

ELECTRICAL

E
N
G
I
N
E
E
R

TECHNICAL REPORT NO. 1

A PHASE STABILITY STUDY SYSTEM FOR VLF
PROPAGATION OVER SHORT DISTANCES

Prepared by

VLF TRANSMISSION LABORATORY

E. R. GRAF, PROJECT LEADER

26 July 1968

FACILITY FORM 602

N 68-31296
(ACCESSION NUMBER)

164
(PAGES)

CR-61922
(NASA CR OR TMX OR AD NUMBER)

(THRU)

1
(CODE)

07
(CATEGORY)

CONTRACT NAS8-20154

GEORGE C. MARSHALL SPACE FLIGHT CENTER

NATIONAL AERONAUTICS AND SPACE ADMINISTRATION

HUNTSVILLE, ALABAMA

ENGINEERING EXPERIMENT

AUBURN UNIVERSITY

AUBURN, ALABAMA



TECHNICAL REPORT NO. 1

A PHASE STABILITY STUDY SYSTEM FOR VLF
PROPAGATION OVER SHORT DISTANCES

Prepared by

VLF TRANSMISSION LABORATORY

E. R. GRAF, PROJECT LEADER

26 July 1968

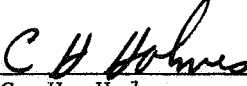
CONTRACT NAS8-20154

GEORGE C. MARSHALL SPACE FLIGHT CENTER

NATIONAL AERONAUTICS AND SPACE ADMINISTRATION

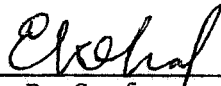
HUNTSVILLE, ALABAMA

APPROVED BY:



C. H. Holmes
Head Professor
Electrical Engineering

SUBMITTED BY:



E. R. Graf
Alumni Professor
Electrical Engineering

FOREWORD

This is a technical report of a theoretical and experimental study conducted by the Electrical Engineering Department of Auburn University under the auspices of the Auburn University Engineering Experiment Station toward the fulfillment of the requirements prescribed in NASA Contract NAS8-20154. This work is a continuation of that described in NASA Technical Report No. 9, Contract NAS8-5231, and this report includes some pertinent text material from that report (No. 9, NAS8-5231) for clarity.

ABSTRACT

An engineering design of a unique transponder system for the phase measurement of VLF signals is developed and evaluated. The phase measurement over a two-way path, which is performed by the system, is independent of the incidental phase errors of the associated transmission equipment and is a result of phase-coherent system design. Hence, the actual measured phase changes, which are twice the one-way phase change, are a function only of the propagation medium.

The system design reviews the basic fundamentals of the propagation of electromagnetic energy within the earth-ionospheric cavity for short distances. The required power and the signal-to-noise ratio for the proposed propagation system are investigated. The design techniques associated with VLF receiving and transmitting antennas are discussed and analyzed in regard to (1) the static antenna capacitance, (2) the effective height, (3) the radiation resistance, (4) the ground system, (5) the radiated field strength, and (6) the antenna pattern factor. The effect of a finite ground conductivity on the over-all propagation in this region is also explored. An engineering design of the system, which meets the requirements for the phase stability measurements, is presented.

An antenna design technique for obtaining increased static antenna capacitance of an umbrella antenna with negligible decrease

in effective height is presented. This antenna design employs a multiple-wire construction which effectively increases the surface area of the antenna rib and, thereby, the total antenna capacitance. Scale model studies with various rib diameters from 1/2 in to 9 in for a 12-rib umbrella antenna indicates that a 20 percent increase in capacitance can be obtained for rib diameter ratios of 18:1. Two full scale antenna structures, which have 12 ribs of 9 in diameters and are 300 ft in height, have been constructed using this technique, and a 24 percent increase in capacitance was obtained as compared to the theoretical value of a similar antenna with a 1/2 in rib diameter.

The system construction, which consisted basically of two 300 ft umbrella antennas and their associated equipment, is described. The over-all experimental system performance is compared to the engineering design data. The measured and theoretical values of the radiated field strengths compared favorably for one propagation path. However, the other path exhibited a somewhat lower propagation efficiency as a result of lower ground conductivity in the area surrounding the transmitting station. The diurnal phase change for the propagation path was measured and predicted to be of the order of 1 μ sec at the operating frequency. The accuracy of the phase measurement was found to be 1 part in 190.

In addition, a computer-aided technique for SNR measurement employing a time interval counter is presented. This technique

yields a measure of the period of the signal-plus-noise in a digital form. This digital data can be recorded along with the phase stability data on magnetic tape, and the SNR can be monitored almost continuously to indicate phase measurement accuracy.

ACKNOWLEDGMENT

The authors wish to express their appreciation to the many members of the group from the Auburn University Electrical Engineering Department, both student and faculty, who contributed to the overall construction of this complex propagation system.

TABLE OF CONTENTS

LIST OF TABLES	ix
LIST OF FIGURES	x
I. INTRODUCTION	1
II. SYSTEM DESCRIPTION	8
III. SYSTEM DESIGN	15
General Concepts	
VLF Propagation Over Short Distances	
Basic Concepts	
The Groundwave	
The Sky Wave	
Signal-to-Noise Requirements	
Sensitivity Requirements	
Accuracy Requirements	
Antenna Requirements	
Transmitting Antenna	
General Discussion	
Vertical Radiator Characteristics	
Ground Resistance	
Top-Loaded Antennas: Theory	
Top-Loaded Antennas: Experimental	
Summary of Antenna Design	
Receiving Antenna	
Effect of Finite Ground Conductivity on Antenna Radiation Characteristics.	
Ionospheric Convergence Factor	
Calculation of Total Field Employing Both Ground and Sky Waves	
Tuning Inductance	
Summary of Design	

IV. CONSTRUCTION AND EVALUATION OF THE PROPAGATION SYSTEM.....	104
V. CONCLUSIONS	128
BIBLIOGRAPHY	134
APPENDICES	138
A. List of Symbols.....	139
B. A Computer-Aided Measurement of SNR Using a Time Interval Counter.....	144

LIST OF TABLES

1. Capacitance Measurements of Scale Model Vertical Radiators with Various Top-Loading Configurations.....	62
2. Magnitudes of Propagated Ground Wave Fields Over the 200 mi Path for Different Conductivities.....	80
3. Magnitude of Individual Sky Wave Field Components.....	88
4. Parameters for Calculation of Sky Wave Components of Table 3.....	89
5. Design Parameters for Phase Stability Study System.....	103
6. Measured Parameters for Phase Stability Study System.....	127

LIST OF FIGURES

1. System Block Diagram for the Proposed VLF Phase Stability Study.....	6
2. Geographical Location of the Propagation Path for the Phase Stability Measurements.....	9
3. Block Diagram of VLF Instrumentation for the Phase Stability Study System.....	12
4. Some Possible Propagation Paths at VLF Frequencies over Short Distances.....	18
5. Variation of Ionospheric Reflection Coefficient Magnitude and Phase as a function of $\cos \phi$	23
6. Variation of Signal-to-Noise Ratios as a Function of Frequency and Power for a 320 km Path Length.....	28
7. Examples of Variation of Atmospheric Noise with Frequency at Various Locations at the Most Noisy Time of Day.....	29
8. Sinusoid Plus Noise.....	32
9. Theoretical Radiation Resistance of a Vertical Antenna for Assumed Linear Current Distribution.....	40
10. VLF Antenna Equivalent Circuit.....	43
11. Capacitance, Reactance, and Required Tuning Inductance as a Function of Antenna Height (No Top-Load).....	44
12. Effective Ground Resistance, R_g , as a Function of Radial Ground Wire Length.....	47
13. Diagram of Umbrella Rib Configuration.....	50
14. Maximum Antenna Base Voltage (rms) as a Function of Antenna Height (No Top-Load).....	55
15. VLF Umbrella Antenna Design (1).....	60

16.	Rib Construction for 100 ft VLF Umbrella Antenna.....	60
17.	(a) Rib Construction for 150 and 200 ft VLF Umbrella Antennas with $d = 3a/7$	61
	(b) Rib Construction for 150 and 200 ft VLF Umbrella Antennas with $d = 5a/7$	61
18.	An Umbrella Antenna Design (2)	68
19.	Multiple-Wire Rib Configuration.....	69
20.	(a) Vertical Radiation Pattern for the Sky Wave of a Short Dipole Located on the Surface of a Flat Earth.....	71
	(b) Vertical Radiation Pattern for the Ground Wave of a Short Dipole Located on the Surface of a Flat Earth.....	71
21.	Magnitude of Launching Loss for $f = 20$ kHz as a Function of Launching Angle.....	75
22.	Convergence Factor Versus Distance.....	77
23.	Cosine of the Angle of Incidence of the Wave at the Ionosphere vs Distance Between Transmitter and Receiver.....	83
24.	The Angle of Arrival of the Wave Above the Surface of the Earth vs Distance, L_g , Between Transmitter and Receiver.....	84
25.	Transmission Delay Time Between Sky Wave and Ground Wave Based on Ray Length.....	85
26.	Field Strength as a Function of Distance for Radiated Power of 1 watt at 20 kHz.....	93
27.	Impedance Matching using Parallel-Tuned Circuit for a Short Vertical Antenna.....	94
28.	Gold Hill VLF Transmitter Station	106
29.	Terminal Construction for the Multiple-Wire Ribs.....	107
30.	Spacer Construction for the Multiple-Wire Ribs.....	107
31.	Vertical View at the Antenna Base Showing Umbrella Construction.....	108

32.	Instrumentation Trailer at Gold Hill Station Housing Tuning Coil, Transmitter, and Remote Control Equipment.....	108
33.	Constant Ground-Wire Current Contours for Gold Hill Station.....	112
34.	View of Antenna Base Showing Feed System, Lightning Arrestor, and RF-AC Isolation Transformer for Tower Lights.....	114
35.	Transmitter Installation in Instrumentation Trailer.....	114
36.	Diurnal Phase Variations (Night and Morning, 3 May 1968 for Fairhope-to-Auburn Transmission (up-path)).....	118
37.	Response of Closed-Loop System to a Step Change in Phase.....	124
38.	Auburn Control Station for VLF Phase Stability Study System....	125
39.	Phase Comparison Accuracy Test of Receiver-Reference Combination.....	126
40.	A Typical Phase Comparison Recording for the Closed-Loop System	
	(a) Control Station Data.....	131
	(b) One-Way Phase Variation, Fairhope Receiver.....	132
41.	The Effects of Uncertainty in Trigger Level on the SNR Measurements.....	148
42.	Actual Versus Computed SNR.....	152

A PHASE STABILITY STUDY SYSTEM FOR VLF PROPAGATION OVER SHORT DISTANCES

C. E. Smith and E. R. Graf

I. INTRODUCTION

The exact prediction of the propagation characteristics of electromagnetic fields in the earth-ionosphere cavity is virtually impossible. The problem is extremely complex and it has been investigated by many engineers and physicists. These investigations have contributed much to our knowledge of the problem, and their results have made possible reliable predictions of the propagation constants of this medium in many cases. The main factors which influence the complexity of the problem are the boundaries of the propagation medium. These actual or apparent boundary surfaces of the ionosphere and earth are neither well defined nor homogeneous with respect to inherent electrical properties. The ionosphere is, of course, the stratum lying between 40 to 50 km and several earth radii. In this region, free electrons exist in sufficient quantities to affect the propagation of radio waves. The region is also divided into layers of different electron distributions, and these distributions vary continually as a result of the ionizing energy and high-energy particles received from the sun. These ionizing effects are then clearly related to the earth's daily and seasonal rotations, the well-known sunspot cycle, solar flares, sudden ionospheric disturbances (SID), and even planetary dynamics through its casual effect on the sunspot cycles.¹ The boundary of the earth's surface is more clearly defined because of the abrupt change in density of the earth-

atmosphere boundary. However, the land masses do not present a uniform surface, and both the electrical conductivity and dielectric constant vary tremendously because of the wide distribution of different minerals within the earth's crust, and, to some extent, because of the ground water level and other tropospheric effects. In addition, the earth boundary can include a mixed path propagation (land and sea) which can influence propagation characteristics. The ionosphere boundary layer, likewise, exhibits some degree of roughness and stratification, and, thus, cannot always be considered a smooth reflecting surface.

It has been found that high frequency (3-30 MHz) propagation in the earth-ionospheric cavity is characterized by:

- (1) unreliability during ionospheric disturbances, and
- (2) fairly rapid and deep fading, both of which are very undesirable.²

These disadvantages are a direct result of the propagation environment. The only major advantage of the high frequency transmission is the relative simplicity and smaller financial investment for the basic terminal equipment. The adverse properties can be minimized by operating at lower frequencies where the propagation characteristics become more stable. This lowering of the operational frequency will eventually lead to the curtailment of the use of high information rates in the network because of the limited usable bandwidth. As a direct consequence of this relative increase in propagation stability, the

interest in the very-low-frequency (VLF) spectrum (3 to 30 KHz) has increased steadily during the past two decades. The stability obtained in voice communications at VLF frequencies has been known from the advent of radio, and as a result VLF transmission has been used by the Navy for long-range communications to ships at sea since about the turn of the century. The increased interest is a result of the discovery that the stability of VLF propagation over long paths (greater than 1000km) approaches that required for precise navigation and dissemination of world-wide time and frequency standards.³ This increased stability for long propagation paths is a result of a waveguide mode of operation which occurs as the height of the earth-ionosphere cavity approaches distances comparable to the wavelength of the operating frequency, and thence the roughness of the boundaries become a smaller portion of a wavelength. If a phase comparison of two stable signal sources is made over such a long path, a regular diurnal change in phase is obtained. This change, on an east-west path, commences some half hour before sunrise at the eastern terminus as the electron density in the ionosphere increases when more and more energy is absorbed from the rising sun. The phase change continues smoothly until just before sunrise at the western terminus, and remains constant until about sunset at the eastern terminus, and, then, it changes smoothly until the nighttime condition is obtained. These diurnal variations are quite regular for long paths and are the major phase variation obtained. By using this relatively stable mode of operation, frequency determinations of better than 1×10^{-11} have been made over short periods of time over such long paths.⁴ Also, as a direct consequence of the

apparent propagation stability, several VLF navigational systems have been investigated, and a dual-frequency system, Radux-Omega,⁵ is being tested and implemented.

However, VLF propagation at short distances is not necessarily as stable, and it is much more sensitive to causal phenomena simply because of the geometry of the problem. The propagation of VLF signals at distances less than 400 km can be described in terms of the summation of a ground wave and single or multiple reflections from the ionosphere. The stability of such a transmitted signal of a one-way path is dependent upon the propagation medium, the atmospheric noise, and the measuring equipment. The major source of phase error in the interconnecting transmission and receiving system employed in the measurement is the transmitting antenna. In large antenna structures there are slow variations caused by changes in transmitter impedance, which are in turn caused by heat dissipation in tuning coils and short time variations resulting from wind-loading and related effects.⁶ The degree of accuracy of the phase comparison measurement of this one-way transmission path is thus inherently limited by any one or a combination of the influencing factors described above; that is, if the phase of a VLF signal received from a high-stability source is compared with a signal received from another high-stability signal source, then the variation or change in the measured phase is interpreted as a change of electrical distance or phase difference between transmitter and receiver. This total phase variation can be attributed to the phase variations in frequency standards, associated interconnecting transmission and receiving equipment, propagation medium, noise, antennas, or a combination of these

phenomena. Numerous investigations,⁷⁻⁹ have been made in order to characterize the propagation characteristics of the region in which the ionosphere affects VLF propagation. One-way phase-comparison measurement does not allow for the determination of absolute phase-change between the two points unless an independent link between the points having a known and stable phase shift is established. The ground wave signal, which is relatively stable, has been utilized as the one-way-path receiving station phase reference at distances up to several hundred kilometers in order to determine VLF ionospheric propagation characteristics on an absolute basis.¹⁰ Commercial telephone circuits have also been employed to transmit reference signals to receiving stations in order to obtain similar information.¹¹

The purpose of this study is to develop a system for studying the absolute phase stability of propagated VLF signals, and which will eliminate errors caused by the antenna and frequency standards or the references of the system. The proposed system is a two-way transmission system, in which a signal at frequency f_1 is transmitted to the transponder station, where it is then re-transmitted at a phase-coherent frequency f_2 slightly offset from f_1 . Frequency f_2 is received at the reference station, and, after being phase-coherent frequency offset, it is compared with the transmitted frequency f_1 , as shown in Figure 1. Thus, the problem of establishing an independent link of known phase shift is by-passed, and the total phase change over the path may be directly attributed to the propagation medium. The phase variation is essentially twice as large since the transmitted signal has traversed the path in both directions. The data obtained from the experiments

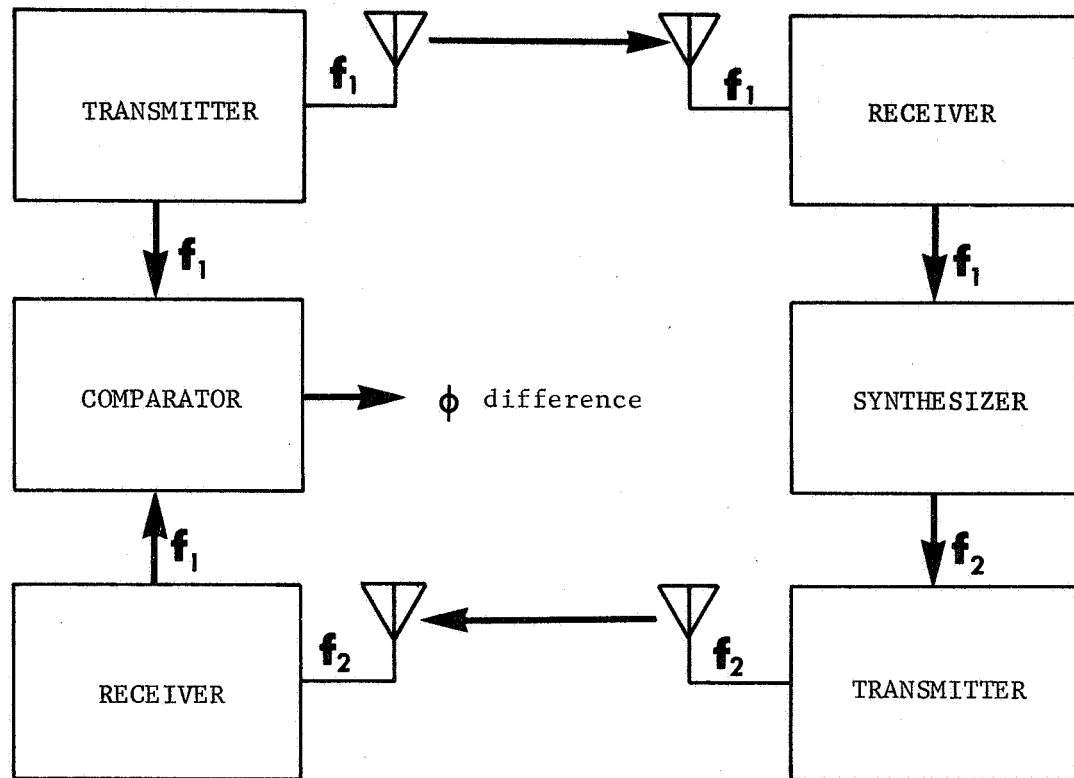


Fig. 1.--System block diagram for the proposed VLF phase stability study.

utilizing this system are to be used to furnish information about phase and amplitude stabilities at very-low-frequencies resulting from variations in the propagation medium and the associated transmission system. It is expected that the data will be useful in determining predictable measures for the short and long term phase stability of the propagation medium, and these measures can be utilized for precise phase comparison measurements over small distances.

II. SYSTEM DESCRIPTION

The proposed phase-stability measurement system has been established over an approximate range of 300 km, between a control station and a transponder station. This distance was selected to insure that the geometry of the propagation path would be intermediate with regard to the long-range (1000 km) condition and the near-vertical incidence condition at the desired operating frequency. The actual propagation path employed is 200 air miles, and it runs between Auburn-Gold Hill, Alabama, and Fairhope, Alabama, as shown in Figure 2. The average electrical conductivity of this path increases monotonically by a factor of two¹² proceeding from the northern to the southern terminus of the system, which is approximately one mile from Mobile Bay. The intervening terrain is characterized by rolling hills gradually sloping towards the South. It is interesting to note that the elevation of the transmitting sites changes from 105 feet on the coast to 715 feet at the inland station. The path is approximately Southwest from the Auburn area. The coordinates of the Gold Hill transmitting station are 32°41'58"N latitude and 85°29'48"W longitude, and those of the Fairhope Station are 30°13'14"N latitude and 87°32'34"W longitude.¹³

Phase measurements will be made over this two-way path by

- (1) transmission of a continuous wave (CW) signal to the transponder station at Fairhope from the transmitting station at Gold Hill,
- (2) synthesis of a phase-coherent CW signal frequency-offset from the

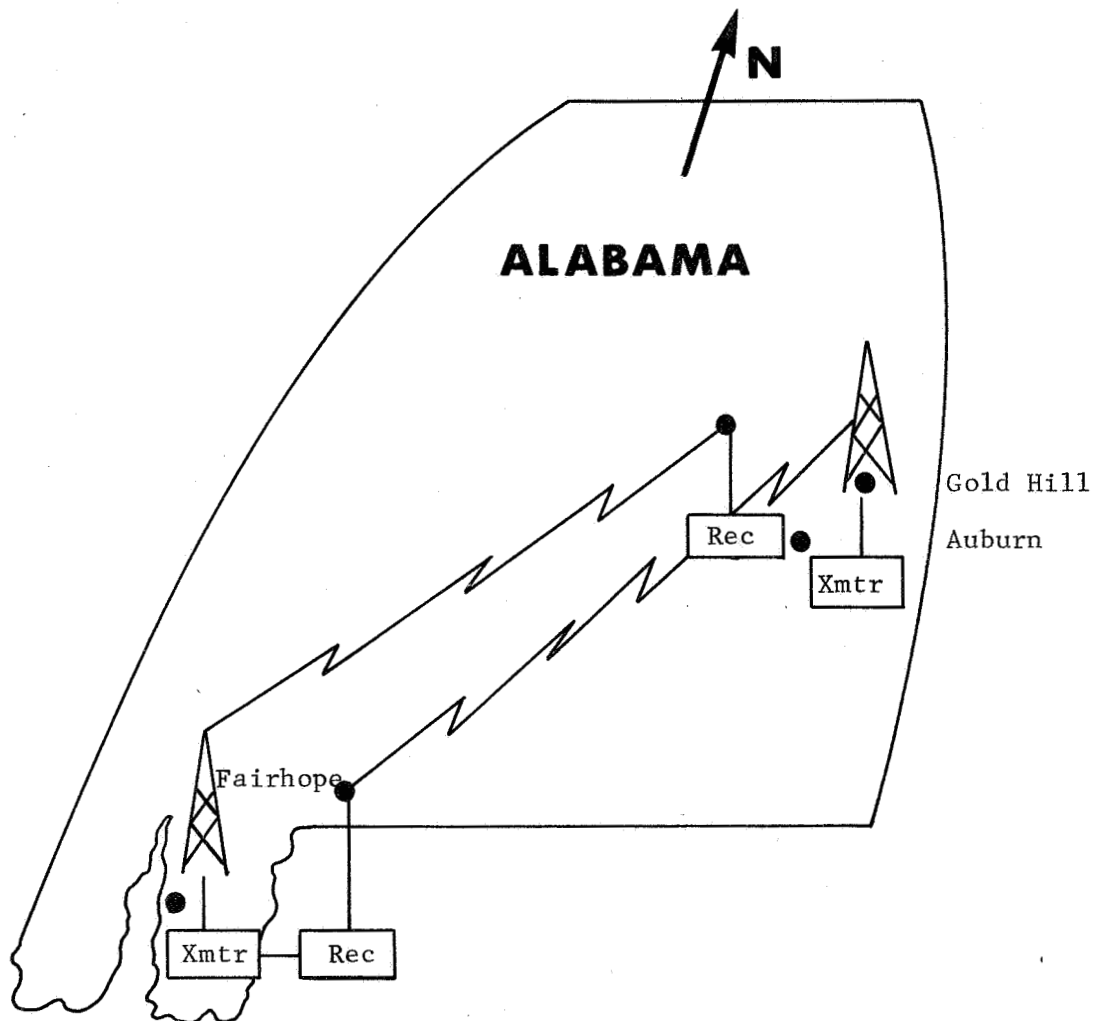


Fig. 2.--Geographical location of the propagation path for the phase stability measurements.

Gold Hill signal, (3) transmission of this phase-coherent signal to a control station at Auburn, and (4) comparison of this received signal with a signal synthesized from a reference signal obtained at the control station. A simple block diagram of this measurement system was presented previously in Figure 1. The measurement technique presented in this figure does not automatically cancel or correct equipment-induced phase errors. Careful control of the terminal operation functions is required to eliminate internal phase variations, and, thus, to insure that the phase data is not contaminated by spurious information which may also be related to the same independent variables as the propagation medium.

The first step taken to insure that these errors were eliminated was the use of separate transmitting and receiving stations at the originating terminus of the signal network. By separating the two stations approximately seven miles along the propagation path (the receiving station is located very nearly on the path between the two transmitting stations), the transmitted signal can be sampled as it is propagated toward the transponder station and then employed as a phase reference for comparison measurements at the control (or receiving) station located at Auburn.

This technique will effectively cancel the phase variations introduced by the transmitted signal in the overall phase measurement because the actual propagated signal, which contains the phase variations, is used as a standard or reference for the measurement. These phase variations are, of course, caused by physical variations of the antenna and its environment, and by effects of the complete transmitter. In

all other sections of the control and transponder stations, phase-lock loops (feed-back control systems which maintain phase input-output relations) are used to maintain phase-coherent operation, and, thereby, phase-stable operation of the system. An in-line phase control loop is employed which also includes the transmitting antenna at the transponder station. The phase of the transmitted signal from the transponder is sampled, and any variations in the phase of the propagated signal caused by antenna changes are cancelled in a manner which maintains coherence between input and output signal phase.

A complete block diagram of the phase measurement system is presented in Figure 3. The basic building blocks of this instrumentation are the four conventional VLF receivers. These receivers act as active filters, which have extremely narrow effective bandwidths, so that signals having very poor signal-to-noise ratios (SNR) can be detected. These receivers are double conversion systems, which use local oscillator frequencies synthesized from a reference source, for reception over a wide frequency range in a phase-locked mode. The phase comparison performed by the receiver is based upon a comparison between the total argument of the sinusoidal input and reference signals. Since the frequencies of both sources will always be slightly different, the receiver continually compensates for this difference (which is sensed as a phase error) as well as for any phase changes. The main functions provided by these instruments are to supply a noise-free output signal which is phase-coherent with the input or received signal, and to supply a record of the total accumulated phase difference

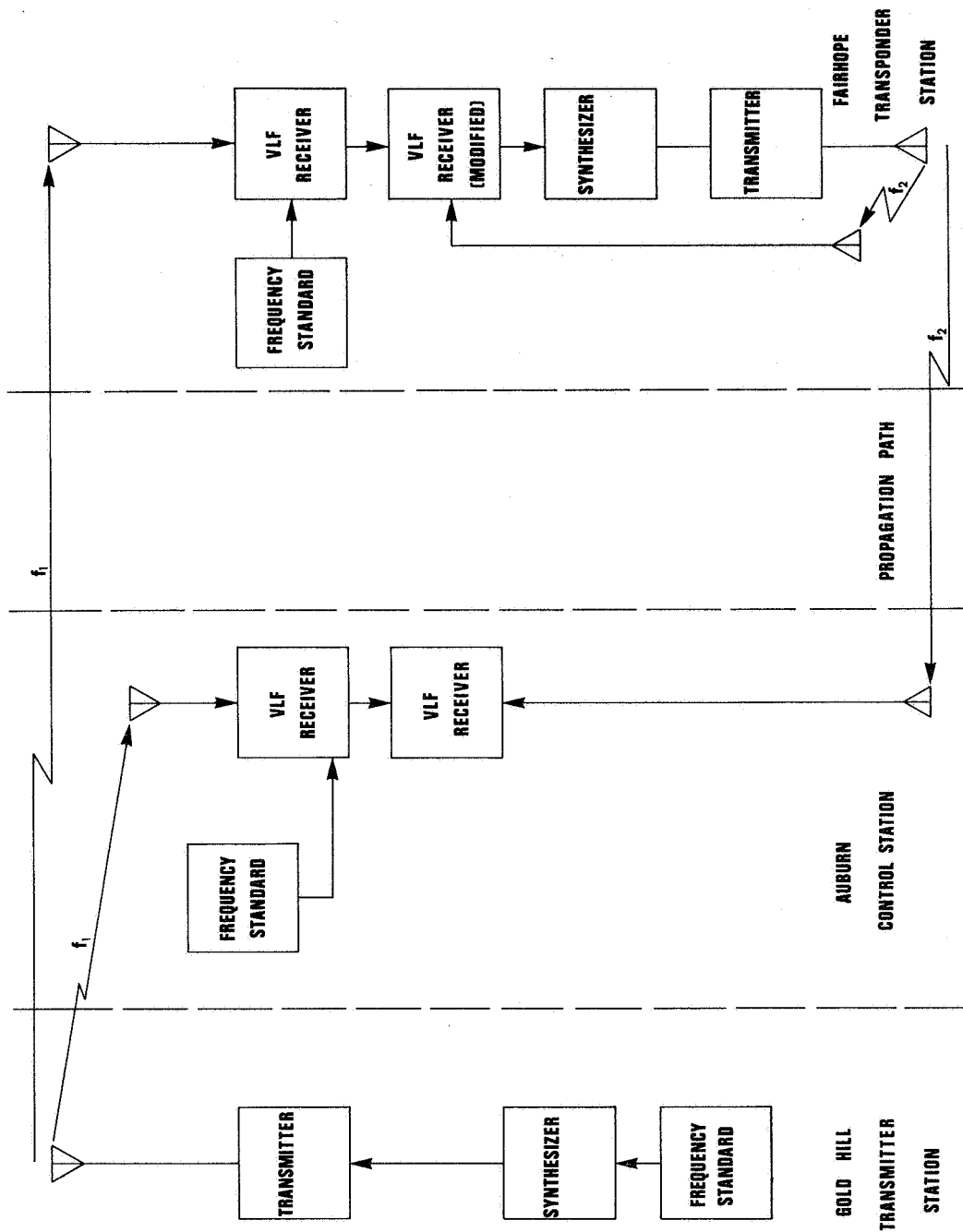


Fig. 3.--Block diagram of VLF instrumentation for the phase stability study system.

between the input and reference signals. The phase stability and response of these units determine the ultimate limit of system accuracy. A phase-lock receiver is not required at the originating transmitter station, which is composed of a frequency standard,* a frequency synthesizer, a power amplifier, a tuning coil, and an antenna. The control station employs one receiver to sample and establish the phase reference from the signal transmitted to the transponder. This reference signal is used as a reference for another receiver to perform a phase comparison, which is related to the two-way phase measurement.

The transponder, which includes standard transmitting equipment, employs one receiver to establish a noise-free signal, which is phase-coherent with the signal transmitted to the transponder. This signal is used to synthesize a phase-coherent signal, which is offset 1 KHz from the received signal. This particular frequency separation was selected to eliminate dispersive effects in the propagation medium, and to minimize receive-transmit interference at the transponder. Another receiver in a modified form is employed to form a closed phase loop around the antenna structure so that the coherence between the received and actual propagated signal from the transponder can be maintained, as also shown in Figure 3. Thus, a signal is transmitted to the transponder, where it is frequency-offset in a phase-coherent mode, and then it is re-transmitted to the control station. At the control station, this

*The stability required depends on the effective system bandwidth and response time.

signal is compared with the reference, which was sampled from the "down-going" signal. The phase measurement obtained is independent of the instrumentation, which is not the case in a one-way phase comparison system, and, thus, it indicates the total two-way or composite phase-shift introduced by the propagation medium.

All modern VLF phase tracking receivers are equipped with a facility for securing amplitude variation data. Amplitude data can be simultaneously recorded and compared for the separate one-way propagation paths. This information indicates the magnitude of the amplitude stability, and also gives a measure of the difference, if any, in the amplitude stabilities in the two propagation paths.

In addition, the phase variations introduced by the transponder transmitting antenna can be obtained from a record of the phase error in the in-line phase-lock loop (modified receiver). These data yield a measure of the phase error introduced by the transmitting antenna utilized in this phase comparison system.

The frequency of operation of the Gold Hill transmitting Station is 20.9 KHz, and the Fairhope Station operates on 21.9 KHz with frequency stabilities in the range of 1 part in 10^{10} . Each station is remote-controlled from the Auburn Control Station by means of commercial telephone circuits, and the phase stability data will be recorded on magnetic tape in digital form to facilitate a computerized statistical analysis of the data.

III. SYSTEM DESIGN

General Concepts

The propagation of electromagnetic energy at the low-frequency (LF) and the very-low-frequency (VLF) portion of the spectrum in the earth-ionosphere cavity has been extensively investigated, both experimentally and theoretically, during the past fifty years. Budden,¹⁴ Wait,¹⁵ and Pierce,¹⁶ as well as others, have contributed greatly to the increased interest in the propagation problem at these frequencies, and to the over-all solution of this problem in the earth-ionospheric cavity. A vast amount of knowledge has been accumulated from all the many studies, and, as a result, relatively accurate predictions of VLF propagation characteristics can be obtained. However, the precision of the predictions of the existing fields is limited, principally because of the complex boundary conditions which exist in the propagation region. Even with the large amounts of experimental and theoretical data and the advancement of related technology, it has only been during the last ten years that improvements in the methods of engineering of LF and VLF systems have been made. Belrose, et al.,¹⁷ have presented one of the first detailed discussions of the factors that influence the design of LF communications systems. Only within the past several months has a very detailed coverage of VLF system design been available for general usage.¹⁸ General design data for specific VLF systems were, of course, available previously.^{19,20}

The solution to the basic propagation problem must satisfy Maxwell's electromagnetic equations within the bounding media. The exact analytical solution of these equations can not be obtained for the actual media because of the complex nature of the physical properties that are involved. In order to obtain a reasonable determination of the propagation theory of VLF waves in this media, simplified models, which are based on idealized boundary conditions, have been used to obtain analytical solutions to the related problem, and the results of experimental studies have been used to describe empirically pertinent propagation characteristics. For distances wherein the near field components are negligible, there are three basic modes of propagation: (1) ground wave, (2) sky wave, and (3) guided wave. For large distances, the total field can be represented as the sum of a number of modes in which the energy is propagated between parallel boundaries similiar to waveguide propagation.^{14,15} For short distances (less than 500 km), the total field existing at a remote point in relation to the source can be considered as the sum of the ground wave and of the sky wave. Since this study is related to short distances, geometrical ray theory can be employed,¹⁸ in conjunction with ground wave propagation theory, to describe the propagation problem.

The major design considerations are involved in two factors which influence system behavior. These are: (1) the propagation medium (including effects of the ground wave, conductivities, the amplitude of the sky wave as a function of transmission distance, frequency, time of day, season, amplitude and characteristics of atmospheric noise), and (2) the antenna system (with special

emphasis on efficiency and economy).¹⁷ This study is an investigation, both theoretical and experimental, of the design and development of a system which will perform the functions outlined in the System Description.

Propagation of VLF Waves Over Short Distances

Basic Concepts

Before the engineering design is approached, the theory of VLF propagation over short distances will be reviewed briefly. This discussion will be limited to the case where both receiving and transmitting antennas are located on the surface of the earth, and only the vertical component of the propagated electric field will be considered.

If a received signal is at a distance L_g measured along the earth's surface from the transmitting source, then it can be thought of as comprising contributions both from the sky waves and the ground wave, as shown in Figure 4. In this simplified case, the generalized form of the received signal will be proportional to the total field strength, \bar{E}_t , where

$$\bar{E}_t = \bar{E}_g + \sum_{m=1}^{\infty} \bar{E}_{s,m} \quad (1)$$

\bar{E}_g = Amplitude of the ground wave,

and

$\bar{E}_{s,m}$ = Amplitude of the sky wave (the required m , the number of reflections, for magnitude determination decreases rapidly so that a good approximation is obtained from a finite number of the components).

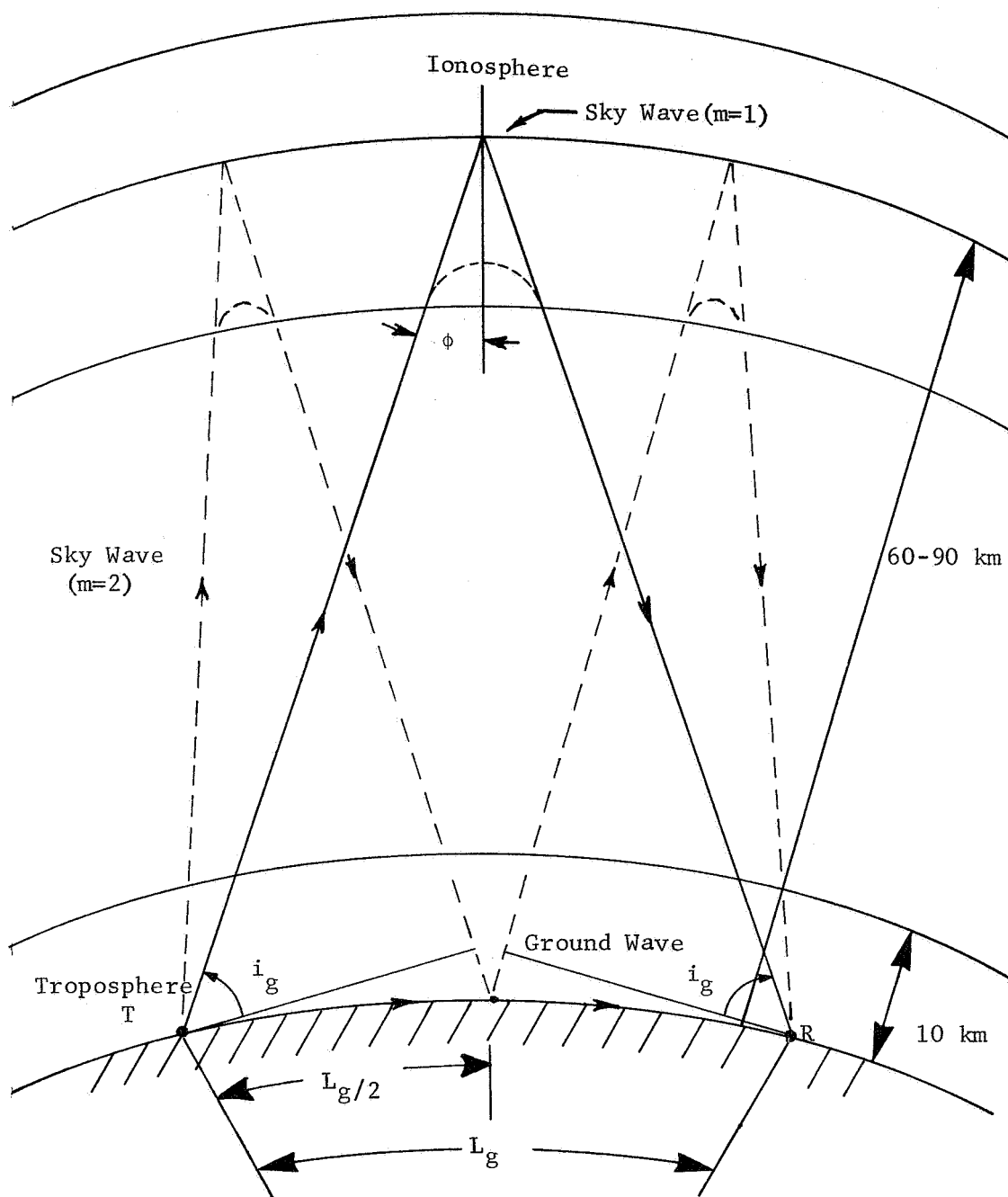


Figure 4.--Some possible propagation paths at VLF frequencies over short distances.

The phase of \bar{E}_t continually changes because there are periodic and nonperiodic variations generated in the sky wave $\bar{E}_{s,m}$, relative to the reasonably constant phase of the ground wave. These variations, in general, are a result of ionospheric phenomena. The magnitude of the total field strength is a function of the reflection height, the reflection coefficient, and the phase of the ground wave. This total phase variation, which is independent of equipment-induced phase error, is the major quantity to be investigated by means of the proposed phase measurement system.

The Ground Wave

The contribution of the ground wave^{12,18} to the received signal strength can be expressed as

$$|\bar{E}_g| = A \frac{|\bar{F}_s|}{L_g}, \text{ and} \quad (2)$$

$$\phi_g = \phi_I + \pi/2 - \beta L_g + \phi_A$$

where $|\bar{F}_s|$ is the unattenuated field strength at one mile from the antenna over a flat conducting plane (which is a direct function of the radiating structure), A is the media attenuation factor, ϕ_I is the antenna current phase, ϕ_A is the media phase change, β is the free space propagation constant ($2\pi/\lambda_0$), λ_0 is the free-space wavelength at the operating frequency, and the $+\pi/2$ and $-\beta L_g$ are two phase factors inherent in \bar{F}_s . This expression is a result of Norton's²¹ work, which reduces an existing complex field solution to a simple numerical evaluation for engineering applications.

The attenuation factor is a function of the frequency, the polarization, the distance with curvature, the effective earth conductivity, and the dielectric constant of the earth. It has been shown that for short numerical distances, the attenuation factor varies almost exponentially with distance as

$$A = e^{-0.43p + 0.01p^2}, \quad (3)$$

where

$$p = \frac{\pi L g}{\lambda x} \cos b; \text{ numerical distance,}$$

$$b = \tan^{-1} \left(\frac{\epsilon_r + 1}{x} \right), \text{ phase constant,}$$

$$x = \sigma / \omega \epsilon_a,$$

$$\sigma = \text{earth conductivity,}$$

$$\epsilon_r = \text{relative permittivity,}$$

and

$$\epsilon_a = \text{actual permittivity}$$

for

$$b < 5^\circ \text{ and } p < 4.5.$$

This theoretical solution (Equation 2) for the ground wave propagation is based upon the assumption that electromagnetic waves are propagated on the surface of a homogeneous spherical earth in the absence of an ionosphere. Thus, the wave propagates on a curved surface and the field decreases because of: spreading of the energy, refraction loss, and absorption at the earth's surface due to the

finite conductivity.¹⁸ There still exists some disagreement about the use of the actual earth's radius or the four-thirds earth's radius concept to account for atmospheric refraction of waves at these frequencies.^{17,18} However, J. R. Wait has indicated recently that the four-thirds concept is valid down to about 10 kHz.¹⁸ This controversy involves a multiplicative factor of about 1.7 in the field calculations. The four-thirds earth's radius concept is used to calculate the resultant fields in this study.

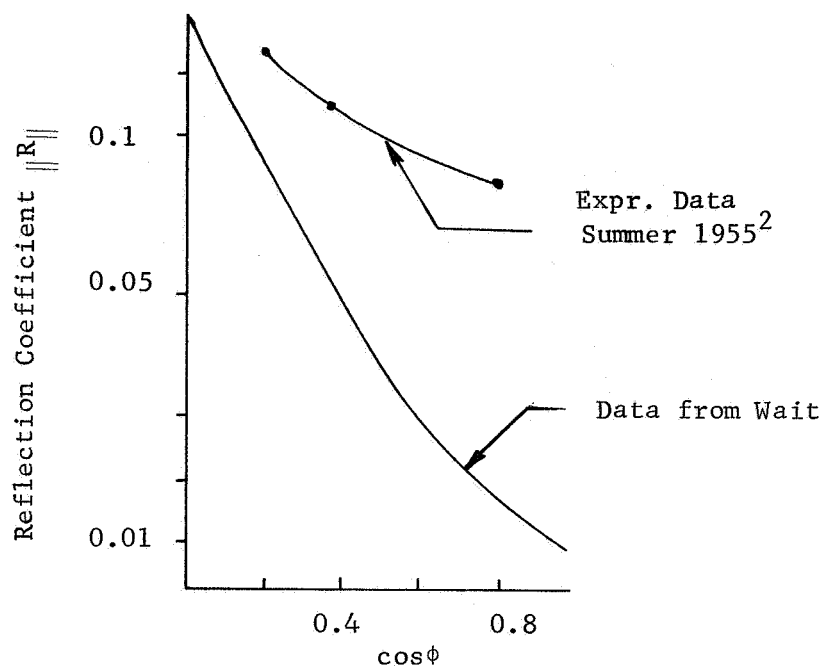
The Sky Wave

The sky wave for the short distance path is obtained by reflection from an apparent surface between 60 to 90 km above the surface of the earth. This actual ionospheric layer of reflection is composed of a region of charged particles with varying density gradient about the earth. The actual electron or ion density of this ionospheric layer, which is basically controlled by absorption of solar energy, is quite sensitive to any ionizing forces and recombination activity. Effects due to meteors, solar flares, sunspots, magnetic storms, thermonuclear explosions, and the normal seasonal and daily rotations of the earth have been observed for a long period of time through the use of electromagnetic waves. The results of these investigations have given a basic characterization of the electric properties of this layer. This layer is immersed in the earth's magnetic field because of its proximity, and, as a result, the incident field can be

converted in polarization.

This polarization conversion is a direct result of the movement (created by the incident electromagnetic field) of the free electrons in the layer in the presence of the earth's magnetic field. The path of the moving electrons do not follow the incident field, and their curved or distorted motions create fields of other polarizations. It is well to note also, that at VLF frequencies the electrons move farther during a cycle, and the collision frequency of the electron with other particles increases. This creates a mechanism of energy loss and the ionosphere has a finite conductivity. These phenomena make the theoretical treatment of the reflecting surface rather complex and difficult to analyze. Therefore, experimentally determined reflection coefficients are generally employed to describe the propagation characteristics of the sky wave. This reflecting ionospheric layer, as has been indicated, varies with time, frequency, geographical location, and, to some degree, direction of propagation. Hence, the calculated values of the actual fields are just reasonable estimates which depend on the precision of the value of the reflection coefficient. Figure 5 presents several curves which indicate some of the variations of the magnitudes and phases of the reflection coefficients with time and frequency.²

The effective amplitude of the sky wave at the receiver location is a function of the distance, the reflection coefficients of the ionosphere and of the earth, and the antenna characteristics. If the finite conductivity of the earth is considered not to alter the vertical radiation characteristics appreciably for this propagation



(See-Wait, J. R., "Reflection of VLF Radio Waves from an Inhomogeneous Ionosphere," J. Res NBS, 670, 519(1963).)

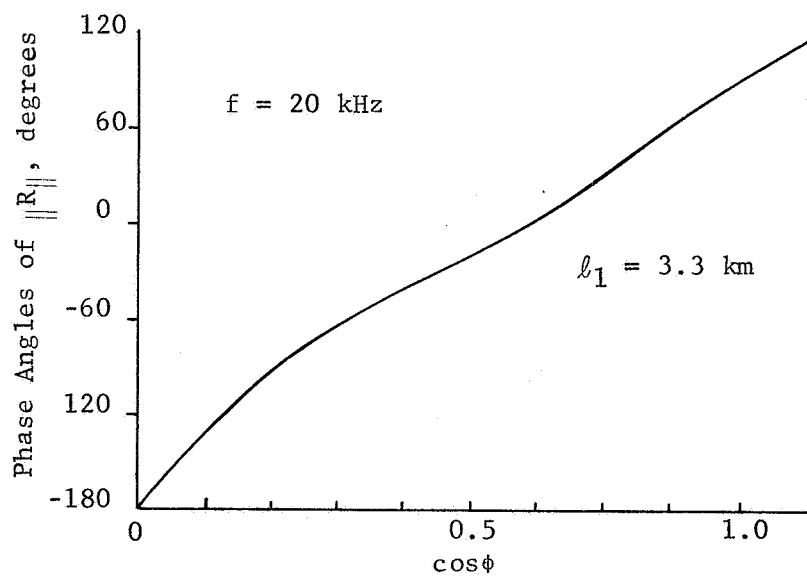


Fig. 5.--Variation of ionospheric Reflection Coefficient Magnitude and Phase as a Function of $\cos \phi$.

path, the amplitude of a m^{th} reflected space wave from a vertical radiator at a distant point is

$$|\bar{E}_{s,m}| = \frac{|\bar{F}_s|}{L_{s,m}} G_t(i_g) R_m D_m \cos(i_g), \quad (4)$$

and

$$\phi_{s,m} = \phi_I + \pi/2 - \beta L_g - 2\pi\Delta T f + \phi_R$$

where $G_t(i_g)$ is the normalized voltage gain of the transmitting antenna, $\cos(i_g)$ is the term which converts the E field of the down-coming wave to a vertical polarization component, (i_g) is the angle of incidence of the sky wave with the earth (see Fig. 4), R_m is the composite reflection coefficient of the ionosphere*, $L_{s,m}$ is the length of the m^{th} sky wave path, D_m is a factor introduced by the focusing or convergence effect of the ionospheric reflecting surface (which will be treated in a later section),²² ϕ_R is the phase of the ionospheric reflection coefficient, $2\pi\Delta T f$ is the additional sky wave delay, ΔT is the time delay between sky and ground waves, and f is the frequency. The total electric sky wave field is then the sum of all possible ray paths between the transmitter and receiver in the earth-ionospheric cavity. On the single-path ray, the amplitude and

* $R_m \approx 20 \text{ mLog} ||R_{||}|| + 20(m-1) \text{ Log} |R_{g||}|$, the subscript notation, $||$, denotes that the electric field of the incident wave is parallel to the plane of incidence and the notation, \perp , means it is perpendicular to the plane of the incidence.

phase of the received vertically-polarized field is simply altered in form by the complex reflection coefficient $\parallel R \parallel$. A field component is also generated and exists in the plane perpendicular to the plane of incidence (plane of vertical polarization). This generated field component is a result of the energy conversion process discussed earlier, and it has a magnitude related to the incident field by a complex conversion coefficient $\parallel R \perp$.

If the case of a multiple-hop path is considered (as in Fig. 5, $m = 2$), the field strength can no longer be simply altered in magnitude and phase by a single reflection coefficient. The received vertically-polarized electric field for $m = 2$ is reflected at three points ((1) the ionosphere, (2) the ground, and (3) the ionosphere) before it arrives at the receiver location. Since the incident field at the first ionospheric reflection is converted into two orthogonal components, and at the ground, these fields are simply reflected for high conductivities; then it is easy to see that the two orthogonal fields may now be converted into four components upon the second reflection from the ionosphere. This reasoning can be extended to higher order reflections, which indicates the degree of complexity of multiple-reflection field strength calculation. In most analyses, the energy loss by conversion is assumed negligible and the total reflection coefficient for a m^{th} order reflection is simply $|R_m| = |\parallel R^m \parallel| |R_g|^{m-1}$. It is well to keep in mind that each reflection coefficient is a function of the angle of incidence, i_g .

Thus, the total electric field over a short distance can be determined in terms of (1) two factors, $|\bar{F}_g|$ and A , (2) the experimentally

or theoretically obtained ionospheric reflection coefficients, and
(3) known constants for the electrical properties of the earth's surface.

Signal-To-Noise Requirements

Sensitivity Requirements

The design of any communications system is based upon the determination of the radiated signal power to noise ratio required to exceed a given threshold which yields a valid estimate of the information content actually transmitted. Since the design of the complete system is dependent upon the determination of the required radiated power, a careful study has been made to determine an estimate of the required power needed for accurate phase measurement. This study was based upon the technique for determining the required power for a VLF transmission path presented by J. A. Pierce,¹⁶ and it was assumed that this data was sufficiently accurate over the range in question (approximately 320 km or 200 miles): Pierce's technique employs the highest measured value of atmospheric noise in the United States, called Kansas noise, as a basis for extracting power requirements for a given signal-to-noise ratio, SNR.

Since the criterion for radiated power is related to receiver sensitivity, it is desirable to base the calculations on a VLF phase tracking receiver system presently available for utilization in the proposed system. A typical receiver* having a sensitivity of 0.01 μ v for a -20 db signal-to-noise ratio into the tracking filter for positive automatic gain control (AGC) action was selected. The

*RMS, Inc. VLF Phase Tracking Receiver, Model 1312, for example.

bandwidth for this SNR is 50 Hz and the tracking filter has a bandwidth of 0.002 Hz. Hence, the SNR existing in the tracking filter is

$$\text{SNR} = -20 + 10 \log_{10} \left(\frac{50}{0.002} \right) = 24 \text{ db.} \quad (5)$$

From the available information for the determination of required power, a curve indicating the variation of SNR as a function of frequency and power of a 320 km path length has been prepared and is presented in Fig. 6. The original calculations are for SNR's for a 1 kHz bandwidth, and are a function of frequency for several powers at the required distance. The right ordinate of this curve is the SNR in reference to Kansas noise for a tracking filter bandwidth of 0.002 Hz. For a transmission frequency of 20 kHz the required power is approximately 2.4 watts, as determined from the curve. It must be noted that the determination assumes that no additional noise is added by the preceeding receiver stages and by the antenna. At these frequencies, the assumption is valid because the noise figure of the available equipment is sufficiently small in most cases (on the order of 3 to 5 db in modern receivers).

Additional examples of atmospheric noise, as a function of frequency at various locations, are presented in Fig. 7. It is important to note that all values of noise are below the recorded Kansas noise. The median value of noise in this latitude (32°N) as presented in Reference Data for Engineers (ITT), is approximately 26 db below Kansas noise at 20 kHz. The measured average of noise peaks at 15 kHz which was measured near Gainesville, Florida (28°N),

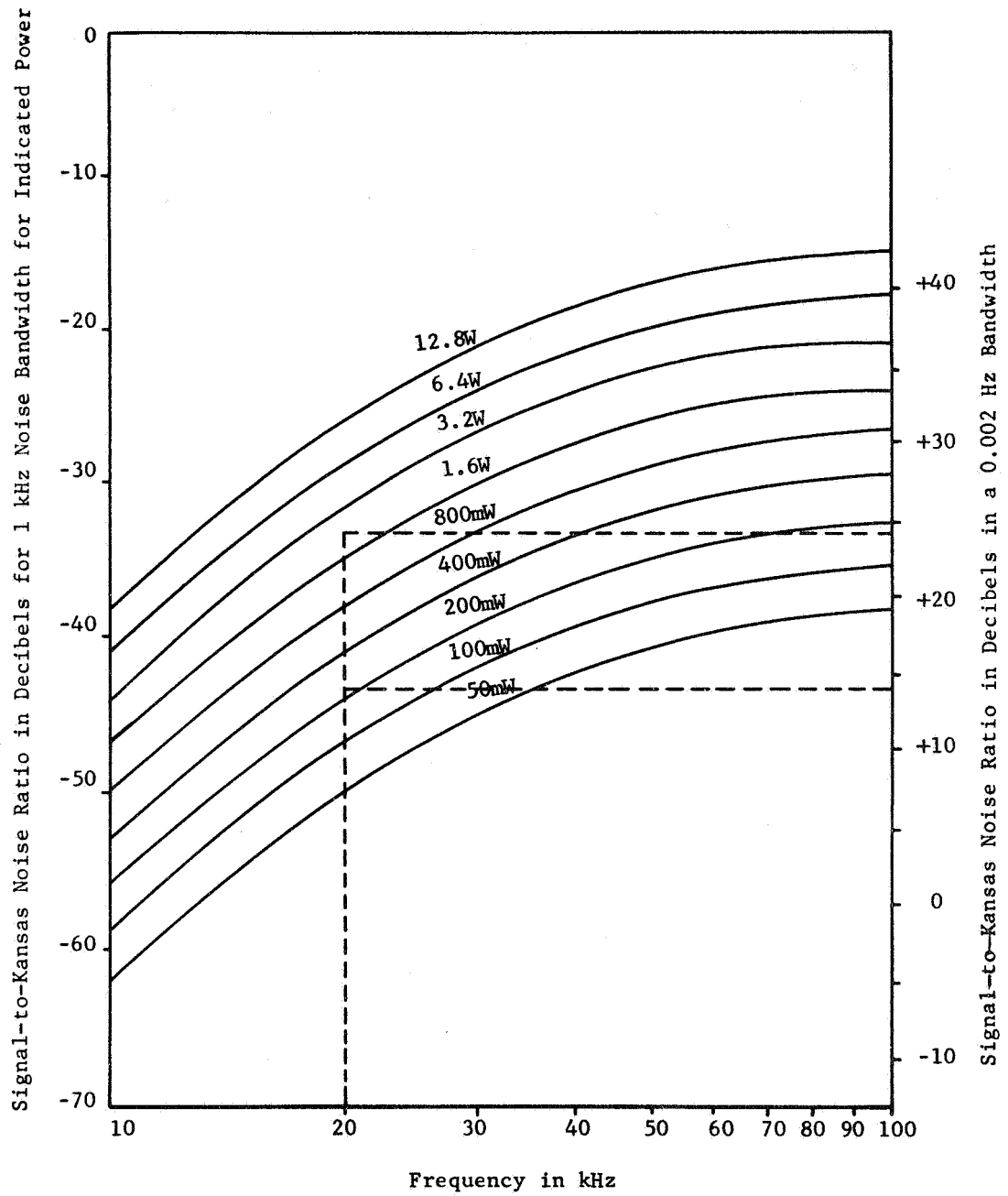


Fig. 6.--Variation of signal-to-noise ratios as a function of frequency and power for a 320 km path length,

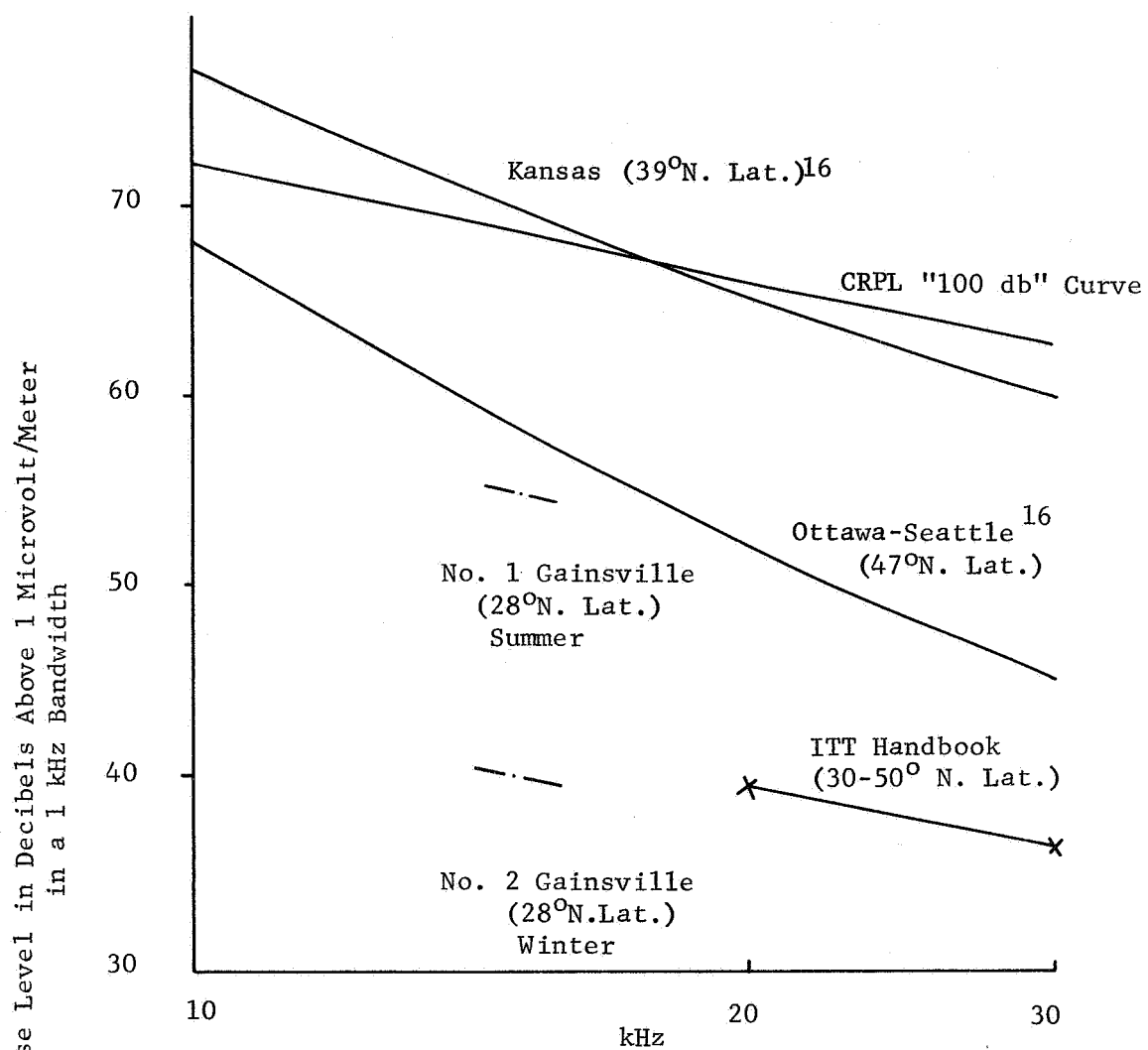


Fig. 7.--Examples of the variation of atmospheric noise with frequency at various locations at the most noisy time of day.

is approximately 16 db below Kansas noise; this average was obtained from a study performed by the University of Florida Electrical Engineering Department.* Because noise levels generally decrease with frequency, the noise as measured in the University of Florida study is seen to be at least 10 db below Kansas noise. Since all recorded noise data indicate that the existing noise level in this region is at least 10 db below Kansas noise, then a shift of 10 db for the SNR to Kansas noise for the 0.002 Hz bandwidth indicates that a radiated power of approximately 100 mw is required for 320 km at 20 kHz.

These curves (Fig. 7) were based upon the required SNR for positive AGC control as specified by the receiver manufacturer; thus, additional receiver sensitivity may be obtained by operating without AGC, which will permit a lower than normal set point for the receiver tracking filter input level. Under the specified conditions, a radiated power of 100 to 200 mw should be sufficient for communications over this path during all periods except those in which ambient noise is excessive.

It is interesting to note that the major source of atmospheric noise in the VLF band comes from radiation due to lightning discharges. The energy from these discharges is scattered by propagation in the earth-ionosphere cavity as a guided wave. The major frequency components peaks about 10 kHz.² Thus, it is easy to understand the variation of atmospheric noise with changes in geographical location since the major storm centers are located in definite regions.

*Private Conversation : Dr. T.S. George, University of Florida, Gainesville, Fla.

Accuracy Requirements

The signal-to-noise ratio existing under measurement conditions for the phase stability study will influence the accuracy of the measured data. The uncertainty of this measurement could detract from the credence of this measured data if the error introduced is of sufficient magnitude. A measure of this error can be calculated as described by Skolnik²³ by considering a continuous sine wave $A_p \sin(2\pi ft + \phi_p)$ where A_p is the amplitude, f is the frequency and ϕ_p is the phase. If a noise component is introduced in the transmission system with the CW wave, it will cause the apparent amplitude to differ from the true amplitude by an amount $\Delta A_p = n(t)$, as shown in Fig. 8.

The measurement of phase can be considered as the measurement of time from a zero-axis crossing of the waveform. The error in time due to the noise is

$$\Delta t = \frac{n(t)}{\text{Slope of Sine Wave at Zero Crossing}}, \quad (6)$$

where

$$\text{slope} \Big|_{t=0} = A_p 2\pi f.$$

Therefore, the rms phase error is

$$\delta \phi_p = 2\pi f \delta t = 2\pi f \frac{(\overline{n(t)^2})^{\frac{1}{2}}}{A_p 2\pi f}, \quad (7)$$

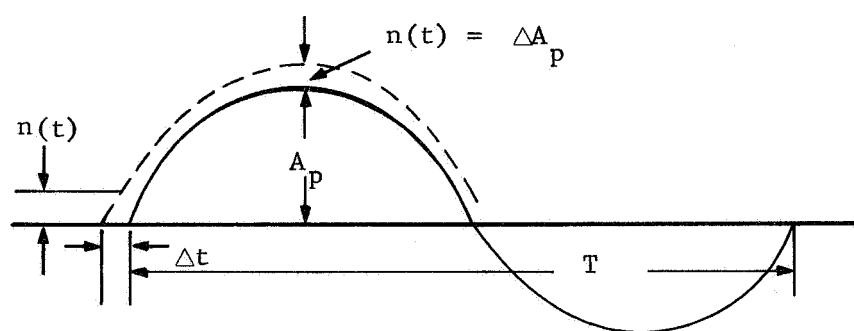


Fig. 8.--Sinusoid plus noise.

where $(\overline{n(t)^2})^{\frac{1}{2}}$ is the rms value of the noise. Now

$$\delta\phi_p = \frac{(\overline{n(t)^2})^{\frac{1}{2}}}{A_p} \quad (8)$$

or

$$\delta\phi_p = \frac{1}{\left(2 A_{rms}^2 / \overline{n(t)^2}\right)^{\frac{1}{2}}} = \frac{1}{\left(2 \text{ SNR}\right)^{\frac{1}{2}}}, \quad (9)$$

where $A_p = 2^{\frac{1}{2}} A_{rms}$ and SNR is the power signal-to-noise ratio.

If the power signal-to-noise ratio in the phase-lock loop (24 db) for positive action of the AGC of the RMS receiver is considered, then

$$\delta\phi_p = \frac{1}{(2 \times 252)^{\frac{1}{2}}} \quad (10)$$

or

$$\delta\phi_p \simeq 1/22.5 \text{ radians or } 2.54^\circ. \quad (11)$$

The deadtime or tracking error of most VLF phase tracking systems is in the order of 0.1 μsec . The mechanical error thus introduced is

$$\delta\phi_m = \frac{\Delta t}{T} 360^\circ, \quad (12)$$

and

$$\delta\phi_m = \frac{0.1 \times 10^{-6}}{50 \times 10^{-6}} 360^\circ \quad (13)$$

or

$$\delta\phi_m = 0.72^\circ \quad . \quad (14)$$

Hence, the measurement accuracy will be determined primarily by the existing SNR of the measurement system and will be less dependent on the introduced mechanical error. This SNR error corresponds to about 1 part in 140. Therefore, the accuracy of the phase measurement will ultimately be determined by the signal-to-noise ratio error of the mechanical control error, whichever is larger.

Antenna Requirements

Transmitting Antenna

General Discussion

Any practical vertical antenna for the propagation of the electromagnetic energy in the VLF spectrum will be electrically short because of the impossibility of erecting self-resonant structures at these long wavelengths. The main considerations of VLF transmitting antenna design are, in most cases, (1) the amount of power required to maintain communication over the required range, (2) the value of antenna quality factor (Q) required to satisfy the bandwidth requirements of the modulated system, (3) the efficiency, and (4) the cost. In this particular system, the power requirement and cost are the determining factors. The quality of a vertical radiator, with respect to efficiency and power capacity, increases with height. However, at the very lowest frequencies, and practical vertical radiator is in the order of

several degrees of electrical length, and hence it is necessary to utilize some form of capacitive top loading in order to obtain even the minimum required performance. The required amount of top loading is usually determined by the maximum allowable antenna voltage for high power installations, although tuning requirements may influence the final choice for low power transmitting installations.

In VLF transmitting antenna design, there is no real optimum design for a particular structural configuration, because additional efficiency or bandwidth can be obtained by increasing the antenna height, top loading, ground plane size, etc. The cost-performance relationship increases rapidly for improved operation because of the increase in price per foot of erecting and maintaining the antenna structures, and the cost of higher voltage insulators required for large transmitted powers.

A survey was made to determine some antenna configuration which would perform under the required conditions, and which would be financially feasible. Two configurations have been considered as possible transmitting antennas. One is a diamond-shaped top-hat antenna fed by one, or multiple, down leads, and the other is an umbrella antenna, which is a simple vertical radiator utilizing guy wires as loading elements. Since the umbrella antenna has the simplest physical configuration, it, in general, costs less to erect and maintain; thus, the umbrella type antenna was selected for utilization in the system.

Vertical Radiator Characteristics

The main disadvantages of VLF propagation are the high cost and the practical difficulty of erecting antenna structures with dimensions appreciable with respect to the operating wavelength.

VLF antennas are usually some form of an electrically short vertical radiator.

The usual model of the simplest and most often used VLF transmitting antennas is a short vertical monopole over a conducting flat plane.

If only the vertical electric field at the plane surface is considered, it can be shown¹² that

$$\bar{E}(t) = \frac{-1}{2\pi\epsilon_0} \left[\int \frac{M(t')dt}{L_g^3} + \frac{M(t')}{V_0 L_g^2} + \frac{dM(t')/dt}{V_0 L_g} \right] \quad (15)$$

where $\bar{E}(t)$ is in volts/meter, $M(t)$ is the changing vertical electric moment, $I_0 \times h_e$, in ampere meters, $I_0(t)$ is the antenna current in amperes, h_e is the antenna effective height in meters, L_g is the distance from the source to the point of observation in meters, v_0 is the wave velocity of free space, and $t' = (t - L_g/v_0)$. The first term on the left of (15) is the electrostatic field contribution, the second term is the induction field, and the third term is the radiation field contribution to the complete field. The tangential magnetic field also has a similar form which consists of both an induction and a radiation field. The electrostatic and the induction fields are related to the actual ground losses in the quasi-static fields in the near vicinity of the antenna; however, the radiation field is of interest to the

propagation problem at this point. At distances far from the antenna the radiation field predominates because it decays only as the inverse of the distance and the other contributions can be considered negligible. Now, if a uniform current distribution is assumed for a single monopole over a conducting plane with a current magnitude I_o , then it can be shown that the unattenuated field strength²⁴ at the surface of a perfectly conducting flat earth one mile from a simple vertical radiator is

$$|\bar{F}_s| = 37.25 I_o \left[\frac{1 - \cos G}{\sin G} \right] \text{ millivolts/meter} \quad (16)$$

where

$$I_o = \left(\frac{w}{R_t} \right)^{\frac{1}{2}}, \text{ antenna base current, or } I_o = \left(\frac{P_r}{R_r} \right)^{\frac{1}{2}},$$

w = total antenna power input,

P_r = radiated power,

R_t = total antenna resistance, $R_t = R_r + R_L$,

R_r = radiation resistance,

R_L = Effective loss resistance,

h = $360^\circ a/\lambda$, angular antenna height,

G = $2\pi a/\lambda$, radian antenna height,

and a = antenna height.

If $G \ll 2\pi$, which is the case for electrically short antennas, and I_0 is expressed in terms of radiated power, the field strength is

$$|\bar{F}_s| = 37.25 \left(\frac{P_r}{R_r} \right)^{\frac{1}{2}} \left[\frac{1 - (1 - G^2/2)}{G} \right], \quad (17)$$

or

$$|\bar{F}_s| = 37.25 \left(\frac{P_r}{R_r} \right)^{\frac{1}{2}} (G/2) \text{ mv/meter}, \quad (18)$$

where the approximations for the series expansions,

$$\cos G \approx 1 - G^2/2$$

$$\text{and } \sin G \approx G,$$

are employed. The established expression for radiation of a short vertical radiator is

$$R_r \approx 10 G^2 \approx h^2/312 \quad (19)$$

for $h < 30^\circ$. The substitution of (19) in (18) yields a field strength of

$$|\bar{F}_s| \approx 5.9 \left(\frac{P_r}{R_r} \right)^{\frac{1}{2}} \text{ mv/meter}, \quad (20)$$

which is independent of antenna height for a constant radiated power. Equation (19) requires that a specific power be radiated regardless of the radiation resistance, which is a function of antenna height as indicated in Fig. 9 for $I_{\text{top}}/I_{\text{base}} = 0$. A comparison of this result with the larger field strength at one mile obtained from a quarter wavelength vertical antenna indicates only an approximate five percent difference. This result is easily deduced from the field strength distribution in the vertical plane around a one-quarter wave length antenna, and a short dipole or infinitesimal antenna above a lossless ground plane.²⁵ The radiation pattern factor of the short dipole is

$$G_t(\theta) = \sin \theta \quad (21)$$

and for the quarter wavelength antenna it is

$$G_t(\theta)\lambda/4 = \frac{\cos(\pi/2 \cos \theta)}{\sin \theta} \quad (22)$$

where θ is measured from the vertical. The pattern of the quarter wave antenna is only slightly more directive than the pattern of the short dipole, and the magnitudes are maximum for $\theta = \pi/2$ (along the ground plane).

A similar, yet different, analysis²⁴ has been made by others wherein the input power w is held constant for a perfectly conducting

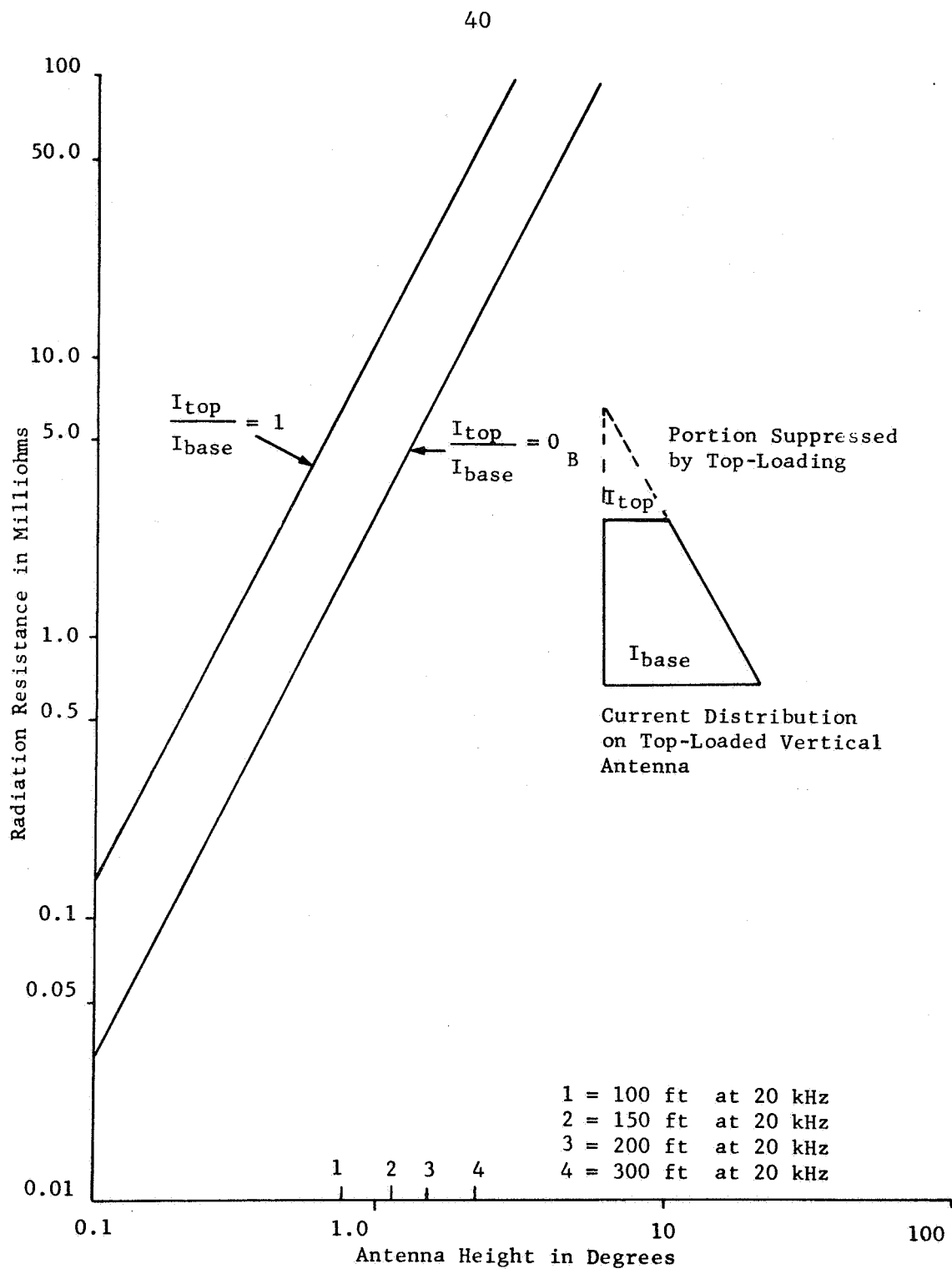


Fig. 9.--Theoretical radiation resistance of a vertical antenna for assumed linear current distribution.

ground. On this assumption, equation (15) becomes

$$|\bar{F}_s| = 37.25 \left(\frac{w}{R_T + R_L} \right)^{\frac{1}{2}} \frac{G}{2} \text{ mv/meter} \quad (23)$$

for $G \ll 2\pi$. For $R_L = 0$, perfectly conducting earth, and a lossless antenna system,

$$|\bar{F}_s| = 5.9 (w)^{\frac{1}{2}} \text{ mv/meter}, \quad (24)$$

which is similar to equation (20), and also indicates that the field strength is independent of antenna height. However, (24) applies for a lossless antenna system. If $R_L \neq 0$ then the field strength decreases with height since

$$\lim_{G \rightarrow 0} |\bar{F}_s| = \lim_{G \rightarrow 0} \left[37.25 \left(\frac{w}{10G^2 + R_L} \right)^{\frac{1}{2}} \frac{G}{2} \right] \rightarrow 0 \quad (25)$$

for $G \ll 2\pi$. Equation (23) is usually plotted for various values of equivalent loss resistance in more relevant references, and hence it can create some misunderstanding if the power is not clearly specified. This type of analysis is certainly correct, and it is employed to emphasize the effect of radiator height on antenna efficiency for a fixed available power input. But, because only small radiated powers are required in the proposed system, the antenna efficiency is not the main concern, and the theoretical field strength can be considered independent of antenna height if power sources are available to maintain a constant radiated power regardless of radiation resistance.

The considerations thus far have applied only for an entirely lossless antenna system. In practice the losses encountered greatly influence system performance because the radiation resistance is extremely small, as indicated in Fig. 9. These losses occur in the tuning inductance, in the vertical radiator, in the insulators, and in the ground resistance as shown in the equivalent circuit given in Fig. 10.

The tuning inductance is required in order to reduce the driving voltage for the antenna reactance which is of the form

$$X_A = Z_0 \cot a \quad (26)$$

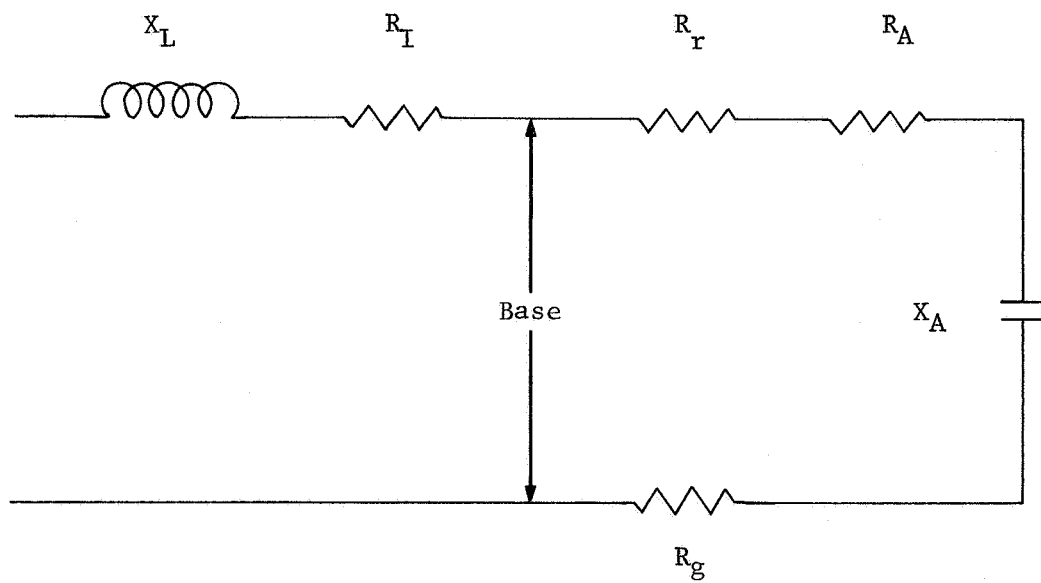
where

$$Z_0 = 60 \ln \left(\frac{a}{r_1} - 1 \right) \quad (27)$$

and

r_1 = effective radius of the antenna.

The reactance, capacitance, and required tuning inductance as a function of height for a simple vertical radiator is presented in Fig. 11. The tuning inductance is excessively large for unloaded towers, which indicates the need for capacitive top loading; however, even with capacitive top loading, practical tuning inductors usually have loss resistances in the many hundreds of milliohms or more. This resistance is much larger than the radiation resistance of an antenna



X_L = Inductive Tuning Reactance

R_I = Inductor Loss Resistance

R_r = Radiation Resistance

R_A = Antenna Loss Resistance

R_g = Ground Loss Resistance

X_A = Antenna Capacitive Reactance (Top Loading)

Fig. 10.--VLF antenna equivalent circuit.

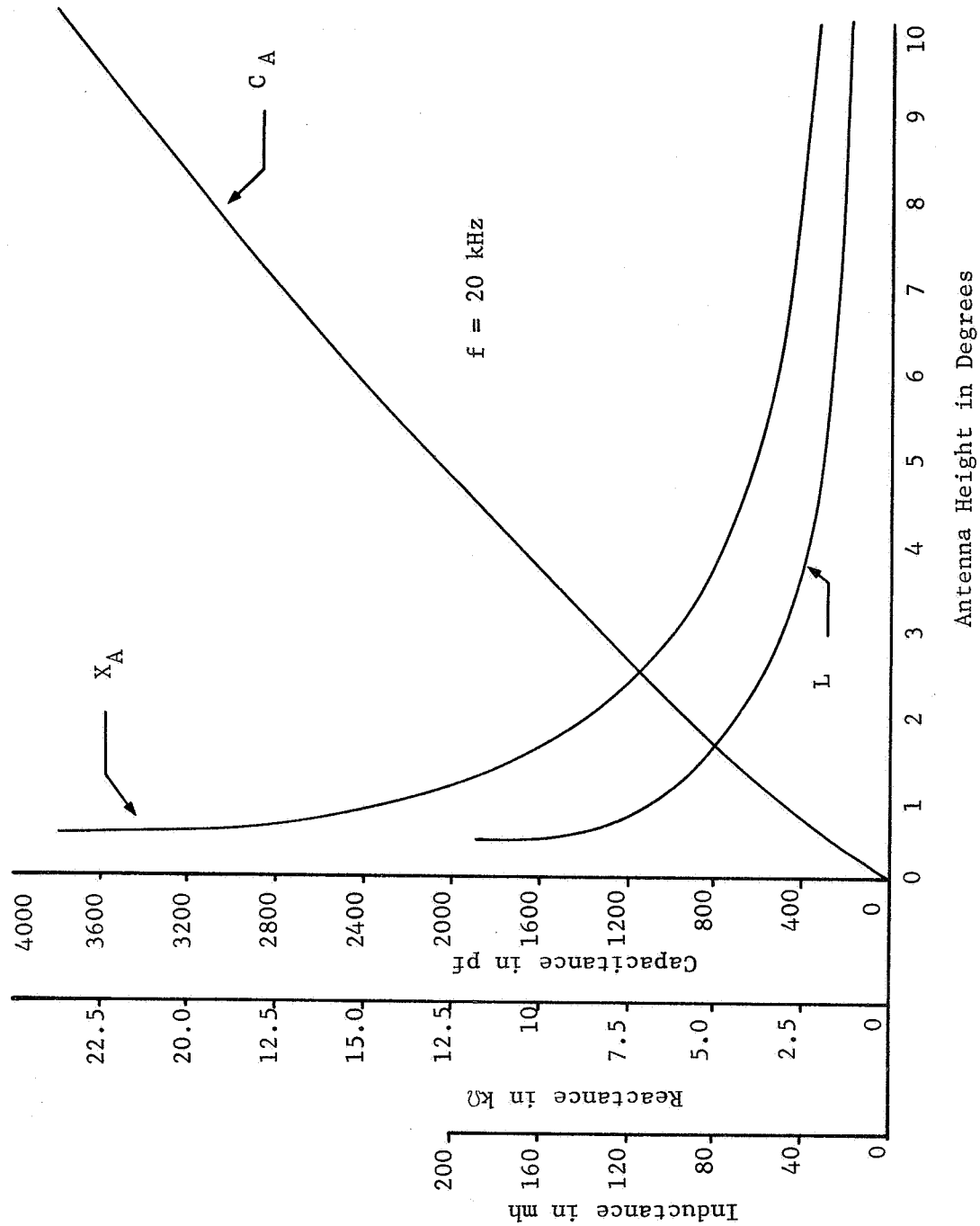


Fig. 11--Capacitance, reactance, and required tuning inductance as a function of antenna height (no top-load).

of several electrical degrees of length. The antenna loss resistance is usually negligible if the component parts of the vertical radiator are bonded together satisfactorily, and are of sufficient surface area.

Ground Resistance

The ground resistance R_g is an effective resistance referred to the antenna equivalent circuit, which is calculated from

$$R_g = \frac{\text{Power Loss in Ground System}}{(\text{Base Current})^2} = \frac{P_G}{I_o^2} \quad (28)$$

Typically, the ground resistance is not less than several hundred milliohms at these frequencies. The power dissipated in the ground is the result of conduction currents induced in the resistive ground system. Radial ground wires are usually employed to minimize this loss, which makes the total power loss in the ground the sum of the power loss in the wires (P_w), the ground adjacent to the wires (P_e), and the ground beyond the ground wires (P_x). Through the placement of a sufficient number of wires of the proper length and size, the power dissipated in the wires, and in the earth adjacent to the wires, can be reduced to an acceptable value. Most sources of information related to the selection of ground plane size recommend that approximately 120 radial ground wires at least 0.3λ long be utilized for minimum ground resistance. However, this is not at all practical for wavelengths in the order of tens of miles because of the space requirement.

Since this requirement is impractical, a study²⁰ has been made to determine the effective resistance of the ground with respect to

a short vertical radiator and a short radial wire ground plane. This simplified study was based upon the assumption that the total power dissipated in the ground system was the sum of the dissipated powers in (1) the wires, (2) the earth adjacent to wires, and (3) the earth beyond the radial wires. The resistance was calculated by the numerical integration of the power loss density about the antenna in the earth's surface down to about one skin depth. The power densities were determined from the current distribution of a vertical radiator over a ground plane of infinite conductivity, and an available expression for the relationship between the current in the wires and in the earth adjacent to the wire for different wire configurations and depths. Results from the study are presented in Fig. 12, which relates the effective ground resistance to ground wire length for several antenna heights. The rapid decrease in effective ground resistance at very short distances from the antenna is a direct result of the very rapid decrease in current distribution as a function of distance from very short vertical radiators.²⁴ It indicates, at least from a circuits viewpoint, that small effective ground resistances for short antennas can be obtained through the use of radial ground systems of lengths less than three-tenths of a wavelength.

Wait and Pope,²⁶ Abbott,²⁷ and others have investigated the calculation of the power loss in buried wire ground systems. Their approach is from a strict or rigorous electromagnetic field point-of-view where the calculated losses are described in terms of the E and H fields. The E field loss occurs as a result of the return ground currents created by the displacement currents surrounding the

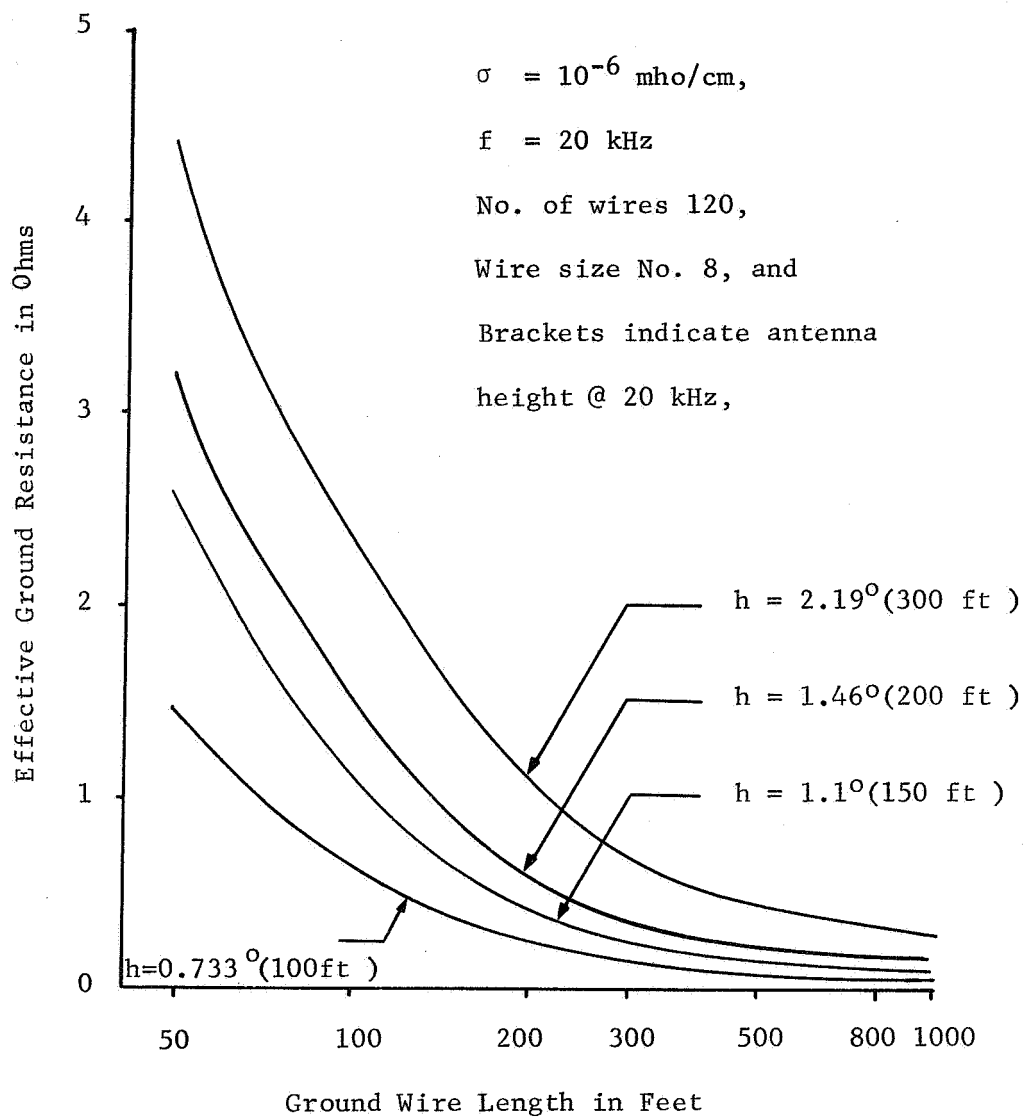


Fig. 12.--Effective ground resistance, R_g , as a function of radial ground wire length.

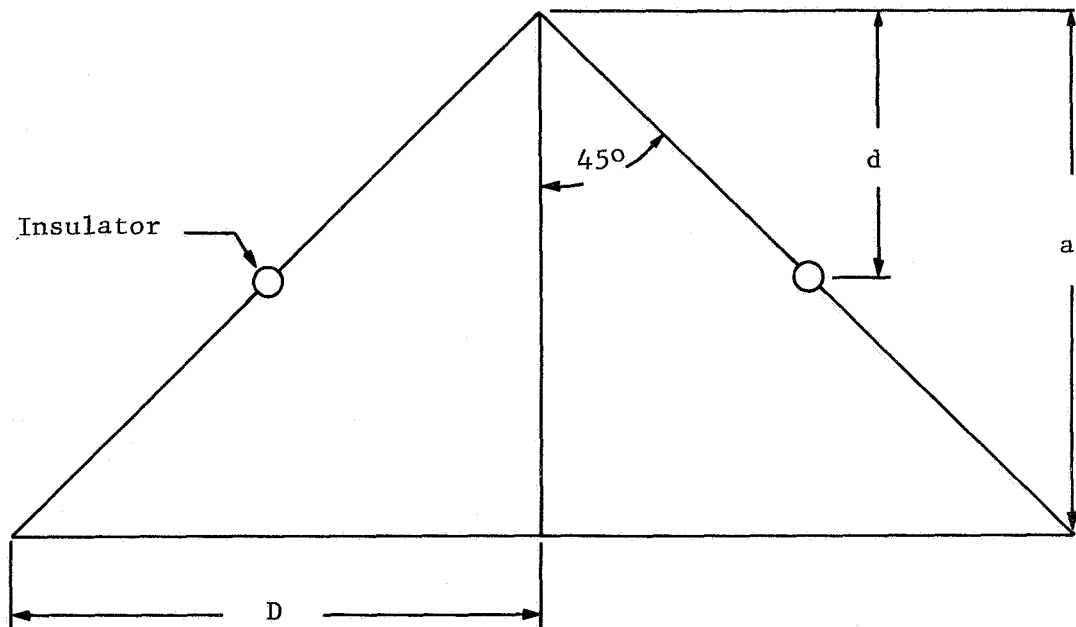
antenna. The H field loss is caused by the existing H field around the vertical radiator which actually forces currents to flow radially toward the base of the antenna. However, the results are for ratios of antenna height, a , to wavelength of greater than $a/\lambda = 0.025$. The ratio of a/λ for this system is smaller by a factor of five or more, and, hence, these results cannot be readily be extended to the system parameters for accurate predictions of ground current losses. The trend of smaller ground resistance for smaller ratios of a/λ at a given distance exhibited in Fig. 12 for the simplified study is quite evident in their results. It is thus felt that the results presented in Fig. 12 give a reasonable estimate for the ground resistance with an accuracy suitable for engineering purposes.

Top-Loaded Antennas: Theory

As indicated in Fig. 11, the reactance of a short vertical radiator increases rapidly as the height decreases. Thus, an extremely large voltage is required to establish the antenna current necessary for a specified power output. This is true because the current on the antenna is determined almost entirely by the reactance which is very much larger than the radiation resistance. It is a common practice to employ a series inductance to resonate the antenna. With this configuration driving voltages and desired current are obtained. For the short vertical antennas the required tuning inductance is quite large, as shown in Fig. 11, which makes it desirable to employ top loading. In this system, top loading, which consists of adding some form of "capacitive hat," serves three desirable purposes: (1) it increases the effective height; (2) it reduces the required tuning induc-

tance; and (3) it lowers the base voltage.

The increase in effective height resulting from top loading is caused by the change in current distribution as can be observed in Fig. 9. The top-loading capacitance prevents the current from decreasing to zero at the top of the antenna such as occurs in the case of a capacitor terminating an open-circuited transmission line. Since the current has a value greater than zero at the top, the average current over the total antenna length is increased. The field strength and effective height of an electrically short antenna is proportional to this average value of current, and any increase in the average current distribution along the length of the antenna tends to increase the measured field parameters. Top loading can increase the effective height by, at the most, a factor of two because of the relationship between the triangular current distribution without top loading and the limiting value of a constant current distribution along the total length of the antenna. The added capacitance may be obtained in several different ways, but the simplest method of achieving large amounts of top loading is the use of the umbrella antenna. The umbrella antenna is basically a vertical radiator with wires extending away from the top of the radiator in a manner similar to that of an extended umbrella as shown in Fig. 13. Additional capacitive top loading may be obtained by connecting the ends of the umbrella rib wires together, as shown in Fig. 15 (connecting wires are called antenna skirt wires). Experimental results indicate that a decided increase in antenna capacitance can be obtained by utilizing this technique in the construction of electrically small antennas. This increased capacitance is a function of the area



d = Distance from top of radiator to insulator

D = Distance to extremities of umbrella support wires

a = Antenna height

Fig. 13.--Diagram of umbrella rib configuration.

enclosed by the skirt wire and of the height of the wire above ground, or a combination of both d and D . The skirt wire does tend to reduce the effective height of the antenna because the enclosed triangular, conic sections tend to shield the vertical radiator. This construction technique is an approach used to reduce the antenna capacitive reactance, thereby minimizing the required tuning inductance. A compromise must be made between the antenna effective height and the required tuning inductance, depending upon the relative importance of each parameter for a given antenna system. Such an antenna configuration has been examined experimentally by C. E. Smith and E. M. Johnson,²⁸ and theoretically by L. C. Smeby.²⁹

From their experimental results, it was concluded that the optimum length of the umbrella wires is not necessarily independent of frequency; however, the optimum radiation resistance is obtained when the value of d is approximately

$$d = \frac{3a}{7} \quad (29)$$

as defined in Fig. 13 for electrically short antennas. (See also Fig. 15). Experimental results for a circular wire, or skirt, attached to the ends of the umbrella wires indicate that the optimum radiation resistance occurs for a given d slightly less than the specified value. If d is increased beyond the point of optimum radiation for a fixed value of D , or, if D is increased with d fixed, then the capacitive reactance of the system is decreased. Through the varying of d , a compromise can be effected between efficiency and

capacitive reactance for the reduction of the tuning inductor requirements, which is, of course, extremely important in this system . Satisfactory results have also been obtained with

$$d = \frac{5a}{7} \quad (30)$$

by others¹⁷ without excessive shielding of the vertical radiator. Their results indicated that radiation resistance increased with an increase in D, and that this dimension should be as large as possible structurally.

The theoretical study by Smeby²⁹ showed that, through the use of the optimum length of the umbrella ribs, the vertical radiation characteristics are the same as they would be from the radiator without top loading. Smeby describes a modified skirt umbrella in which the umbrella wires are connected at the outer periphery by a skirt-wire, and in which the alternate rib wires have an insulator at the top of the antenna. This configuration was suggested as an approach to obtain larger radiation resistance. The skirt on the standard umbrella was thought to be mechanically undesirable, in practice, in view of the fact that the same resistance can be obtained with an umbrella of slightly greater radius.

An expression for the base terminal voltage can be developed from the antenna equivalent circuit of Fig. 10. For a given antenna height, the base voltage is

$$V_b = I_o Z \quad (31)$$

where

$$|Z| = \left[(R_r + R_A + R_g)^2 + X_A^2 \right]^{\frac{1}{2}} . \quad (32)$$

From the theoretical discussion it can be seen that

$$R_t = R_r + R_L = R_r + R_A + R_g \quad (33)$$

and

$$|X_A| \gg R_t;$$

thus,

$$|V_b| \approx I_o X_A , \quad (34)$$

$$|V_b| \approx \left(\frac{W}{R_t} \right)^{\frac{1}{2}} X_A = \left(\frac{P_r}{R_r} \right)^{\frac{1}{2}} X_A, \quad (35)$$

or

$$|V_b| \approx \frac{0.32 (P_r)^{\frac{1}{2}}}{G} X_A . \quad (36)$$

If the antenna capacitance is increased by means of top loading for a given antenna height, the base voltage will decrease. The base voltage is of primary interest since it determines the quality of the base insulator required for a specified radiated power. The base

voltage varies inversely with antenna height as described by (36), and it is presented in Fig. 14 for a radiated power of 1w. The base voltages for several umbrella antennas discussed in a later section of this chapter are also recorded in this figure, and are based upon experimental scale model capacitance measurements. The curves can be extended to other voltages by multiplying the ordinate values by the square of the ratio of desired power normalized to 1w.

The voltage distribution over the antenna tends to follow a cosine law of distribution, with the maximum voltage occurring at a point on the antenna most distant from the base terminals. This voltage distribution is a function of the terminal voltage, of the antenna self-inductance, and of the capacitive fringing effects. The voltage at the most distant point on the antenna³⁰ is usually approximated as

$$V_f = 1.05 I_o X_A \left[1/\cos 90^\circ(f/f_o) \right] \quad (37)$$

where f is the operating frequency and f_o is the frequency at which the antenna is electrically $\lambda/4$ in length. In this case, $f \ll f_o$, and hence

$$V_f \approx 1.05 |V_b|. \quad (38)$$

This result should be expected since the entire antenna structure is only a fraction of a wavelength. The voltage at any point on the structure should be approximately equal to the base voltage, where

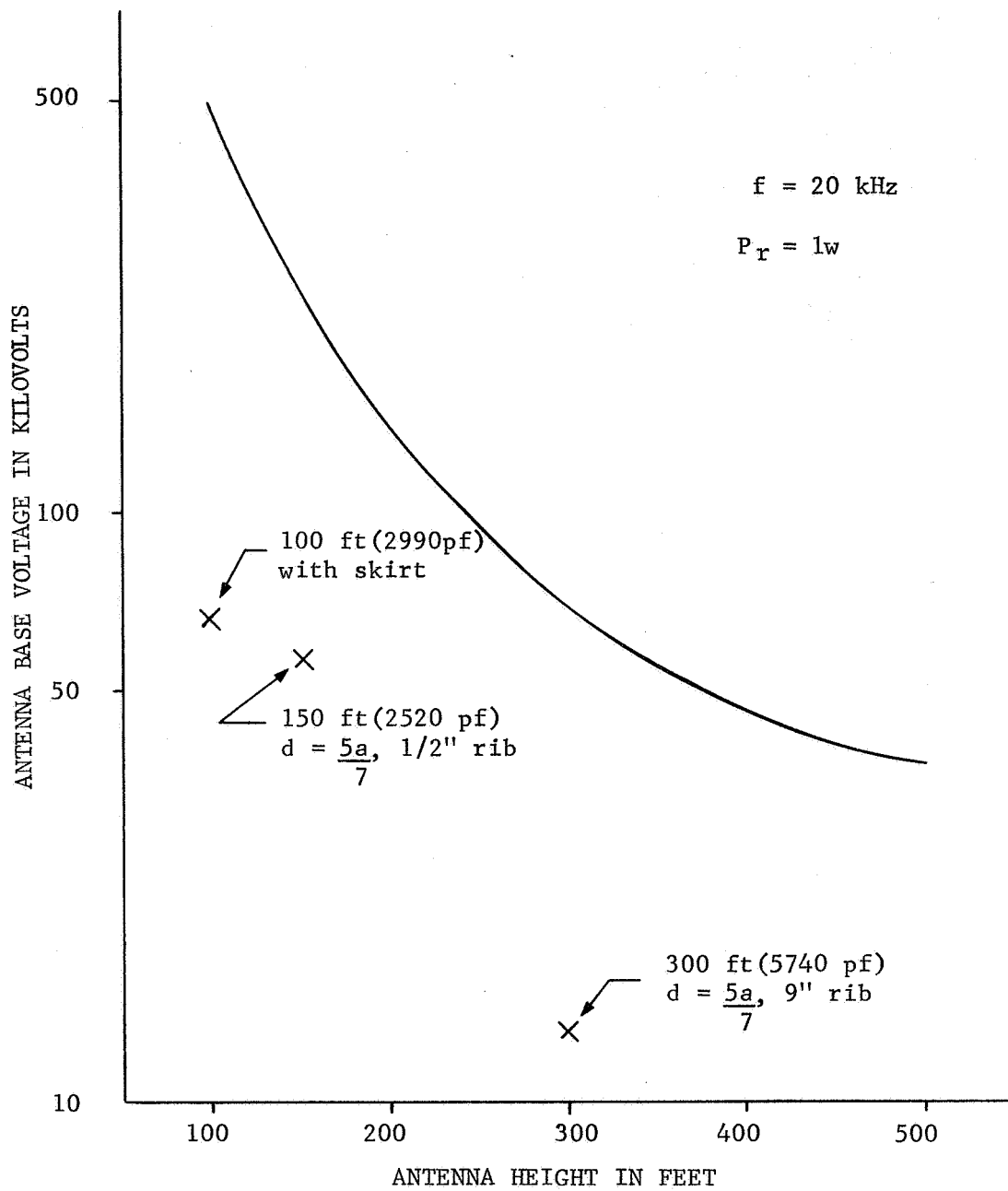


Fig. 14.--Maximum antenna base voltage (rms) as a function of antenna height (no top load).

edge effect may cause a variation of up to 10% of this value.

The basic efficiency of antennas such as these is

$$\eta = \frac{\text{Power Radiated}}{\text{Power Input}} \times 100\%, \quad (39)$$

which can be expressed in terms of the equivalent circuit parameters of Figure 10,

$$\eta = \frac{R_r}{R_I + R_r + R_A + R_g} \times 100\%, \quad (40)$$

where the inductance X_L with loss resistance R_I is included as a part of the antenna system. This inductance may be replaced in practice by a Pi, T, or an L matching section; however, for the present purpose, a series inductance with a loss resistance is satisfactory. The radiation resistance (see Fig. 9), with top loading will have range values of:

$$\begin{aligned} 1.6\text{m}\Omega < R_r < 6.8 \text{ m}\Omega & \text{ for a 100 ft. antenna,} \\ 4\text{m}\Omega < R_r < 15 \text{ m}\Omega & \text{ for a 150 ft. antenna,} \\ 7\text{m}\Omega < R_r < 27 \text{ m}\Omega & \text{ for a 200 ft. antenna, and} \\ 16\text{m}\Omega < R_r < 60 \text{ m}\Omega & \text{ for a 300 ft. antenna.} \end{aligned} \quad (41)$$

The maximum top loading becomes more difficult to obtain as height increases for umbrella antennas because of the shielding of the vertical radiator; and, furthermore, maximum top loading cannot be obtained with simple structures.

A recent investigation of electrically short umbrella top-loaded antennas³¹ has indicated that the static effective height of such structures can be determined by approximating the integral equation describing the antenna charge distribution. This is accomplished by dividing the integral (or antenna configuration) into a finite number of segments over which the charge density is assumed constant, and wherein the integral is represented by a set of simultaneous linear equations. The results of this computation of the integral are presented in the form of nomograms relating the capacitance, the effective height, and the quality factor Q of the umbrella antenna as a function of height, d , D , and the number of umbrella ribs where

$$r_1/a = 1 \times 10^{-3},$$

$$r_2/a = 10^{-5},$$

r_1 is the effective radius of the antenna tower, and r_2 is the effective radius of the umbrella rib wires. From these nomograms, the effective height h_e of an umbrella antenna wherein

$$N = 12,$$

$$d = 5a/7, \text{ and}$$

$$D = a$$

is determined to be

$$h_e \approx 0.5a ,$$

(42)

which is exactly the effective height of an unloaded vertical antenna. This decrease in the anticipated effective height results from the fact that the rib length exceeds the value for optimum radiation. This particular choice of an antenna configuration was investigated because maximum static capacitance is desired. The configuration will be discussed in the following section. A feasible estimate of the system performance can hence be based upon the radiation resistance of a vertical radiator with no top-loading capacitance.

Top-Loaded Antennas: Experimental

In the design of antennas, considerable information related to the impedance characteristics and the radiation pattern of a given structural configuration can often be obtained from a scaled model mounted on a large ground plane.³² Scale factors as large as one-hundred to one (100:1) can be utilized to obtain useful information if the structural design is carefully scrutinized. Intricate details, such as lattice structures, wire configuration, etc., can be idealized through the use of some simple geometric forms wherein the measurements are corrected accordingly.

Four scale model VLF umbrella antennas of 100, 150, and 300 feet have been constructed for the determination of the static capacitance of the structures. The value of antenna capacitance is extremely important since it determines the required tuning inductance, and the total base voltage, for a given transmitted power. The 100-foot antenna consists of an ungrounded, triangular, vertical radiator, which is three feet on each side, and an umbrella, consisting

of eight ribs with skirt. Each rib is in a cage form of four wires on a four-foot square, as shown in Fig. 15 and 16. The 150- and 200-foot antennas consist of ungrounded triangular, vertical radiators with eight single-wire ribs with skirt at a 45° angle from the vertical, as shown in Fig. 17. Static capacitance measurements were made at a frequency of one thousand cycles per second, using a simple audio frequency bridge with the antenna mounted on an effective 20-foot-square ground plane. The corrected full scale measured capacitance values are recorded in Table 1 for several structural variations of the basic designs including some structures with 12 ribs. In addition, capacitance measurements were made at the proper scaled frequency for these models in an effort to determine the actual operating capacitance. The results are also presented in Table 1. Since the scale factor was extremely large (in some cases 200:1), it was impossible to scale all the physical parameters of the structure so that more information could be obtained (loss and radiation resistances, for example.) Although there was some difficulty in modeling the structures, the wire sizes, the tower dimensions, and the lattice construction were approximated as closely as possible.

The static capacitance of top-loaded umbrella antennas can be determined using the nomograms developed by Gangi, et al.,³¹ described earlier in this chapter. The capacitance of a vertical radiator where

$$a = 300 \text{ feet,}$$

$$d = 5a/7,$$

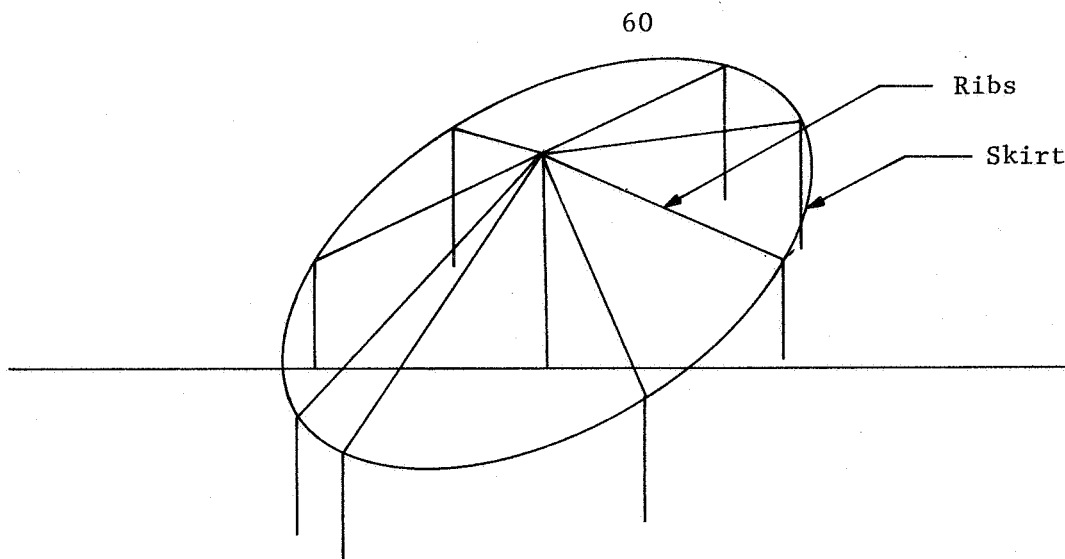


Fig. 15.--VLF umbrella antenna design (1).

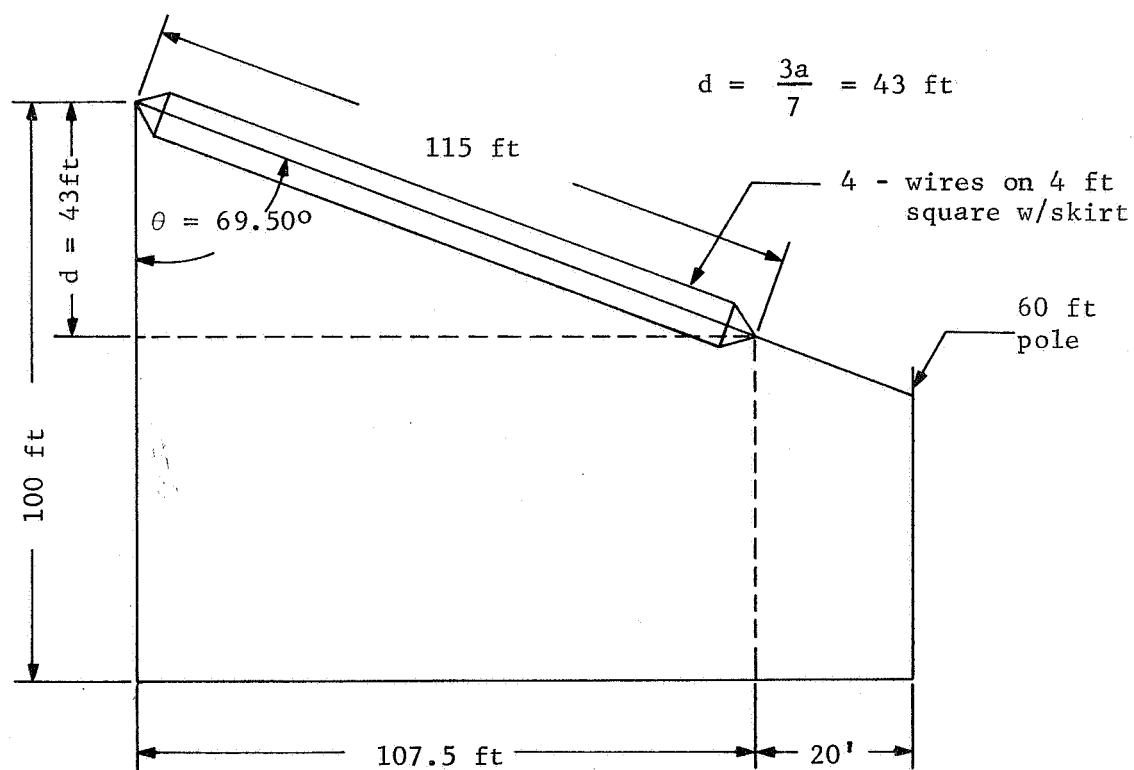
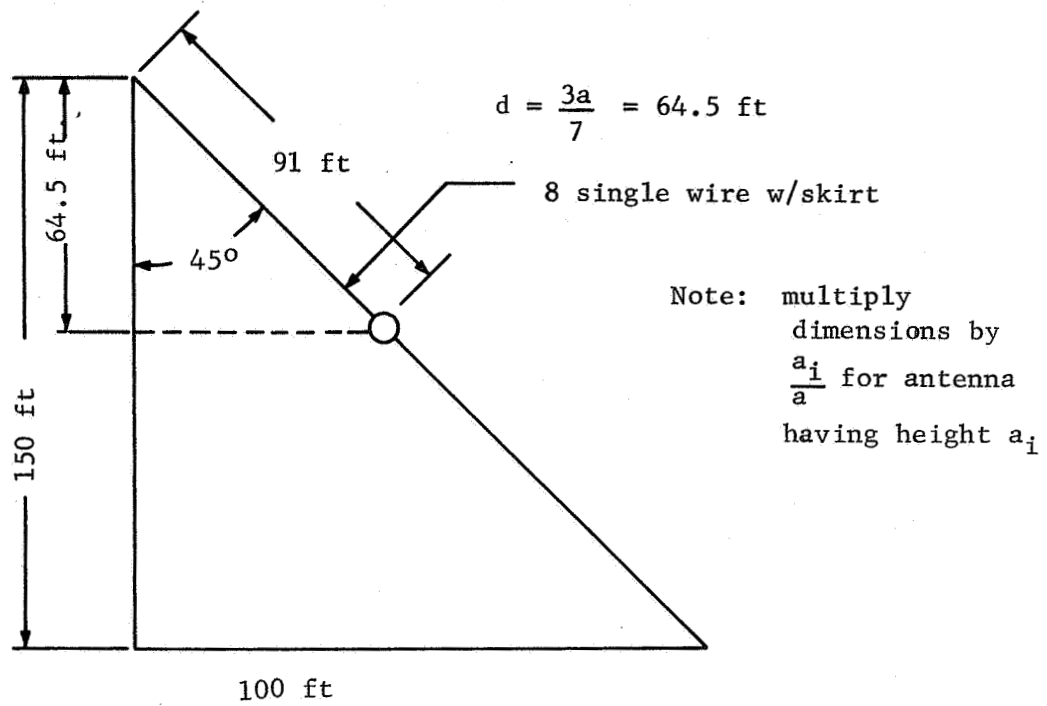
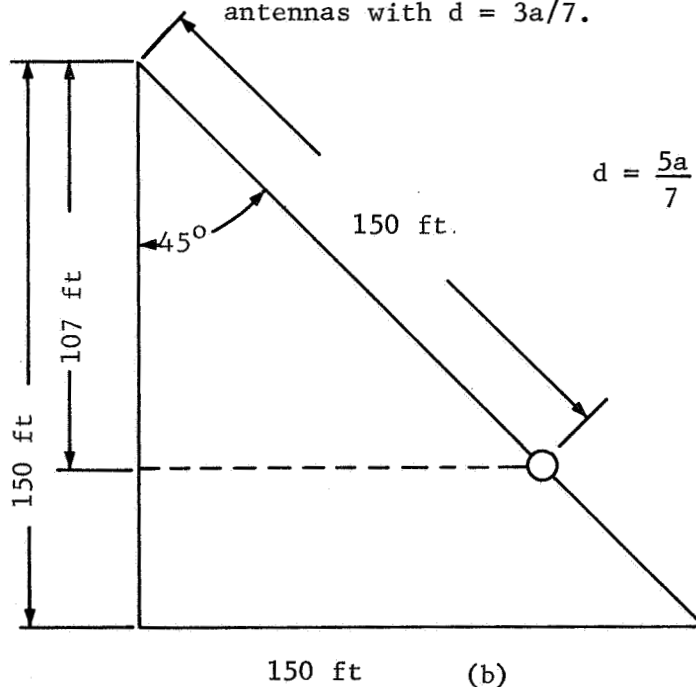


Fig. 16.--Rib construction for 100 ft VLF umbrella antenna.



(a)

Fig. 17a--Rib construction for 150 and 200 ft VLF umbrella antennas with $d = 3a/7$.

(b)

Fig. 17b--Rib construction for 150 and 200 ft VLF umbrella antennas with $d = 5a/7$.

TABLE 1

CAPACITANCE MEASUREMENTS OF SCALE MODEL
VERTICAL RADIATORS WITH VARIOUS TOP-LOADING CONFIGURATIONS*

No.	Height In Ft	Wire Size in Inches	Skirt	UMBRELLA				D	Capacitance	
				No. of Ribs	No. of Wires in Rib	d	0 ft	0 ft	Static	Operating
1	100	0.5	No	0	0	0 ft	0 ft	470 pf	420 pf	
2	100	0.5	No	8	1	43	267	1770	1720	
3	100	0.5	Yes	8	1	43	267	2480	2320	
4	100	0.5	Modified ²⁹	8	1	43	267	2440	2320	
5	100	0.5	No	8	4	43	267	2490	2320	62
6	100	0.5	Yes	8	4	43	267	2990	2820	
7	150	0.5	No	0	0	64.5	150	690	520	
8	150	0.5	Yes	4	1	64.5	150	1050	920	
9	150	0.5	No	8	1	64.5	150	1400	1320	
10	150	0.5	Yes	8	1	64.5	150	1580	1570	
11	150	0.5	Modified ²⁹	8	1	64.5	150	1580	1570	

*Vertical radiator scaled for a triangular shape 3 feet on each side.

TABLE 1 (Continued)

No.	Height in Ft	UMBRELLA				Capacitance		
		Wire Size in Inches	Skirt	No. of Ribs	No. of Wires in Rib	d	D	Static Operating
12	150	1.0	No	8	1	107 ft	150 ft	2100 pf
13	150	1.0	Yes	8	1	107	150	2880
14	150	1.0	No	12	1	64.5	150	1620
15	150	1.0	Yes	12	1	64.5	150	1820
16	150	1.0	No	12	1	107	150	2520
17	150	1.0	Yes	12	1	107	150	3120
18	300	0.5	No	12	1	211	300	4800
19	300	9.0	No	12	1	211	300	5740

*Vertical radiator scaled for a triangular shape 3 feet on each side.

$$D = a,$$

$$\text{and } N = 12$$

is determined to be

$$C_A \approx 4140 \text{ pf}, \quad (43)$$

for the nomograms given in the referenced report. The value is within fifteen percent of the measured scale mode capacitance (Table 1, No. 18 which has a slightly larger rib radius) of

$$C_A \approx 4800 \text{ pf} \quad (44)$$

for such a structure. The calculated value obtained from the nomograms are only valid for a ratio of rib radius to height (r_2/a) of 10^{-3} and a ratio of two radii to height (r_1/a) of 5×10^{-5} . Gangi, et al.,³¹ state that an order of magnitude change (larger or smaller) in r_2/a affects the parameters by less than ± 20 percent. A comparison of the data from Table I indicates that the static capacitance for these structures, which can be predicted from both scale model and nomograms, can be determined to a satisfactory degree for design purposes. The data also indicated that a considerable increase in capacitance can be obtained from increased rib diameters.

The umbrella antenna exhibits, in most cases, a significant improvement in antenna performance over the simple vertical radiator. However, the umbrella has the distinct disadvantage of increasing the

mechanical load on the supporting tower. Taller vertical radiators, such as the 150 and 200 foot antennas, are more difficult to load capacitively, with minimum shielding of the radiator, unless additional tall, rib-supporting structures are utilized. However, a strong 100 foot tower can be heavily top loaded, through the use of shorter inexpensive supporting structures, without shielding the vertical radiator. In any case, the maximum capacitive loading is required at these frequencies in order to reduce the base voltage and the tuning inductance required for reasonable transmitter output voltages.

Summary of Antenna Design

Unless electrically large structures are employed, the design of the transmitting antenna to be utilized in this system is electrically very small because of the long wavelengths involved. The design of electrically small structures presents a class of unique problems. The large antenna capacitive reactance, for antennas of less than two degrees of electrical length, is by far the most important consideration in the design of electrically small antennas. In order to obtain even small radiated powers, the antenna base voltages reach enormous proportions, and large tuning inductances are required in order to reduce the driving voltage of the untuned antenna. Since the loss resistance increases as the inductance increases, it is mandatory that the required tuning inductance be reduced if reasonable antenna efficiencies are to be obtained.

It has been shown that the radiation characteristics, for a specified radiated power, are independent of antenna height. Employing this philosophy, several antenna configurations were constructed, and

the reactance characteristics measured. Two basic designs were used. In the first case, d (the length of the ribs) and in the other case, D (determining factor of the angle from the vertical for a fixed rib length) were each varied in order to obtain the antenna reactance characteristics. A 100-foot umbrella antenna, using multiple wire ribs with $D > a$, has a larger capacitance (2900 pf) than any of the 150 ft antenna structures investigated. This large static capacitance can be obtained by means of the proposed utilization of inexpensive supporting structures (creosote poles) for the rib support, and D would thereby be made as large as structurally possible. At larger heights, a structure using physical supports for the umbrella ribs would be even more expensive than a simple top hat supported by four large towers. By extending the tower heights to 200 or 300 feet, and by using the maximum length for 12 ribs without skirts ($d = 5a/7$), capacitances of 3390 and 5740 pf, respectively, can be obtained, (See Table 1, and use a linear scale change). The 200-foot antenna, loaded in the specified manner, yields only slightly more capacitance than the heavily loaded 100-foot structure. The 300 foot antenna with large diameter ribs produces an almost 2:1 increase in capacitance over the 100 foot antenna, which results in a large improvement in over-all efficiency because the loss resistance decreases with required tuning inductance (in the order of 12 mh), and because the radiation resistance increases with the increase in height.

After considering the cost-performance characteristics of several different antenna configurations, the 300 ft umbrella antenna design which had the largest ribs diameter(9 in) was selected as a transmitting

antenna. The cost was, of course, somewhat higher than the other structures, but it was felt that the taller antenna would have much better coupling efficiency and a more reliable and predictable radiation pattern.

The antenna final design consists of a 300-foot tower (3 ft triangular cross-section) top-loaded as shown in Fig. 18. Each rib is constructed of a multiple-wire configuration, which in turn consists of six wires equally spaced on nine (9) inch plastic spacers, as shown in Fig. 19. This particular configuration is employed to increase the effective rib diameter so that a larger over-all antenna area and a greater capacitance can be obtained. Parasitic inductance is increased somewhat by this configuration; however, it should be negligible in this case since the total length of each rib is only a fraction of a wavelength.

Receiving Antenna

The receiving antenna requirements are less severe than those of the transmitting antenna at VLF frequencies. Since the ambient atmospheric noise is much greater than the inherent noise introduced by the receiver, the SNR is established on the basis of the atmospheric noise, independent of the receiver characteristics. The efficiency of the receiving antenna is thus of minor importance, since both the noise and the signals are reduced in the same proportion for any given efficiency for non-directional antenna systems. The only requirement of the antenna is that the effective height, or aperture, be large enough to ensure that the received signal is above the receiver sensi-

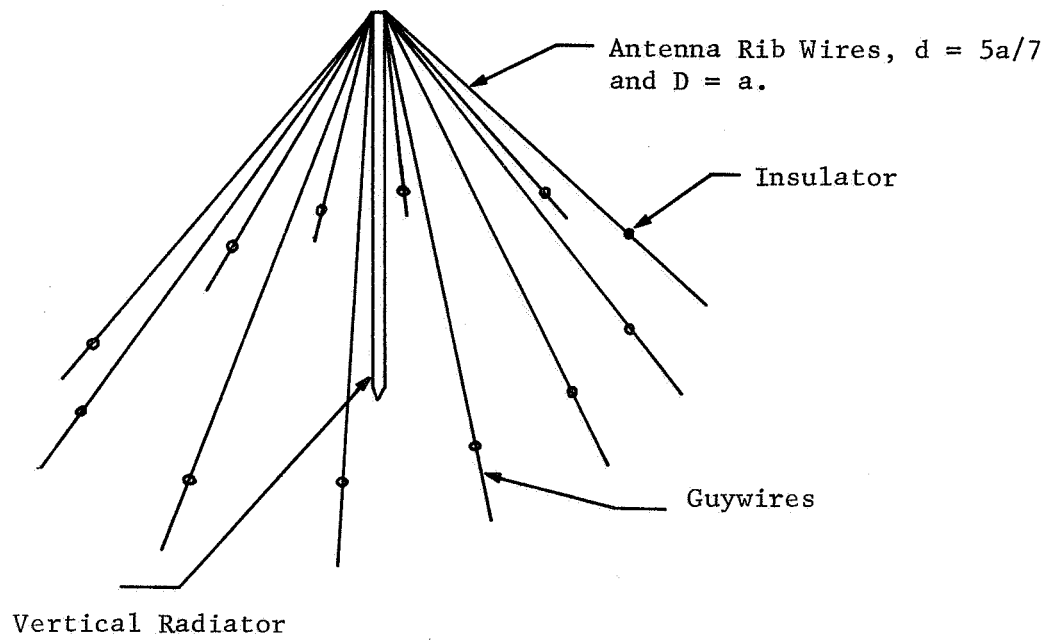


Fig. 18--An umbrella antenna design (2).

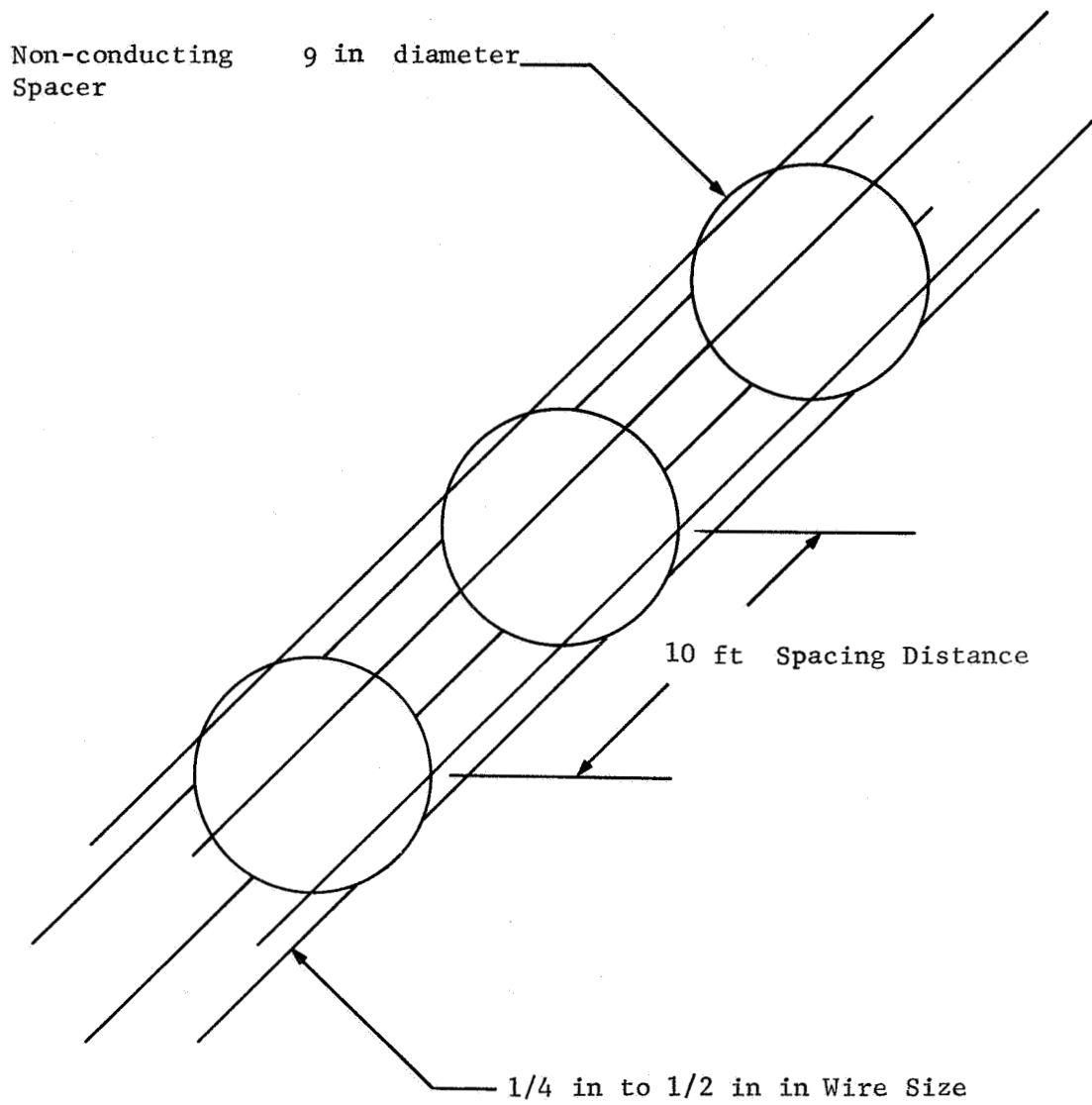


Fig. 19--Multiple-wire rib configuration.

tivity for a sufficient SNR.

The receiving antenna usually employed in such investigations is a standard whip antenna of about 3 meters physical height and 0.3 cm to 100 cm of effective height. If both the field strength and the receiver sensitivity are known, a compromise can be made to obtain an antenna structure which will satisfy all requirements.

Since the SNR is set independent of the receiving system, directive arrays are of considerable importance, because the total noise received is reduced, thereby yielding higher SNR's. Loop and wave antennas have been utilized in certain applications to some advantage; however, neither the small effective height of the loop antenna, nor the large physical dimensions of the wave antenna are desirable for the present system requirements. For future requirements the loop antenna might possibly have some applications, even though the effective height is very small.

Effect of Finite Ground Conductivity on Antenna Radiation Characteristics

In the foregoing discussion of the radiation characteristics of a short dipole, the earth was considered a flat perfect conductor. While this assumption may be satisfactory in some cases, the effect of a finite conducting earth upon the radiation characteristics of a short dipole in the VLF frequency range merits further consideration. The major effect of the finite conductivity of the earth upon the radiation pattern of the space wave is that it reduces the magnitude of the field, at low angles, from its value over a perfectly conducting earth,¹² as shown in Figure 20. The functional parameter n is

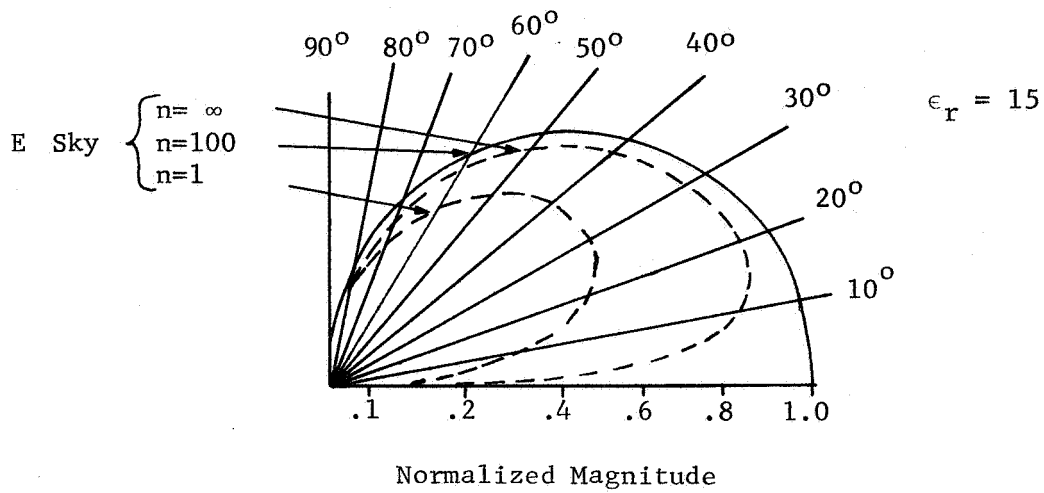


Fig. 20a--Vertical radiation pattern for the sky wave of a short dipole located on the surface of a flat earth.¹²

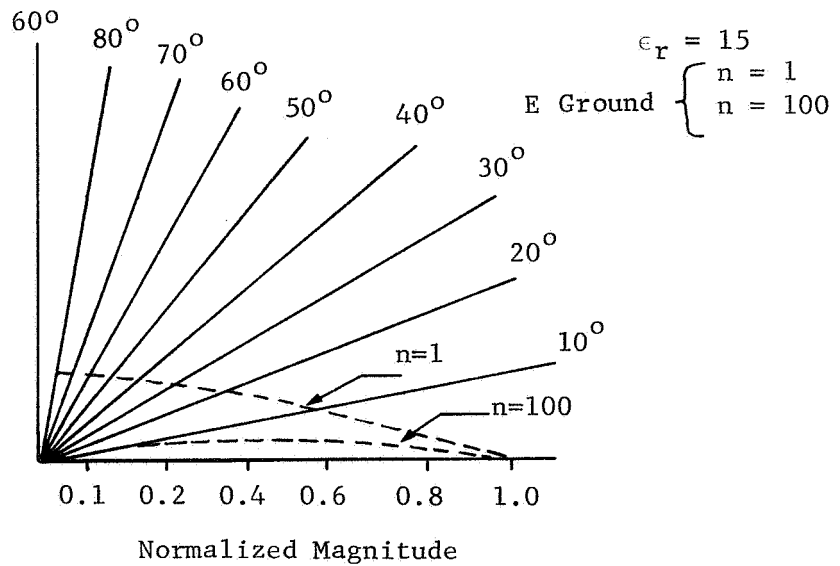


Fig. 20b--Vertical radiation pattern for the ground wave of a short dipole located on the surface of a flat earth.¹²

$$n = \frac{18 \times 10^5 \sigma}{f_{\text{MHz}} \epsilon_r} \quad (45)$$

where

ϵ_r is the relative dielectric constant,
 f_{MHz} is frequency in megacycles, and
 σ is the earth conductivity in mhos per cm.

The reduction in field magnitude is caused by the rapid changes of the ground reflection coefficient for angles near the pseudo-Brewster angle, which is a function of earth conductivity. At angles of incidence below the pseudo-Brewster angle, the phase of the reflection coefficients is approximately zero, and at angles above it is 180 degrees. Thus, the reflected wave tends to cancel the propagated wave below the pseudo-Brewster angle, and tends to reinforce the propagated wave above the angle. If an average value is assumed for ϵ_r , and if a frequency of 20 kHz is considered, with conductivities ranging from 1×10^{-6} mho/cm (poor) to 2×10^{-5} mho/cm (average), then

$$6 \leq n \leq 120, \quad (46)$$

where $\epsilon_r = 15$. The dielectric constant is reasonably stable for different conductivities, and these values of n will not vary appreciably as a function of the dielectric constant. It is apparent that the effect of the finite conductivity is to reduce the signal

strength at low angles for these values of n , as indicated in Figure 20. The reduction of field strength at low angles indicates that the selection of the transmitter location is extremely important for long range space wave communications, which require radiation at low elevation angles. Whenever possible, a site having high conductivity in the first few wavelengths from the antenna should be selected in order to minimize this effect.

In this particular system, the communications path is approximately 320 km, which is relatively short. The angle of incidence measured from the horizontal is of the order of 25 degrees, if a mean height of 75 km is assumed for the ionosphere. Since the lowest conductivity for any portion of the proposed propagation path is 3×10^{-5} mhos/cm, ($n = 180$).^{*} the angle of elevation of the vertical radiation space wave pattern will be less than 25 degrees. This fact indicates that the finite conductivity of the earth will alter the radiated reflected sky wave magnitude only slightly over the proposed propagation path.

The magnitude of the ground wave radiated from the vertical radiator is also dependent on the finite conductivity of the earth. For large values of n (low frequencies and good conductivity), the unattenuated radiated ground wave is very small, except near grazing angles near the earth's surface. For smaller values of n , the unattenuated ground wave has an appreciable value at higher angles, as shown in Figure 19. The attenuation of the ground wave received at a remote point on a flat earth is, thus, a function of the earth conductivity. This effect

^{*}FCC Map of Ground Conductivity in the United States.

of the earth's conductivity on ground wave signal strength is, however, accounted for in the calculation of the attenuation factor.

Wait and Conda³³ have treated the problem of the effect of the earth conductivity on the antenna radiation pattern of a vertical radiator over a curved lossy surface. This investigation indicates that the over-all effect of the curved lossy surface can be included in the calculation of the field strength as a multiplicative correction factor. The modification of the radiated antenna pattern can be described in terms of a "cutback-factor," C_f . This factor can be described as

$$C_f = 1 + R_{g\parallel} \quad (47)$$

for $i_g > 5^\circ$ which is of interest to the study. $R_{g\parallel}$ is the complex plane wave reflection for vertical polarization at the ground which has been studied by many workers.^{2,12} The launching loss is also defined in terms of the terrian "cutback factor" as

$$L_t = -20 \log_{10} C_f. \quad (48)$$

A typical curve of launch loss as a function of launching angle is presented in Fig. 21 for a frequency of 20 kHz.

It is interesting to note that this effect is a direct result of the curvature and conductivity of the earth. Hence, the sky wave field intensity is reduced under some conditions by being propagated over a lossy curved surface, and Equation (4) can now be

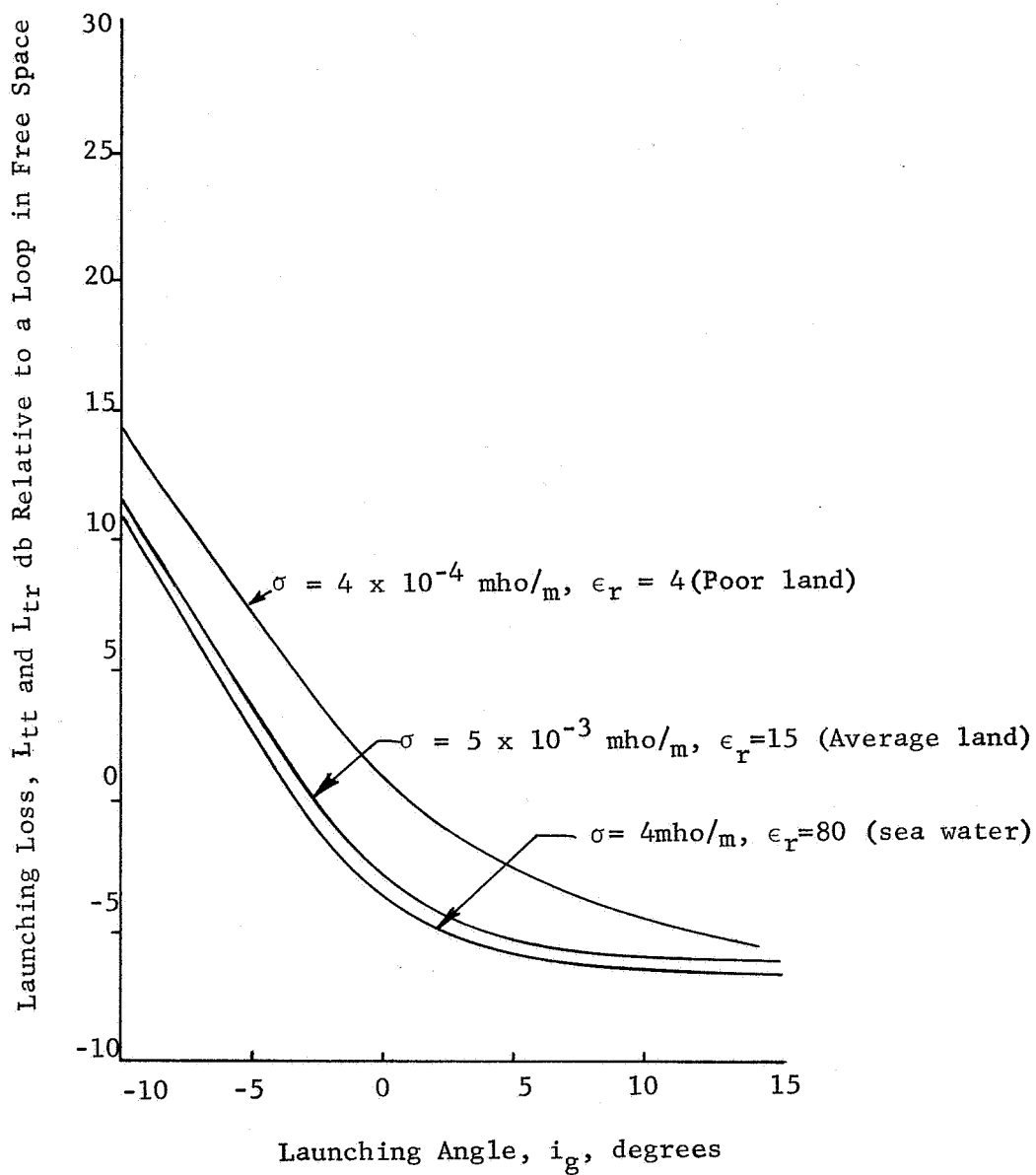


Fig. 21.--Magnitude of launching loss for $f = 20 \text{ kHz}$ as a function of launching angle.

modified as

$$|\bar{E}_{s,m}| = \frac{|\bar{F}_s|}{L_s} G_t(i_g) R_m D_m \cos(i_g) C_{ft} C_{fr} \quad (49)$$

where C_{ft} = cutback factor at the transmitting location
and C_{fr} = cutback factor at the receiving location, and the phase of each cutback factor must be included in the equation for total phase shift. Equation (49) describes the vertical electric field strength of the m^{th} reflected wave as would be received by an antenna located on the earth's surface.

Ionospheric Convergence Factor

Another geometrical phenomenon that tends to reduce the effective sky wave field strength is related to the fundamental spreading property or inverse square law of propagated waves. As an electromagnetic field propagates from the transmitting antenna, the wave front is spherical in nature with a radius of curvature equal to the distance traveled, and the intensity of the wave decreases with increasing distance because the power per unit solid angle is spread over a correspondingly larger surface area. If the wave is reflected from a flat mirror-like surface, the wave front continues to diverge; however, in the case of the curved ionosphere, it may continue to diverge or it may even converge at larger distances. This effect can be corrected in a manner similar to the "cutback factor" where the field strength magnitude is altered to account for the effect. Norton³⁴ has treated this problem extensively and an example of this work for a one skip or hop reflection is presented in Fig. 22 for $f = 30\text{kHz}$. It is evident from this curve

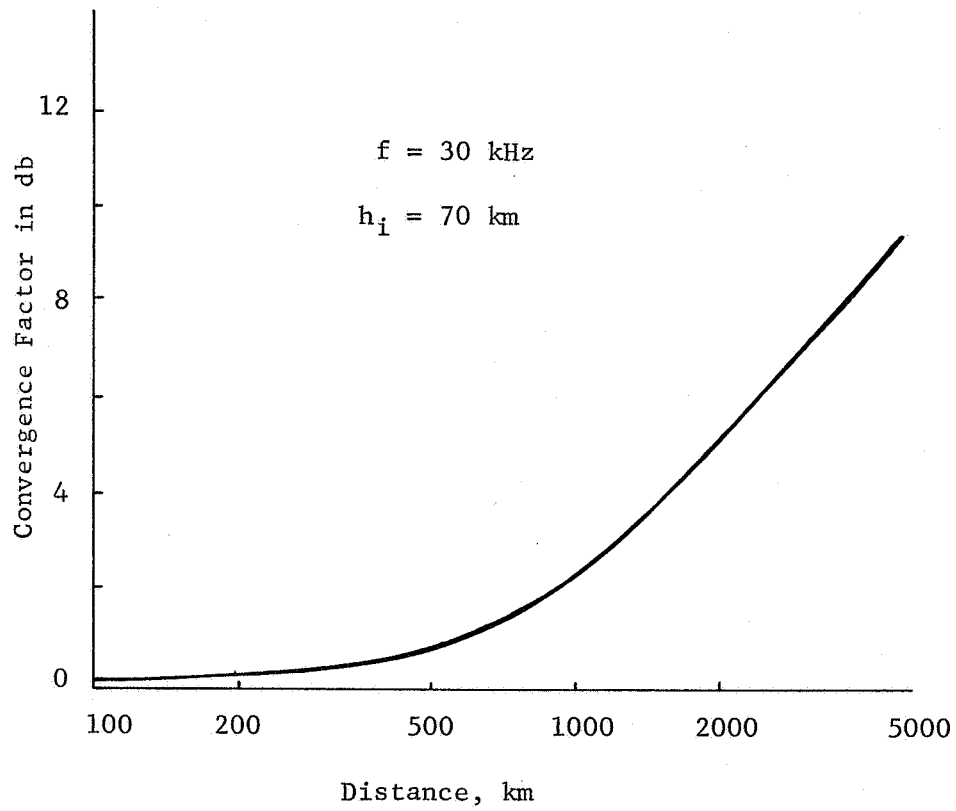


Fig. 22.--Convergence factor versus distance.³⁴

that at the distances involved here (200 miles or 320 km), the effect of the convergence factor is almost negligible.

Calculation of Total Field Employing both Ground and Skywaves

The total vertical electric field propagated over the 200 mi (320 km) path can be calculated from (1) if the various amplitude and phase modification terms are included when appropriate to the specified condition. This can best be accomplished by first calculating the ground and sky wave components separately before a composite solution is attempted.

Using this approach, the magnitude of the ground wave field contribution can be expressed in terms of radiated power from (2) and (20) as

$$|\bar{E}_g| = 5.9A (P_r)^{\frac{1}{2}} (L_g)^{-1} 10^{-3} \mu\text{V/m} . \quad (50)$$

Equation (50) can be expressed in decibel form which will simplify the calculation of $|\bar{E}_g|$; hence,

$$|\bar{E}_g| (\text{db}, 1\mu\text{V/m}) = 75.4 + 20 \text{ Log } A + 10 \text{ Log } P_r - 20 \text{ Log } L_g \quad (51)$$

where the field strength in db is referenced to 1 $\mu\text{V/m}$. If a propagation distance of 200 mi is assumed for a radiated power of 1 watt, then (51) becomes

$$|\bar{E}_g| (\text{db}, 1 \mu\text{V/m}) = 29.4 + 20 \log A. \quad (52)$$

The value of A, the ground attenuation factor, can be obtained from (3) or from available curves in Jordon,¹² Watt,¹⁸ or Norton.²¹ This factor may also be obtained from Wait's surface impedance concept.³⁵ Since the conductivity varies by a factor of about $2(6 \text{ to } 3 \times 10^{-3} \text{ mho/m})$ over the propagation path, a median value of $4 \times 10^{-3} \text{ mho/m}$ is used in the calculation of ground wave field intensity. Additional calculations of field intensity over the 200 mi path are presented so that the effect of reduced conductivity can be obtained. The Gold Hill Station is located on a geological boundry between a plain and mountainous region (the Piedmonts), and as a consequence, the geology varies greatly in this region. This particular site appears to have a fairly high content of mica in the clay soil, and the actual conductivity at the transmitter is, in all likelihood, lower than that anticipated. The probable conductivity is somewhat between that of rocks (10^{-8} mho/m) and dry ground ($1 \times 10^{-3} \text{ mho/m}$). This will certainly influence the over-all propagation on the "down-path," (Gold Hill to Fairhope) because the conductivity in the immediate vicinity of the transmitting antenna has a major influence in the radiated power. Thus, from Table 2, the magnitude of the ground wave field intensity for the "down-path" is

$$15.4 \text{ (db, } 1\mu\text{V/m)} < |\bar{E}_g| < 28.4 \text{ (db, } 1\mu\text{V/m)} \quad (53)$$

*FCC Map for Ground Conductivity in the United States.

TABLE 2

MAGNITUDES OF PROPAGATED GROUND WAVE FIELDS OVER
THE 200 MI PATH FOR DIFFERENT CONDUCTIVITIES.*

Quantity	Frequency and Conductivity		
	20kHz 4×10^{-3} mho/m	20kHz 10^{-4} mho/m	20kHz 10^{-5} mho/m
A	0.99	0.71	0.1
ϕ_A	-50°	-85°	-90°
n	220	5	0.6
Constant(52)	29.4db	29.4db	29.4db
20 Log A	-1.0db	-3.0db	-20.0db
$ \bar{E}_g $ (db, $1\mu V/m$)	28.4db	26.4db	9.4db
$ \bar{E}_g $ $\mu V/m$	26.3 μV	21.0 μV	2.95 μV

* $\epsilon_r \approx 15$ and $P_r = 1$ watt.

or

$$5.9 \mu\text{V/m} < |\bar{E}_g| < 27 \mu\text{V/m}$$

and that of the "up-path" is

$$|\bar{E}_g| \approx 28(\text{db}, 1\mu\text{V/m}) \quad (53)$$

or

$$|\bar{E}_g| \approx 27 \mu\text{V/m}$$

for 1 watt radiated power as calculated for $f = 20$ kHz. This frequency is used because almost all the available data is measured or calculated in this region. The effect of the poor conductivity upon the radiation characteristics of a vertical monopole is quite evident from Fig. 20 for the calculated values of n also given in Table 2.

The magnitude of the sky-wave field contribution can be obtained from the summation of the singly-reflected wave and all possible multiple-hop or multiple-reflection waves which have significant magnitudes. Hence, the m^{th} -hop sky wave intensity from (49) is

$$|E_{s,m}| = 5.9 \times 10^{-3} (P_r)^{\frac{1}{2}} (L_{s,m})^{-1} G_t(i_g) R_m D_m \cos(i_g) C_{ft} C_{fr} \mu\text{V/m} \quad (54)$$

or

or

$$\begin{aligned}
|\bar{E}_{s,m}| \text{ (db, } 1\mu\text{V/m)} &= 75.4 + 10 \text{ Log } P_r - 20 \text{ Log } L_{s,m} + 20 \text{ Log } G_t(i_g) \\
&+ 20 \text{ Log } R_m + 20 \text{ Log } D_m + 20 \text{ Log } \cos(i_g) \\
&+ 20 \text{ Log } C_{ft} + 20 \text{ Log } C_{fr}.
\end{aligned} \tag{55}$$

An example of the calculation of the sky wave field contribution for a 200 mile path with a radiated power of 1 watt is given as follows. (The single-hop field contribution ($m = 1$) is determined). For this calculation, the first parameters to be determined are i_g , the angle of incidence at the earth, and ϕ , the angle of incidence at the ionosphere, as defined in Fig. 4. From Fig. 23, $\cos\phi$ is 0.435 at the approximate height of 75 km, which is the average height of the apparent reflection surface of the ionosphere at VLF frequencies. Then, $\phi \approx 64^\circ$. From Fig. 24 $i_g \approx 22^\circ$, the time delay, which can be obtained from Fig. 25 is approximately 175 μsec . Now, since velocity of propagation is $v_o = \text{distance}/\text{time}$, then the sky wave path is longer than the ground path by

$$\Delta L_g \approx \Delta T v_o = 175 \times 10^{-6} \times 186 \times 10^3 \approx 33 \text{ mi.} \tag{56}$$

Then

$$L_{s,1} \approx L_g + \Delta L_g \approx 233 \text{ mi.} \tag{57}$$

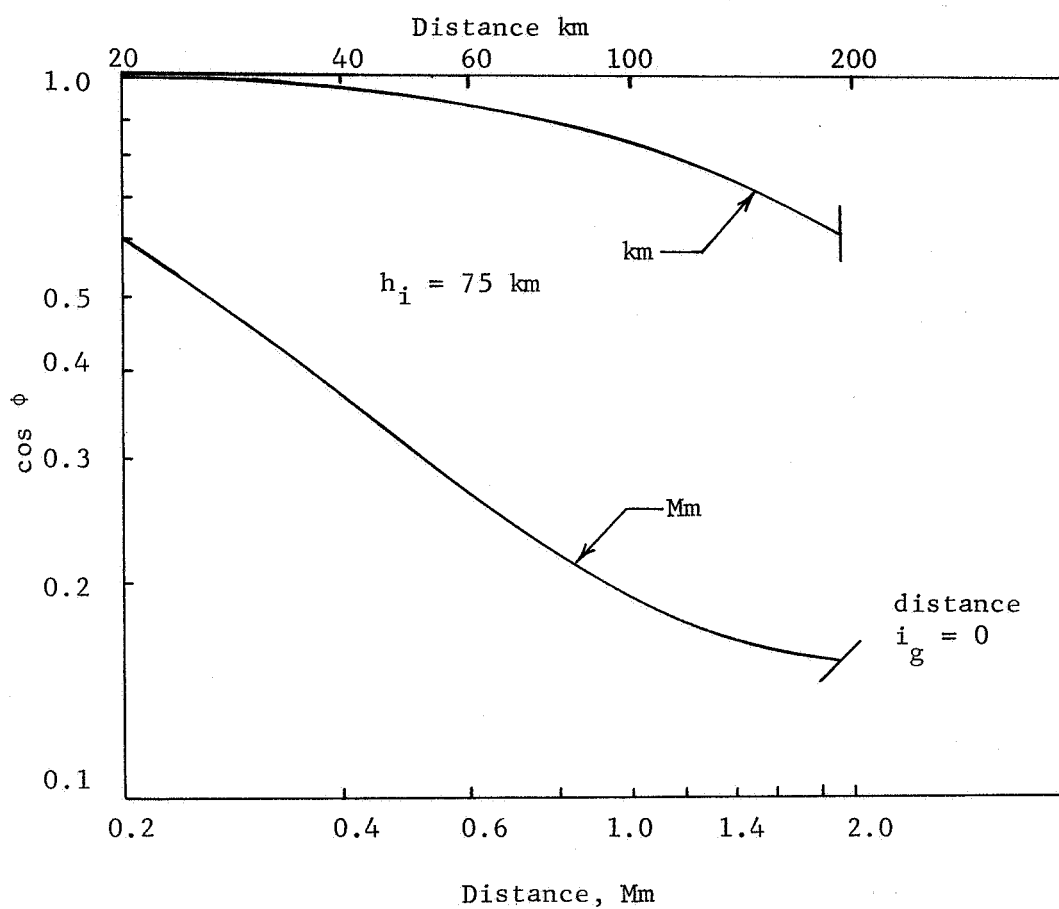


Fig. 23 --Cosine of the angle of incidence of the wave at the ionosphere vs distance between transmitter and receiver.¹⁸

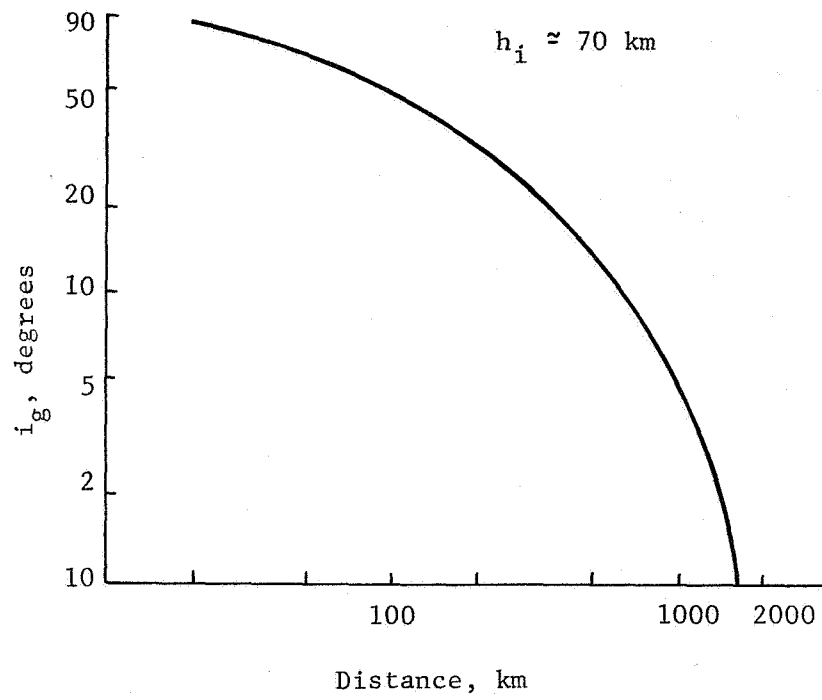


Fig. 24.--The angle of arrival of the wave above the surface of the earth versus distance, L_g , between transmitter and receiver.¹⁸

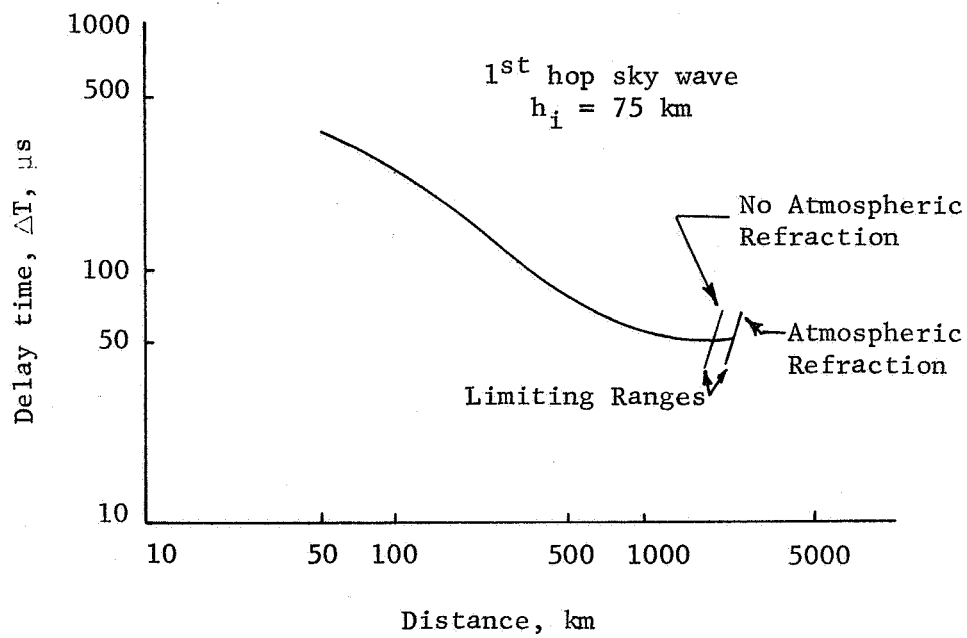


Fig. 25.--Transmission delay time between sky wave and ground wave based on ray length.¹⁸

The vertical antenna pattern factor for a short vertical dipole (which is assumed symmetrical in azimuth) is

$$G_t(i_g) \approx \cos(i_g) \quad (58)$$

from (21) where i_g is measured from the horizontal. The magnitude of this factor is

$$G_t(i_g) \approx \cos 22^\circ = 0.926 \quad (59)$$

and the magnitude of the loss factor due to the electric field not being vertical is also

$$\cos(i_g) \approx \cos 22^\circ = 0.926 \quad (60)$$

The convergence factor D_1 can be determined from Fig. 22 and it is almost negligible as would be expected over this short distance ($20 \log D_1 \approx 0.3$ db). The launching factor, which becomes quite important even at short distances if the conductivity is low, cannot be determined from Fig. 21 because $i_g > 15^\circ$. However, (48) can be used to calculate the launching factor directly using the magnitude and phase of the flat-earth reflection coefficient from Terman's Radio Engineering Handbook or from Watt.¹⁸ These factors are

$$\begin{aligned} C_f, \text{ Fairhope} &\approx -0.3 (F = 1.94) \text{ and} \\ C_f, \text{ Gold Hill} &\approx -0.4 (F = 1.91) \end{aligned} \quad (61)$$

where $R_{g\parallel} \approx 0.94/\underline{0}^\circ$ for 6×10^{-3} mho/m and $R_{g\parallel} \approx 0.91/\underline{0}$ for 3×10^{-3} mho/m. The calculated launching loss for a conductivity of 10^{-5} mho/m decreases to approximately -3.0db ($R_{g\parallel} \approx 0.3/\underline{75}^\circ$). The decrease means that the power output of a transmitter at this location, for example, is reduced by a factor of one-half, which is a drastic reduction of over-all efficiency.

The evaluation of the ionospheric coefficient of reflection is not so straight-forward. One approach is to employ a theoretically-determined value of reflection coefficient and phase angle for a given frequency and time being studied, which can be correlated to the existing experimental data. This approach can be rather complex if all components (actual and connected) of the multiple-hop wave are included. A simple solution can be obtained which does not include the conversion effects of the incident wave upon reflection as indicated earlier in (4). For the 200 mi path with f assumed at 20 kHz and an average ionospheric height of 75 km, the magnitude of the sky wave field components can be evaluated for $m = 1$ from the reflection coefficient $||R_{||}$ and phase ϕ_R from Fig. 5. The magnitude and phase of the single-hop sky wave field intensities as well as the multiple-hop cases of $m = 2$ and 3 are presented in Table 3. The parameters used for the determination of the sky wave components are indicated for clarity in Table 4. It is evident from the values of the individual sky wave field contributions ($m = 1, 2, \text{ and } 3$), that the single-hop field strength predominates. Therefore, in the subsequent calculation only the single-hop field will be used.

TABLE 3
MAGNITUDE OF INDIVIDUAL SKY WAVE FIELD
COMPONENTS ($P_r = 1$ watt, $\epsilon_r \approx 15$)*

Quantity	m = 1	2	3
Constant (53)	75.4 db	75.4 db	75.4 db
$10 \log P_r$	0.0	0.0	0.0
$20 \log L_{s,m}$	-47.4	-48.2	-52.0
$20 \log G_t(i_g)$	-0.6	-3.0	-8.1
$20m \log R $	-17.7	-61.0	-113.0
$20(m-1) \log R_{g }$	0.0	0.0	0.0
$20 \log D_m$	-0.3	0.0	0.0
$20 \log \cos(i_g)$	-0.6	-3.0	-8.1
$20 \log C_{ft}$	-0.3	-0.3	-0.3
$20 \log C_{fr}$	-0.4	-0.4	-0.4
$ E_{s,m} $ (db, $1\mu V/m$)	8.1	-50.5	-106.5
$\phi_m \approx m\phi_R + (m-1)\phi_g$	-30°	44°	-75°
$ E_{s,m} $ $\mu V/m$	$2.54\mu V$	$3.1nV$	20 pV

* $\sigma_{Fairhope} = 6 \times 10^{-3}$ mho/m and $\sigma_{Gold Hill} = 3 \times 10^{-3}$ mho/cm.

TABLE 4

PARAMETERS FOR CALCULATION OF SKY WAVE
COMPONENTS OF TABLE 3. ($f = 20$ kHz)

Quantity	m = 1	m = 2	m = 3
ϕ	64°	45°	22°
i_g	22°	45°	67°
ΔT	$175\mu s$	$200\mu s$	$350\mu s$
ΔL	33 mi	64mi	186 mi
$L_{s,m}$	233 mi	264mi	386 mi
$G_t(i_g)$	0.935	0.707	0.39
$\cos(i_g)$	0.935	0.707	0.39
$ R $	0.14	0.03	0.013
ϕ_R	-30°	22°	95°
$ R_g $ [See(61)]	1	1	1
ϕ_g	0°	0°	0°

The phase of both the ground wave and composite sky wave must be determined. Since the launching factor phase delay is approximately zero, then

$$\phi_g + \beta L_g - \pi/2 + \phi_A \quad (62)$$

$$\text{and } \phi_{s,1} + \beta L_g - \pi/2 - 2\pi\Delta T f + m\phi_R$$

The phase difference between the terms on the right of each equation is the relative phase between the ground and sky waves, which is referenced to the antenna current. Using these equations and the results of Tables 2, 3, and 4, the total vertical electric field at a terminal end of the propagation is

$$\begin{aligned} \bar{E}_t &= \bar{E}_g + \bar{E}_s \\ &= 26.3e^{j\omega t - \beta L_g + 40^\circ} + 2.54e^{j\omega t - \beta L_g - 120^\circ} \\ &= 24e^{j(\omega t - \beta L_g + 38^\circ)} \mu\text{V/m} \end{aligned} \quad (63)$$

where ω is the operating radian frequency ($2\pi 20\text{kHz}$) and βL_g is phase delay of the wave due to the propagation path.

This approximate calculation is based upon the basic reciprocal property of the two paths and the assumption that the parameters are not extremely sensitive to frequency, since 20 kHz was employed for the calculation. These assumptions are valid and (63) is a reasonably accurate measure of the expected field strength for a radiated power

of 1 watt. It is quite evident from (63) that the field intensity is predominately the ground wave at this short distance. Hence, even if the launching factor is influenced by a poor conductivity at the Gold Hill Station, the total field strength will not be affected by the sky wave field component to any major degree. However, the magnitude of the ground wave could be decreased severely if the conductivity of the Gold Hill Station affects the overall average path conductivity by an order of magnitude or more. The small magnitude variation which will be induced by the sky wave will vary by a large amount during the course of a year, as evident from the experimental data for the reflection coefficient in Fig. 5. The magnitude of the diurnal phase variation will be quite small if the results of (63) are reasonably valid.

$$\phi_d < \arctan \frac{2.54}{26.3} < 6^\circ \quad (64)$$

or less than 1 μ s in time at 20 kHz. It should be noted that if a study devoted exclusively to the space wave, reflected from the ionosphere, is performed at a later time, the required transmitted power will increase somewhat or overall efficiency must be improved.

The field strength calculated from (63) is shown on a plot of the field strength as a function of distance from Pierce's equation,¹⁶

$$|\bar{F}_s| = 210 (P_r / \sin \theta_1)^{\frac{1}{2}} 0.27 f^{3/4} \theta_1 \mu\text{V/m} \quad (65)$$

where

θ_1 is the angular distance in radians,

P_r is in kilowatts,

and

f is in kiloHertz in Fig. 26.

This equation was used in the section on signal-to-noise requirements to establish a basis for minimum communication conditions. The equation is a modified form of the "Austin-Cohen" formula, which was developed on a semi-empirical basis to fit experimental results for long propagation distances.³⁶

Tuning Inductance

The input impedance of an electrically short vertical antenna is almost entirely a capacitive reactance of large magnitude, as indicated previously (See Fig. 11). Thus, to establish any significant magnitude of current distribution on the antenna, large voltages are required, as indicated in Fig. 14. Top-loading of the antenna structure of course, minimizes this high voltage by decreasing the magnitude of the reactance. However, in almost every case, the capacitive antenna is tuned for resonance with an external inductance whereby the large voltages required for appreciable power outputs are generated by resonant current flow. In a series-tuned antenna circuit similar to that of Fig. 10, the high voltage requirement is eliminated; but, the current capacity of the driving source may be quite large because the input impedance is essentially that of the resistive losses (on the order of 3 to 5 ohms depending on the system). To circumvent any high source current

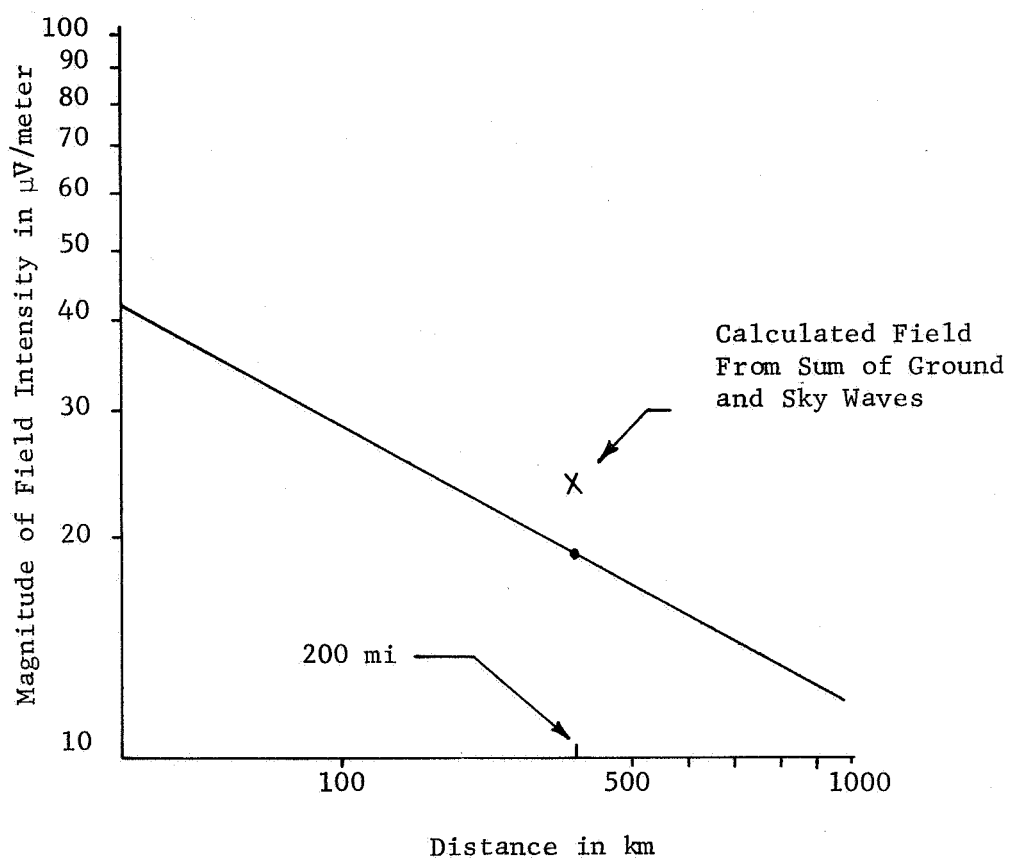
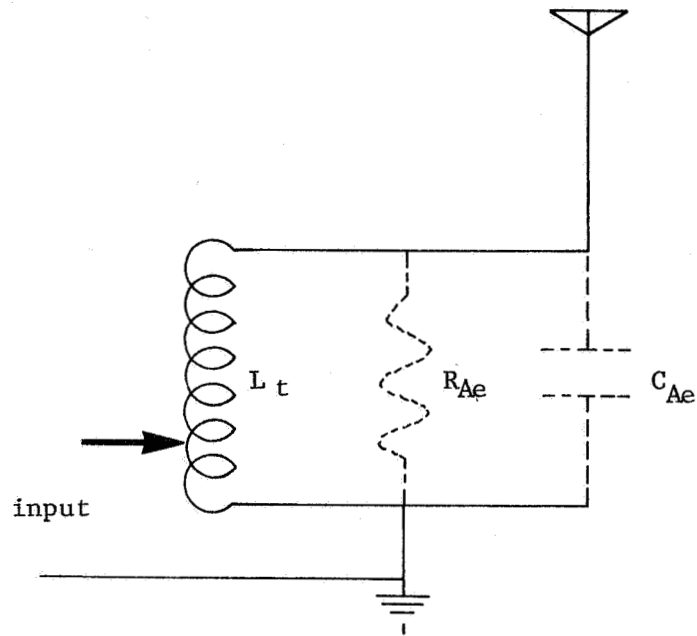


Fig. 26.--Field strength as a function of distance for a radiated power of 1 W at 20 kHz.¹⁶



L_t = Tuning Inductance,

C_{Ae} = Equivalent Antenna Capacitance, and

R_{Ae} = Equivalent Antenna Shunt Resistance (a function of R_r , R_A , R_I , and R_g).

Fig. 27.--Impedance matching using parallel-tuned circuit for a short vertical antenna.

requirement, a "tapped parallel-tuned" circuit configuration, Fig. 27, is employed for impedance-matching between source and antenna. The "tapped" inductance acts as an auto-transformer to transform the large effective resistance in shunt with the "tuned-tank" circuit. A 3000 ohm input impedance level was selected for design purposes using this technique. It is well to note, that this matching technique provides a ground return external to the source for lightning protection. In addition, it is well to remember that the voltage on the base of the antenna is still in the high kV range, and, hence, a corona problem can exist.

The actual tuning inductor can be designed in a number of ways using low-loss litz wire, ferrite cores, and special winding techniques. In this application, a simple single-layer solenoid is employed simply on the basis of construction simplicity and economic feasibility. An inductance of approximately 10 mH is required to resonant the effective capacitance of the 300 ft antenna with a 9 in rib diameter. Based upon this requirement, a slightly larger singly-layer inductor having a total inductance of 12 mH was designed and constructed.

The low-frequency inductance of a single-layer solenoid or helix³⁷ can be obtained from the well-known expression

$$L_t = F n_t^2 d_i \quad (66)$$

where L_t is tuning inductance, F is a magnitude factor which is determined by d_i/ℓ , n_t is the number of turns, d_i is coil diameter and ℓ is coil

length. Now if $d_i/\ell \approx 1$, and $d \approx 6$ ft for $L_t = 12\text{mH}$, then

$$n_t \approx 96 \text{ turns} . \quad (67)$$

If $n_t = 96$ is assumed, then the turns spacings in a 6 ft. length is

$$s = n_t/\ell \approx 0.75 \text{ in} . \quad (68)$$

The selection of the wire diameter for the spacing is determined by voltage gradient across the coil, resistance loss in the wire as a function of skin depth, and the effective increase of the resistance of each turn as a result of the adjacent turns. This proximity effect is caused by induced eddy currents in the adjacent wires, and it increases rapidly as spacing to wire diameter decreases. The actual resistance in a single-layer solenoid, which has been studied extensively by Butterworth,³⁸ can be calculated from

$$R_{ac} = R_{dc} (\alpha H + (\beta \mu_1 + \gamma \mu_2) G' \left(\frac{do}{c} \right)^2), \quad (69)$$

where α , β , γ , μ_1 , μ_2 , G' and do/c are numerical parameters determined by the geometry and conductivity of the coil. Tables of the values are given in Terman.³⁷ If a wire diameter of 0.5 in is assumed for a copper conductor, then

$$R_{ac} = 19.7 R_{dc} \quad (70)$$

where R_{dc} can be obtained from another well-known relation

$$R_{dc} = \frac{1}{\sigma} \left(\frac{\text{length}}{\text{area}} \right). \quad (71)$$

In this case for $\sigma_{\text{copper}} \approx 1.7 \times 10^{-8}$ ohm, then $R_{dc} \approx 73 \text{ m}\Omega$, and

$$R_{ac} \approx 1.4\Omega. \quad (72)$$

This value of loss resistance results in a Q of

$$Q = \omega L / R_{ac} \approx 1075 \text{ for } f = 20 \text{ kHz}. \quad (73)$$

A 6:1 scale model was constructed and tested to verify the basic design. Although specific information concerning the quality factor of the actual structure cannot be obtained from this study, the design equations predicted measured parameters to a high degree of accuracy. The winding capacitance was very low (approximately 4pf) which indicates a very high self resonance can be obtained in the actual coil. The measured voltage gradient was almost linear except near the ends of the 6:1 structure where flux leakage became evident. This means that the difference of potential between turns, V_t , should be low even at kilovolt potentials; i.e.,

$$V_t = \frac{V_{\text{base}}}{n_t} \quad (74)$$

or $V_t \approx 260 \text{ volts}$

for $V_{\text{base}} = 25 \text{ kV}$. These results of the scale model study were obtained in the presence of a shield or a model of the proposed helix house to simulate actual operating conditions.

A basic design for the tuning inductor based on this analysis is as follows:

Inductance	12 mH	
Turns	96	
Length	6 ft	
Diameter	6 ft	
Wire Diameter	0.5 in	(75)
Wire Spacing	0.75 in	
Material	copper	
Q	≈ 1000	
R_L	1.4Ω	

This basic design has been quite simple to construct and it is economically feasible in both construction time and financial investment.

Summary of Design

The major factors which influence the design of this phase stability study system have been discussed in the previous sections of this chapter. If the derived data are employed, a complete theoretical description can be made once the basic decisions are reached as to (1) transmitting antenna type, (2) the required radiated power or specific SNR requirement, and (3) the ground system size.

As previously discussed, the antenna design employed will be a 300 ft multiple-wire umbrella antenna which has $R_r \approx 0.16 \text{ m}\Omega$ ($h_e \approx 0.5a$) and $C_A \approx 5740 \text{ pf}$. This multiple-wire rib construction increases C_A

with only a negligible decrease in effective height for a fixed rib length.

The radiated power required for a 2.54° phase error (SNR = 24 db) is approximately 100 mW. as seen in Fig. 6. However, the received signal predicted from the summation of the theoretically-obtained ground and sky wave fields for this short propagation path is 2 db above that predicted from Pierce's field intensity equation.¹⁶ Thus, the actual theoretical SNR is 2db higher (26db) than anticipated. Even with this slight increase in SNR, the rms phase error for a sinusoid plus noise is still greater (about 2°) than the inherent mechanical error introduced by the finite resolution of the receiver. If the radiated power is increased by a factor of 10 to 1W effective radiated power, ERP, then the rms phase error is reduced by a factor of $10^{\frac{1}{2}}$ and

$$\delta\phi_p \approx 0.6^\circ. \quad (76)$$

This is less than the over-all equipment induced phase for a single receiver. A comparable rms phase error which is introduced by all the equipment can be based on the accuracy of $\pm 1\mu s$ for a single receiver. If $\delta\phi_m$ of a single receiver is assumed to be $1\mu s$, the total rms phase error introduced by the four receivers all of which process the phase information in the measurement system is

$$\delta\phi_{mt} = (\delta\phi_{m1}^2 + \delta\phi_{m2}^2 + \delta\phi_{m3}^2 + \delta\phi_{m4}^2)^{\frac{1}{2}} \quad (77)$$

where

$\delta\phi_{mt}$ = total equipment induced rms error, and

$\delta\phi_{mn}$ = equipment induced error of the n^{th} receiver.

Hence,

$$\delta\phi_{mt} = 1.42^\circ, \quad (78)$$

and the phase error existing due entirely to SNR is, in a similar manner,

$$\begin{aligned} \delta\phi_p &= 0.6(2)^{\frac{1}{2}} \\ &= 0.85^\circ. \end{aligned} \quad (79)$$

The calculation, (79), is essentially independent of the phase error introduced by the two reference receivers because the existing SNR is much greater than that of the other receivers. An estimate of total system phase error is

$$\delta\phi_t = (\delta\phi_p^2 + \delta\phi_{mt}^2)^{\frac{1}{2}} = 1.65^\circ. \quad (80)$$

This corresponds to a system measurement accuracy of 1 part in 220 at 20 kHz. On the basis of these calculations, a radiated power of 1 watt is specified for the basic system design.

From (40), it can be seen that the loss resistance of the ground system does influence the over-all system efficiency. In addition, the curves of Fig. 12 indicate that the ground resistance is inversely

related to the ground wire length or ground system diameter. On the other hand, the selection of a ground system is strictly based upon a compromise between economic feasibility and transmission efficiency. The over-all cost increases rapidly with increased system diameters for a low value of R_g , as a result of the increased required acreage and copper costs. It should be noted that for ground wire lengths longer than about 500 ft, the relative decrease in R_g becomes much smaller for a given increase in length. A 500 ft radial ground wire system of 120 wires, which requires on the order of 30 acres, was specified to reduce ground power losses to a minimum, based on over-all cost. Thus, from Fig. 12,

$$R_g \approx 0.35\Omega @ 500 \text{ ft. length} \quad (81)$$

for a 300 ft. antenna structure. From (40), the efficiency is

$$\eta = \frac{16m\Omega}{16m\Omega + 1.4 + 0.35} \times 100\% \quad (82)$$

$$\approx 0.9\%$$

where R_A , the antenna structural loss is assumed to be negligible.

From (81), the required power input P_i to the antenna system for 1W ERP is

$$P_i = 100P_r/\eta = 111\text{watts} \quad (83)$$

A transmitter output capability of 2kW was specified to meet the power input requirement calculated in (82) and to supply additional power input as might be required at some later time.

These design parameters for the basic propagation problem related to this phase stability measurement system are summarized in Table 5.

TABLE 5

DESIGN PARAMETERS FOR PHASE STABILITY STUDY SYSTEM

Electrical Characteristics	
Parameter	Value
Power Input	2kW
Power Radiated	1W
Radiation Resistance	16 m Ω
Antenna Efficiency	0.9%
Ground Resistance	0.35 Ω
Tuning Coil Resistance	1.4 Ω
Tuning Inductance	12mH
Received Field Intensity	24 μ V/m
SNR (Phase Loop)	36 db
Phase error (rms)	1.65 $^{\circ}$

IV. CONSTRUCTION AND EVALUATION OF THE PROPAGATION SYSTEM

The engineering design of this transponder propagation system did not require a tremendous financial outlay. However, a large monetary investment, a vast number of man hours, and many items of equipment, both of commercial and "in house" design, have been used or expended on the basis of this design in the fabrication of this complex propagation system. The design and construction has been spread over several years, principally because of the time required to purchase, fabricate, instrument, and test this expensive and physically large structure outside ideal laboratory conditions.

The over-all development of this system has involved many varied systems and sub-systems which were required for operational integrity. A simple "doubly-redundant" logic system together with its associated coders and decoders was constructed to remote-control the transmitter stations over commercial phone lines in conjunction with "data-phone" sets. Automatic coding devices for amplitude modulation of the station call signs on the transmitter outputs were constructed, and these units are used in conjunction with specially designed diode switches for modulation purposes. Various extremely narrow-band notch and band-pass filters have been developed for signal processing at both stations. All these, and many more sub-systems and related design techniques were required for an operational propagation system. However, these design problems are of a support nature only, and conse-

quently, they are not of any significant importance to this study.

The actual fabrication and erection of the two 300 ft, multiple-wire rib, umbrella antennas was completed under the direction of Andrews Tower, Inc., Fort Worth, Texas. The site construction was accomplished in two phases after the station land was cleared. First, the 500 ft, 120-wire (No. 10 copper), ground system and the tower supports (base and "dead-men") were installed. Then, the tower and rib sections were constructed and erected at the site. The Gold Hill transmitter station is shown in Fig. 28. This view is almost directly South, and the direction of propagation is, in this case, Southwest. The complete antenna structure was made according to the electrical design of Chapter III with the exception that all insulators were designed for 50 kV in anticipation of possible changes in power-output requirements. Figs. 29 and 30 indicate the construction techniques utilized in the fabrication of a multiple-wire rib. A vertical view of the antenna structure from the tower base which gives a better perspective of the umbrella-type construction is shown in Fig. 31. In addition, a view of the instrumentation trailer at the Gold Hill Station which houses the tuning coil, transmitter, and remote-control equipment is shown in Fig. 32.

The static capacitance of the two full-scale antennas was measured at 1 kHz with a capacitance bridge. These measured values are

$$C_{A, \text{Gold Hill}} \approx 5160 \text{ pf and}$$

$$C_{A, \text{Fairhope}} \approx 5200 \text{ pf.}$$

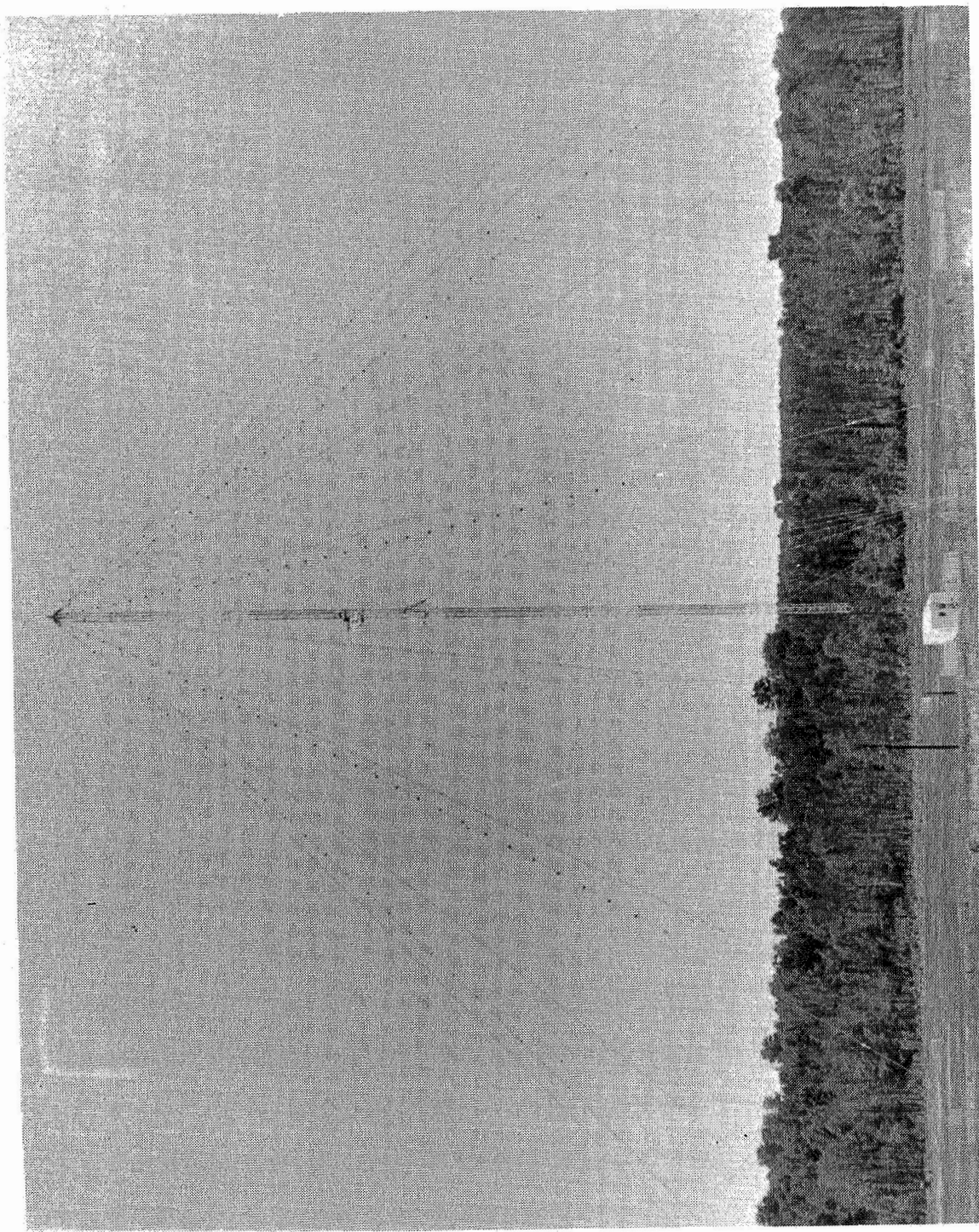


Figure 28.--Gold Hill VLF Transmitter Station

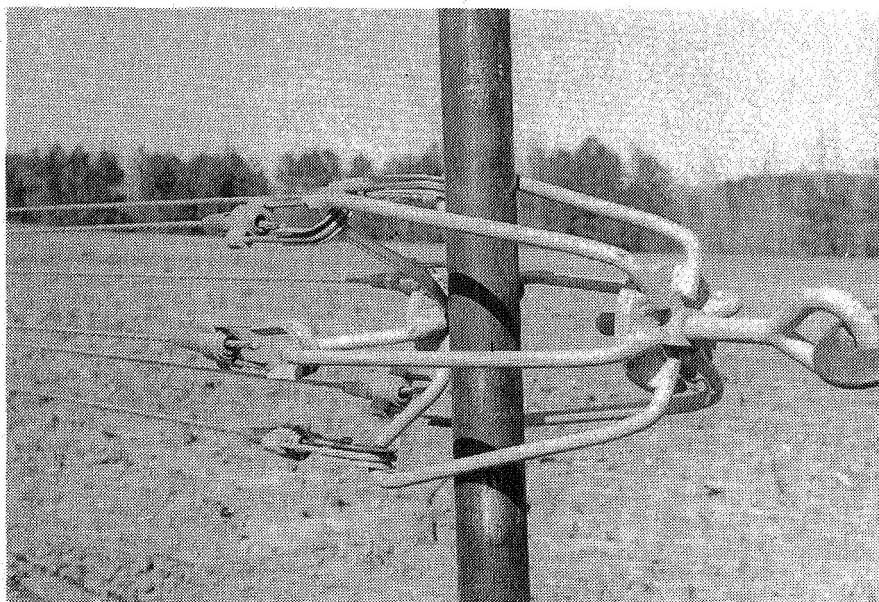


Fig. 29--Terminal construction for the multiple-wire ribs.

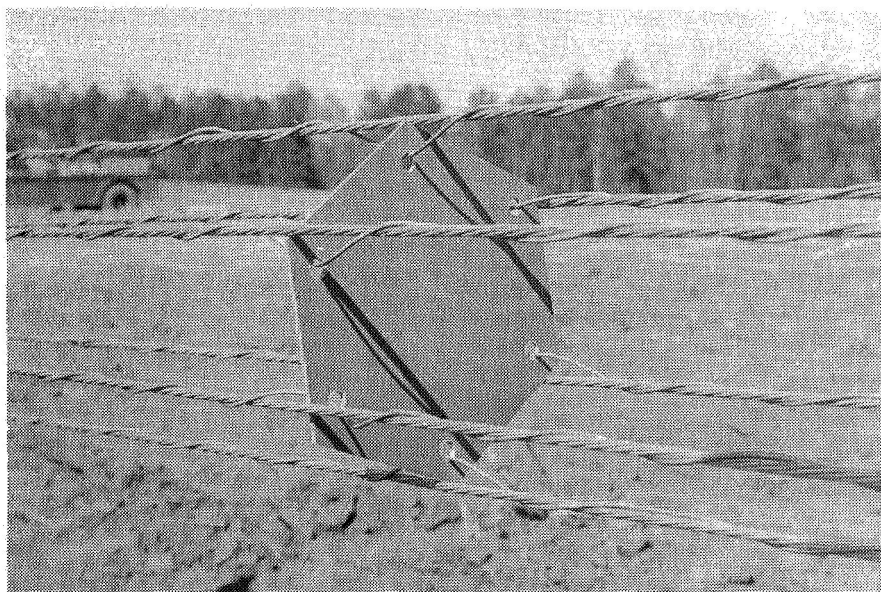


Fig. 30--Spacer construction for the multiple-wire ribs.



Fig. 31.--Vertical view at the antenna base showing umbrella construction.



Fig. 32.--Instrumentation trailer at Gold Hill station housing tuning coil, transmitter, and remote control equipment.

A comparison of the scale model and calculated data for an umbrella antenna with $\frac{1}{2}$ in rib diameters indicates about a 16 percent difference (see Table 1, nos. 18 and 19, and (43)). Gangi, et al.³¹ has shown that accuracies on the order of 10 percent between full-scale measurements and calculated values can be obtained from the nomograms. Thus, the results of this scale model study yield measured values that are higher than the expected measured capacitance for a full-scale structure. These higher measured values for the scale model study are a result of the inaccuracies of the non-ideal large-ratio scaling of the actual structure. The scale model study does, however, indicate an increase in capacitance of 20 percent if the rib diameter is increased to 9 in. These data more significantly show that a considerable increase in capacitance is also obtained with the increase in rib diameter as a result of the comparison between the actual measured data and calculated values. The capacitance is increased about 1000 pf above the calculated value, which is a 24 percent increase in total capacitance in this case. Thus, this multiple-wire construction can be used to considerable advantage to increase the effective height of such structures with shorter rib lengths and/or the total capacitance can be increased for a given antenna configuration. The effective capacitance for either antenna at the operating frequency is reduced about 4 percent as a result of the parasitic inductance. The total capacitance of the completed structure at the Gold Hill Station measures 5812 pf ($Q=525$) which includes the added stray capacitance of the base insulator and isolation transformer ($C_{AFairhope} = 5830 \text{ pf @ } 21.9 \text{ kHz, } Q = 545$).

No extensive antenna pattern measurement have been made for either of the antenna systems. Ground wire currents have been measured, however, and constant ground current contours for the Gold Hill Station are shown in Fig. 33. These contours are indicative of the electric field pattern of the antenna structures since these ground currents are related to the displacement currents of the fields and the magnetically-induced currents. The current distribution of a short vertical radiator over an ideal ground plane is symmetrical in the radial direction, and the current decreases rapidly as a function of distance from the base of the antenna.^{20,24} These current contours indicate that the distribution is not symmetrical and that the current contour magnitudes are small as well as distorted in a northeastern direction. This reduced current indicates that electrical conductivity in this direction is not homogenous around the base of the antenna (it could be larger or smaller since either changes the ratio $I_{\text{wire}}/I_{\text{ground}}$). In this case, these smaller values of current indicate that the displacement currents are small, and thereby the electric field is small, because a localized area of fairly high mica content lies in this particular direction from the antenna. This nonhomogeneity in conductivity affects the propagation characteristics of the antenna in the azimuthal direction by reducing the effective value of the unattenuated field field strength $|\bar{F}_s|$ more than the ground propagation constant A. However, in the direction of propagation, the currents are larger. The strongest radiated field intensity will probably be in a southernly direction, if this current-field correlation is employed.

The construction of the tuning coil consists of twelve grooved lami-

nated oak, 2 in x 4 in x 7.5 ft boards equally spaced around a circular form 6 ft in diameter. The grooved oak supports were saturated with paraffin at elevated temperatures to reduce the moisture content and to reduce and maintain the electrical conductivity for a more stable and a better Q. The coil winding is 0.5 in diameter copper tubing which was hand-wound on the forms at the 3/4 in turn spacing specified in the coil design of (75). The total inductance L_t of the coil is 13.2mH and $Q \approx 95$ at 20.9kHz. This indicates a total loss resistance of 18.5 ohms and a loss resistance R_I of 17 ohms for the portion of the coil required for actual tuning (10.82 mH at Gold Hill Station). The measured bandwidth B of the tuned antenna and transmitter system is approximately 543 Hz (Δf between 3 db points). Now, from a well known communications theory equation for a parallel-tuned L-C circuit,

$$Q_{Load} = \frac{f}{b} = 21.14 \text{ kHz}^* / 543\text{Hz} = 38.9 \quad (85)$$

where f is the frequency at which Q is measured, if the Q of the capacitor is much greater than that of the inductor. This assumption is quite adequate in this case, $Q = X_A/R_T \approx 1600/16 \times 10^{-3} = 10^5$, if the ground loss is considered along with the inductor loss resistance. Since the required tuning inductance and Q of the coil is known, then an estimate of the ground resistance can be obtained as follows:

$$Q_{Load} = X_L/R_{Load} \quad (86)$$

* measurement frequency

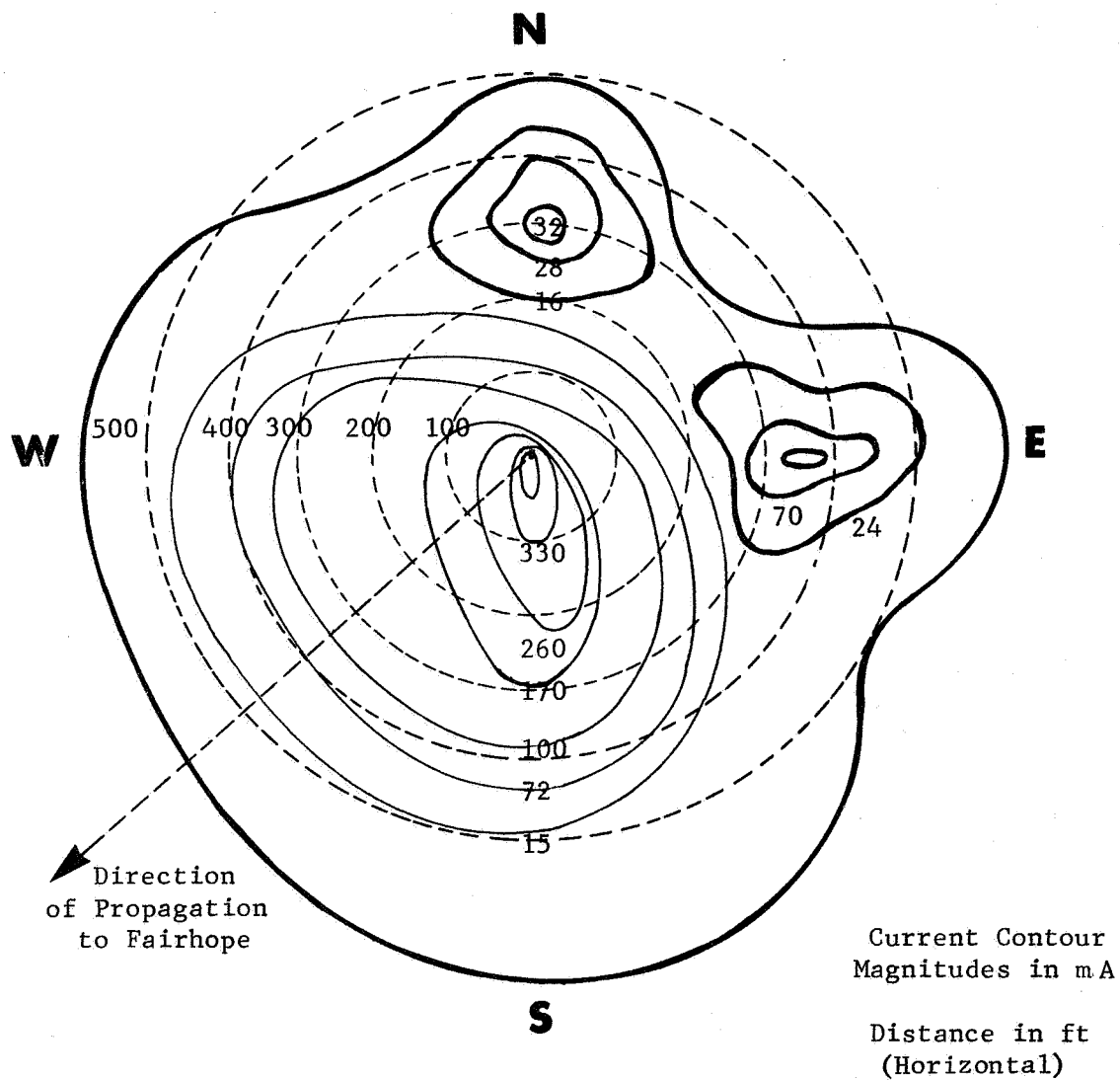


Fig. 33.--Constant ground-wire current contours for Gold Hill Station.

by definition; hence,

$$R_{\text{Load}} = X_L / Q_{\text{Load}} = 2\pi \times 10.82 \times 21.14 \text{ kHz} / 38.9 = 37\Omega. \quad (87)$$

Now, since the transmitter is matched to the resistive tank circuit, the total loss resistance is

$$R_t = R_{\text{Load}} / 2 = 18.5\Omega. \quad (88)$$

If (33) is substituted in (88), then

$$R_g = R_t - R_I$$

or

$$R_g \approx 1.5\Omega \quad (89)$$

if the structural loss resistance and radiation resistance is assumed negligible in comparison to both R_I and R_g . This value of R_g , which is determined on the basis of system bandwidth, is of the same order of magnitude as the ground resistances of 2.3Ω (Fairhope) and 2.5Ω (Gold Hill) which are specified by the measured values of actual Q's.

Fig. 34 shows the feed-through insulator and associated connecting line to the base of the antenna. A shunt-lightning arrester can be seen attached to this line. The RF-AC isolation transformer for the antenna lightning system can be seen to the left of the tower base. The transmitter installation, which consists of (1) power amplifier, (2) frequency synthesizer, (3) frequency standard, and (4) call-sign code modulator, is shown in Fig. 35. These units are located on the wall in front of the coil room so that the RF signal can be matched to the coil over the shortest transmission path. The coil room consists

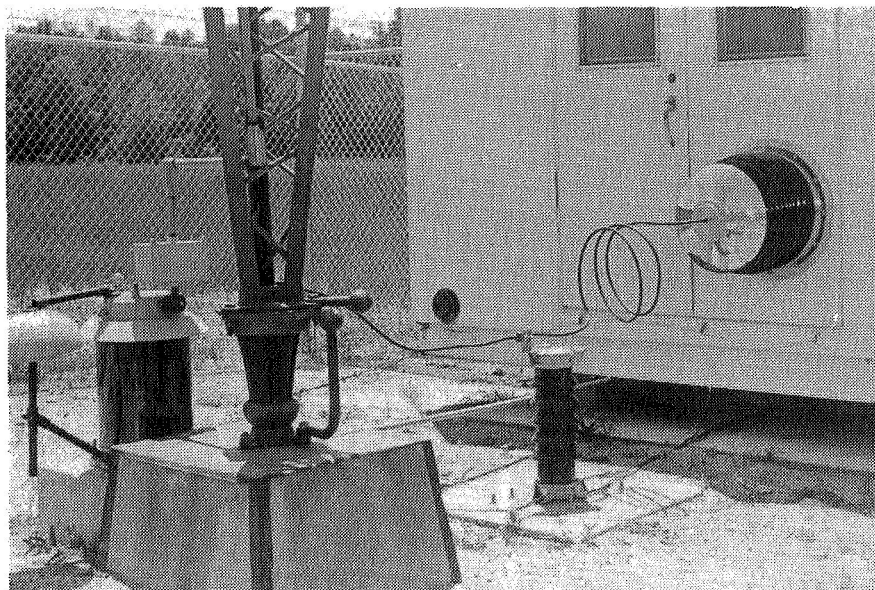
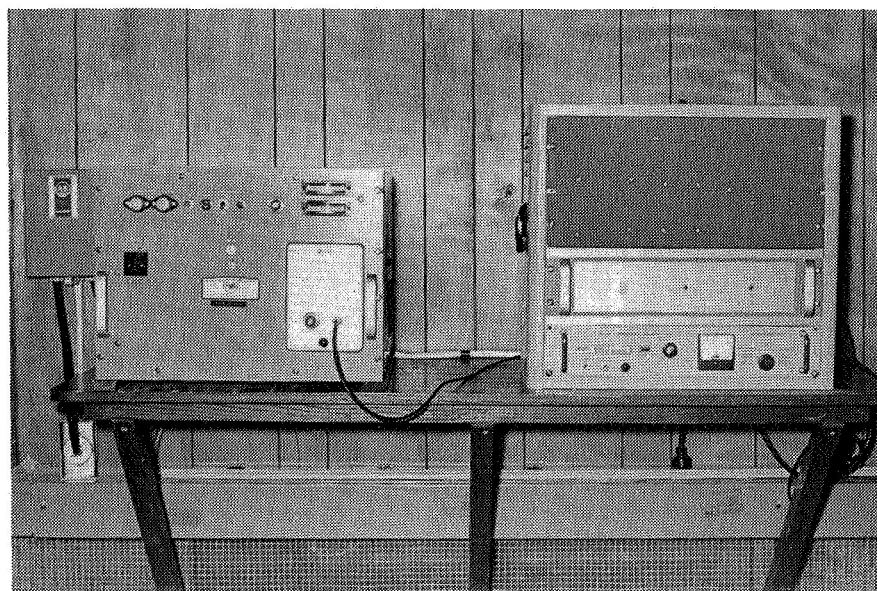


Fig. 34.--View of antenna base showing feed system, lightning arrestor and RF-AC isolation transformer for tower lights (left).



Power Amplifier (2kW)

Standard, Synthesizer and Coder

Fig. 35.--Transmitter installation in instrumentation trailer.

of a 12 ft closed-in section of the instrumentation trailer nearest the antenna tower (see Fig. 32). The remaining portion of the trailer is used as an instrument and equipment room and a work area. Both transmitting stations have identical installations with the exception of the added receiving systems at the Fairhope Station.

The absolute measurement of electromagnetic field intensity radiated from a transmitting source over a given range with a known power input for determination of propagation characteristics can be a most difficult problem. The problem is quite similar to that encountered in the engineering design where not only does the antenna and the propagation characteristics affect the measurement, but the accuracy of the measurement equipment becomes involved. Field strength measurements have been made over the "up" and "down" paths using the receivers and antennas procured for this study. The voltage amplitude calibration for each receiver was verified to insure accurate measurements, and a simple broadband whip antenna having $h_e = 0.3$ cm was used to sample the vertically polarized component of the electromagnetic field. The average field strength magnitude measured over the Gold Hill-Fairhope path was $3.3 \mu\text{V}/\text{m}$ during the winter and spring of 1968. A variation of a factor of three above and below this measured amplitude was observed. The field strength of the Fairhope-Auburn path was measured somewhat higher on the average, about $10.5 \mu\text{V}/\text{m}$ (measured voltage $0.0317 \mu\text{V}$), with about the same amplitude variation during the same period. These values are somewhat lower than the predicted values for the mean conductivity of the path; the error in both cases is approximately -17.2db (1 to 7.3) and -7.2 db (1 to 2.28) respectively. Some of this error

may be attributed to the specified effective height of the field sampling antenna which was employed in the determination of the field strength ($|\bar{E}|h_e = \text{volts}$).^{*} However, the error in the Fairhope-Auburn path is quite reasonable for the theoretical engineering design of this type.

An estimate of radiation resistance can be made from (20) if the antenna base voltage is known, and the radiated power is assumed to be $P_r = I_o^2 R_r$ and $I_o \approx \frac{V_b}{X_A}$. If the measured field strength intensity is now transferred to the reference distance of one mile using (2) where from Table 2, $A = 0.99$, then

$$R_r = (X_A/V_b) (|\bar{E}_g| L_g 10^{-3}/5.9A)^2. \quad (90)$$

The sky wave is assumed negligible in the calculation of (90). For full transmitter power input to the antenna, $V_b \approx 17\text{kV}$ and $C_A \approx 5200 \text{ pf}$, hence

$$R_{r \text{ Fairhope}} \approx 10 \text{ m}\Omega \quad (91)$$

which is slightly less than the $16 \text{ m}\Omega$ predicted. The effective radiation resistance of the Gold Hill antenna is less by a factor of the square of the ratio of the two field strengths (about $1 \text{ m}\Omega$). The over-all system efficiencies can also be estimated on the basis of (39), i.e.,

$$\eta = \frac{P_r}{P_{in}} 100\% = \frac{I_o^2 R_r}{P_{in}} 100\% = \frac{V_b^2 R_r}{X_A^2 P_{in}} 100\%. \quad (92)$$

^{*}Private conversation; Dr. S. N. Witt, RMS, Inc., Atlanta, Georgia.

Thus,

$$\eta_{\text{Gold Hill}} \approx 0.01\% \quad (93)$$

and,

$$\eta_{\text{Fairhope}} \approx 0.082\% \quad (94)$$

where $C_A \approx 5200$ pf, $V_b \approx 17\text{kV}$, $P_{\text{in}} = 2\text{kW}$. The efficiencies are an order of magnitude lower than the predicted values which indicates higher effective losses. However, these losses may include other effects besides the resistive components, such as the antenna radiation pattern effects. The efficiency can also be calculated from the determined values of R_r , R_l , and R_g from (40); hence,

$$\eta_{\text{Gold Hill}} \approx (1 \times 10^{-3}/17 + 2.5 + 0.001) \times 100\% \approx 0.0051\% \quad (95)$$

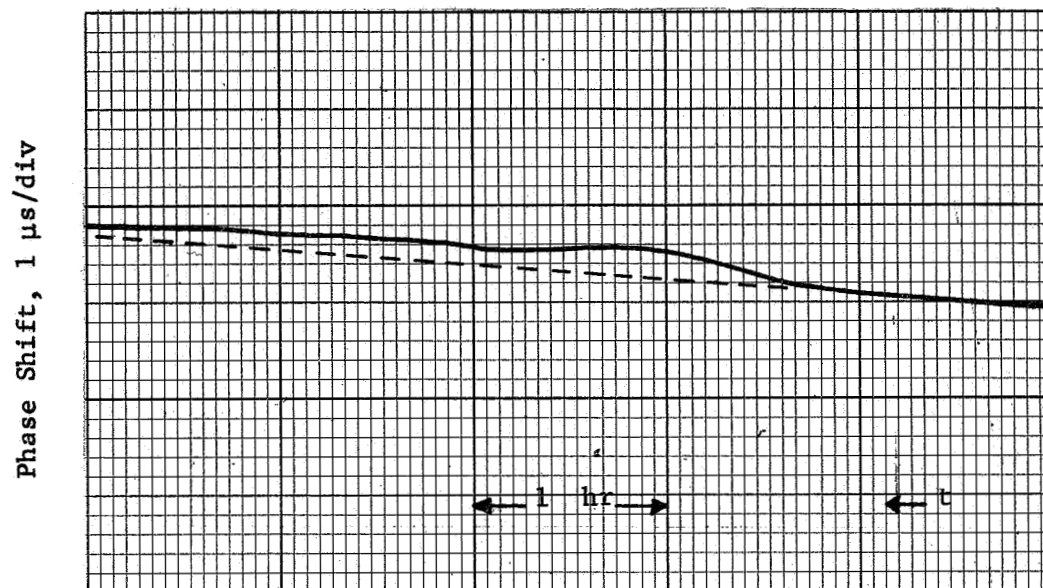
and

$$\eta_{\text{Fairhope}} \approx (10 \times 10^{-3}/16 + 2.3 + 0.01) \times 100\% \approx 0.0543\% \quad (96)$$

These values are of about the same order of magnitude as those values of (93) and (94).

The diurnal phase variations of these propagation paths have been observed and recorded several times recently for the sole purpose of estimating the interference between the sky wave and the ground wave. In Figure (36), a typical morning and night

Night



Morning

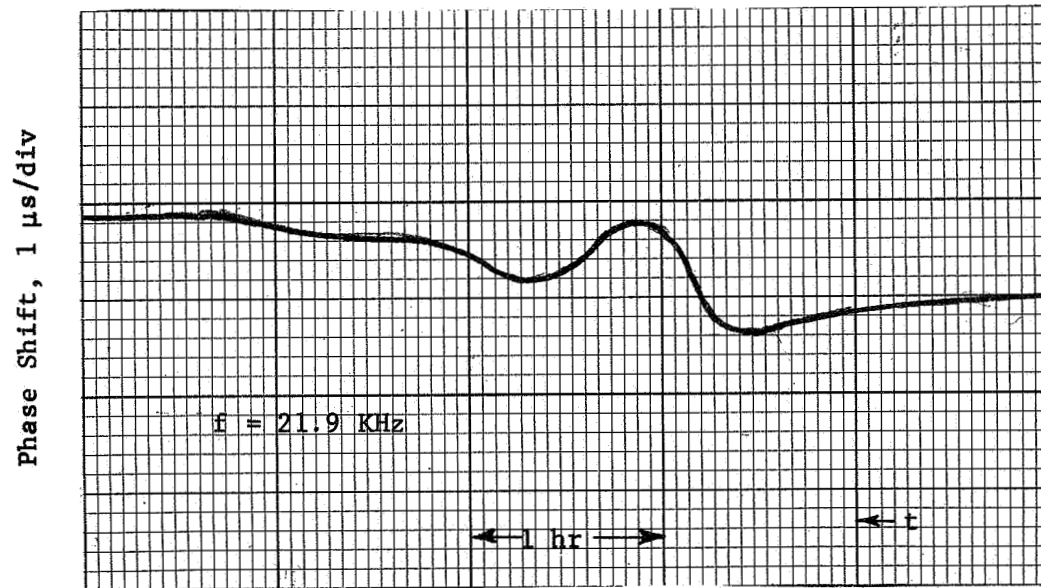


Fig. 36.--Diurnal phase variations (night and morning),
3 May 1968 for Fairhope-to-Auburn transmission
(up-path).

diurnal phase change for the "up-path" is presented. It is very difficult to estimate the total phase from the morning change in phase because of the "over-shoot" and the probable drift between the phase reference (this is an "open-loop" measurement). This overshoot phenomenon is quite pronounced if transmission occurs along the sunrise line, and, as yet, it is not fully explained.* However, a comparison of the slopes of the phases curves (see dotted lines in Fig. 36) before and after sunset indicates approximately a $1.5 \mu\text{s}$ phase shift. This measured phase change compares quite favorably with the maximum phase shift of $1 \mu\text{s}$ predicted from (63).

Extensive measurements of the atmospheric noise power densities at the two stations have not been made in the course of this work. Some samples of effective noise field strengths have been made, however, during winter and spring of 1968 employing a tuned voltmeter (noise bandwidth $\approx 10 \text{ Hz}$). Measurements were made on a frequency of 21.9 kHz with a standard broadband whip antenna at the Auburn Control Station. The average value of the rms noise level in a 1 kHz noise bandwidth varied between 3 mV/m to 10 mV/m (72 to 80 db above $1 \mu\text{V/m}$ at 1 kHz bandwidth). This is approximately 10 decibels above the level predicted and is possibly a result of the control station location. The control station is located in the Textile Building on the Auburn University Campus, which is surrounded by a small, densely-populated, town. The man-made noise from this environment is most likely the factor creating a large background noise level at this frequency. Noise

*Private Conversation: D. D. Crombie, Head, ELF - VLF Lab, NBS, Boulder, Colorado.

peaks as high as 450 mV/m to 600 mV/m have been observed during local thunderstorm activity; however, normal peak values are on the order of 60 mV/m or less. This increase in ambient noise levels directly reduces the over-all signal-to-noise ratio. The reduction in SNR leads to more uncertainty of the actual signal phase, and the accuracy of the phase measured is reduced by an appropriate factor. In the case of a 10 db increase in noise, the rms phase error due to atmospheric noise (assumed equal at both locations) is increased $(10)^{\frac{1}{2}}$, and hence,

$$\delta \phi_t = (10\delta \phi_p^2 + \delta \phi_{mt}^2)^{\frac{1}{2}} \quad (97)$$

from (80). Hence, from (78) and (79)

$$\delta \phi_t \approx 3.05^\circ . \quad (98)$$

This corresponds to an accuracy of about 1 part in 120.

A technique for continuously monitoring the SNR of the VLF phase stability measurements has been developed to indicate the relative precision of the phase comparison. The technique (See Appendix B) is based on a computer-aided measurement of SNR using a time-interval meter or counter. The time interval meter is used to present a digital output related to the signal period. This actual period count contains the SNR information. Hence, the period data can be recorded simultaneously with the phase data, and the SNR can be calculated on an almost continuous basis as the phase data is analyzed. The signal-to-noise ratio measured for the reference receiver at the control station (20.9 kHz from Gold Hill) is

$$\text{SNR} = 76.8 \text{ db} \quad (99)$$

which corresponds to an rms phase jitter of less than 0.49 degrees. The SNR of the "up-path" from Fairhope employing this technique is

$$\text{SNR} = 69.9 \text{ db} \quad (100)$$

which corresponds to a phase error of 0.72 degrees.

The phase stability study system was designed so that commercially available equipment could be employed as functional parts of the system if the equipment requirements and specifications were compatible. The basic type of receiving equipment procured for the system was the RMS, Inc. Model 1320 VLF phase tracking receiver. These receivers are constructed with the very latest state-of-the-art technology employing electronic phase control. Many features of this receiver are advantageous when compared to the older receivers using mechanical phase control; but, there are two features that are most important to this system. These are (1) sensitivity (an increase of a factor of 10) and (2) variable effective bandwidths (.002 Hz to .007 Hz at 20 kHz). The corresponding control system time constants, τ , are 33 seconds and 2 seconds, respectively. The upper cut-off frequency response (f_c) due to phase variations is

$$0.3 \text{ cycles/min} < f_c < 4.8 \text{ cycles/min} \quad (101)$$

where $f_c = 1/2\pi\tau$. These frequency responses are quite adequate for this study since the highest frequency component of the phase variation even considered in the study is on the order of 0.16 cycles/min. However, the over-all system response is related to the response times of all four receivers. An estimate of the total time constant, τ_t , of the system can be obtained from

$$\tau_t = (\sum_n \tau_n^2)^{\frac{1}{2}} \quad (102)$$

where τ_n is the response time constant of the n^{th} receiver, and the phase-lock is assumed to be continuous (no loss of a cycle or multiple thereof during a phase change). It is quite evident that the reference receivers should be operated at the fastest tracking rates (larger bandwidth), so that the over-all response time (small time constant) can be as rapid as possible. Thus, if $\tau_1 = \tau_2 \gg \tau_3, \tau_4$, then, from (102),

$$\tau_t = (2)^{\frac{1}{2}}\tau_1 \quad (103)$$

and the time constant and the cut-off frequency are altered by a factor $(2)^{\frac{1}{2}}$. Hence, the over-system cut-off frequency is

$$f_c = 0.212 \text{ cycles/min} \quad (104)$$

for $\tau_2, \tau_1 = 33 \text{ sec}$ and $\tau_3, \tau_4 = 2 \text{ sec}$. The system response under these

conditions is virtually independent of the reference receiver time responses. The response of the over-all phase study system operating in a closed-loop mode is shown in Fig. 37 for a step change in phase. The total response time t_t for this step of phase change is approximately 200 seconds which is somewhat longer than the predicted time of (104) where $t_t \simeq 0.35/f_c \simeq (99 \text{ sec.})$.

A view of the Auburn Control Station showing the receivers, frequency standard or reference, and the data acquisition system is presented in Fig. 38. As is indicated in Fig. 3, an output signal from the reference receiver, which is phase coherent with the received signal of the reference receiver, is employed as the reference for a second phase comparison receiver. Consequently, if both receivers are tuned to the same signal frequency, the phase error sensed in the second receiver is essentially zero because both the input and reference signals are in phase as a result of the phase coherence maintained in the reference receiver. This technique is employed to test the accuracy of the receiver-reference combination for long term stability. A typical test curve is presented in Fig. 39. The curve indicates a possible $1 \mu\text{s}$ error over the long-term measurement; however, this error is a result of the long term stability of the recorder.

A summary of the measured parameters are presented in Table 6 together with the design parameters.

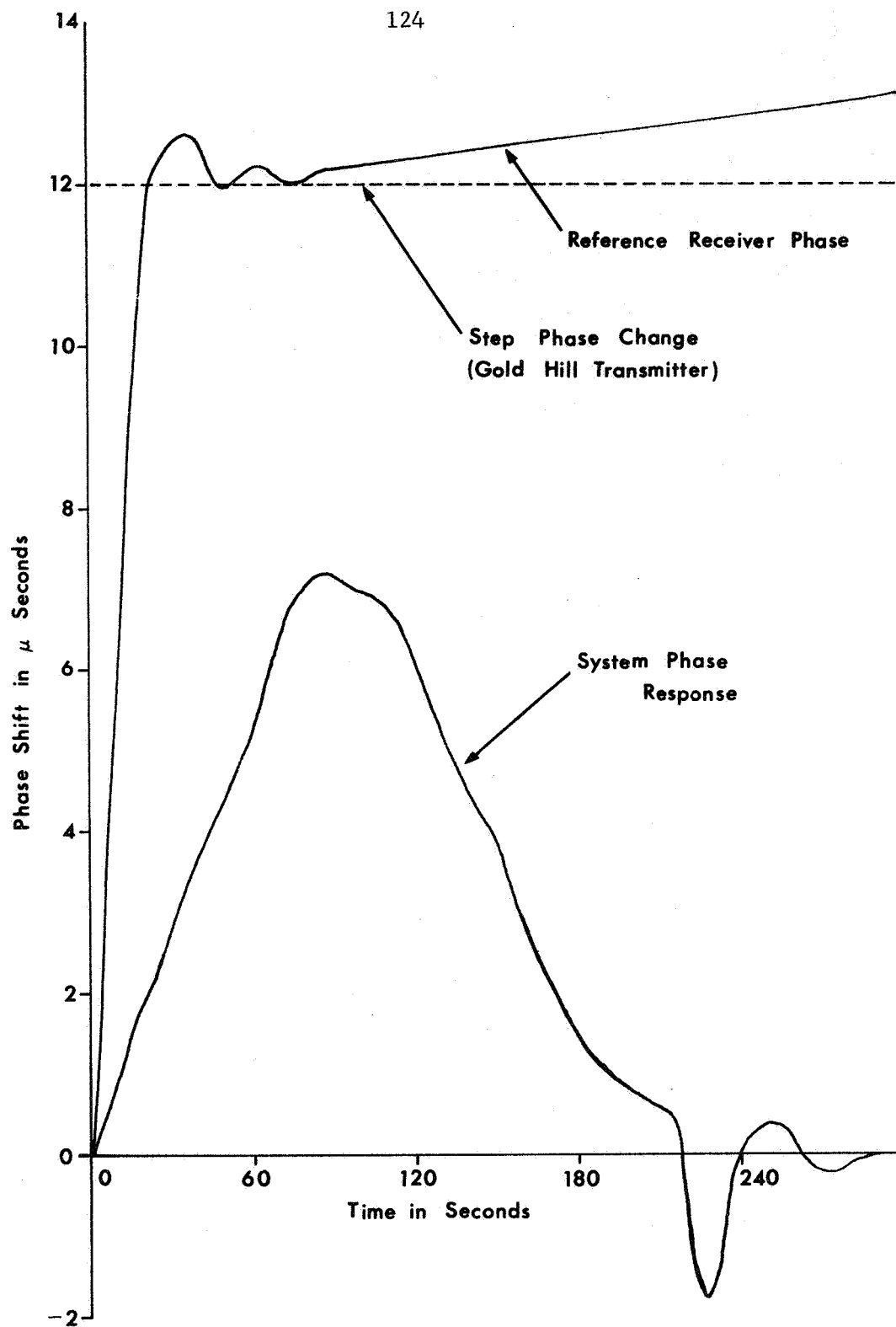
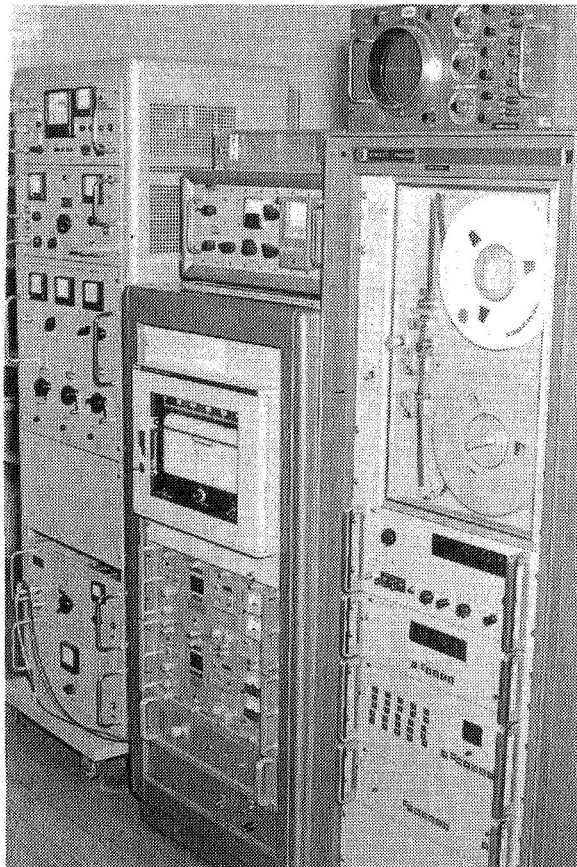


Fig. 37--Response of Closed-loop System to a Step Change in Phase.



Frequency
Standard

Receivers and
Recorder

Data Acquisition
System

Fig. 38--Auburn control station for VLF
phase stability study system.

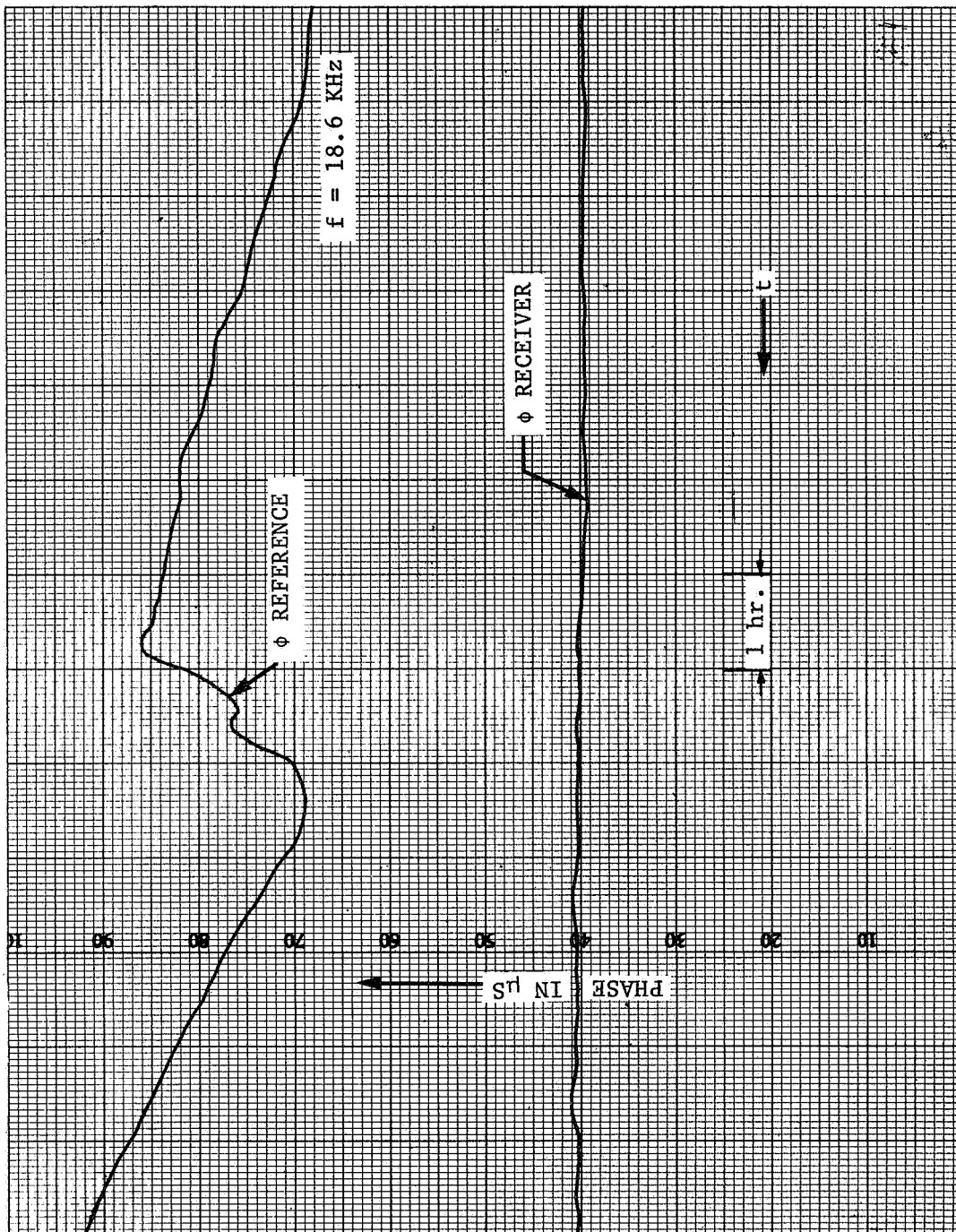


Fig. 39 -- Phase comparison accuracy test of receiver-reference combination.

TABLE 6

MEASURED PARAMETERS FOR PHASE STABILITY STUDY SYSTEM

Quantity	Fairhope	Gold Hill
C_A (Static)	5200 pf	5160 pf
C_A (Operating) *	5830 pf	5812 pf
Q (Antenna)	545	525
L_t	9.9 mH	10.82 mH
Q (Helix)	≈85	≈84
R_I	16Ω	17Ω
R_r	10 mΩ	1 mΩ
R_g	2.3Ω	2.5Ω
B	≈550 Hz	≈543 Hz
$ \bar{E}_t $	10.5 μV/m	3.3 μV/m
η	0.082%	0.01%
SNR (Control)	69.9db @ B = 2×10^{-3} Hz	76.8db @ B = 7×10^{-2} Hz
t_t (Control)	200 sec (system response time)	

* This value includes all stray capacitance.

V. CONCLUSIONS

This study has presented the basic theoretical design considerations for any VLF communications system for propagation over short distances. Using this basic design information, the propagation problem related to the described VLF transponder system for a 200 mi path is analyzed and design parameters are specified in Table 5. The engineering design of this system was implemented and tested during the years 1967 and 1968. The experimental results obtained from the implemented system are presented in Table 6.

These experimental results compare quite favorably with the predicted values in most cases. The largest difference appears in the predicted values of tuning coil Q's (1000 compared to 525) and in the value of ground resistances (2.3Ω compared to 0.35Ω). Both of these errors, of course, reduce the efficiency somewhat; however, a possible over-all loss in radiated power due to differences in design and actual system parameters had been anticipated, and the specified transmitter power output is sufficient to radiate 1 watt ERP.

The design of the antenna structures was most satisfactory. The scale model study and the theoretically calculated values for the antenna structure indicate that a 20 per cent increase in capacitance can be obtained with rib diameter increase of 1:18. The capacitance actually obtained (5200 pf) indicates that a 24 per cent increase in total capacitance

can be obtained for such a 300 ft structure employing the multiple-wire construction. This multiple-wire type construction can thus be used to considerable advantage to increase the effective antenna height of such structures with a shorter rib length and/or the total capacitance can be increased for a given antenna configuration. The antenna radiation resistance of the Fairhope antenna is of the same order of magnitude as that predicted. The radiation resistance of the Gold Hill antenna is somewhat lower and this may be a result of the local conductivity.

The measurement of signal-to-noise is one very important aspect of establishing the performance characteristics of this propagation system. The technique presented here, which uses a time interval counter in conjunction with a digital computer, can determine system SNR's accurately at the same time as the phase data is being analyzed. Thus, the SNR can be monitored on a long-term basis almost continuously. The results of a signal-to-noise measurement at the noisiest time of day using this technique (see (99) and (100)) indicates that a system accuracy of about 1 part in 190 can be obtained for the specified equipment error if the SNR at both locations are equal. This result is slightly better than that determined from a cursory measurement of rms ambient noise as specified in (97) and (98).

The closed-loop operation of this system with full power output was obtained only recently. This mode of operation had been hindered as a result of the interference of the transmitter signal at 21.9 kHz and the received signal at 20.9 kHz. This, of course, is a direct

result of the large difference in power levels, and the close spacing in operating frequencies (1 kHz) which is required to minimize dispersive effects in the propagation media. A cascaded band-pass and notch filter has been used to minimize this problem so that a closed-loop mode of operation can be obtained. A typical plot of the phase comparison recording for the closed-loop transponder system is shown in Fig. 40a. It is interesting to note that the composite phase plot does not have a definite slope like that of the reference phase, since there is no frequency error and, thus, no "ramp-type" accumulated phase. The jump in reference phase of about 7 μ s appears to be a result of the Gold Hill frequency standard or the frequency synthesizer because it does not appear in the total phase response and, thus, it was canceled by the reference receiver in the over-all phase plot. The total diurnal phase variation for the closed-loop appears to be about double that of the one-way path (3 μ s) and a definite change in the slope of the phase data is indicated before and after sunset. The phase plot also exhibits the "noisy" characteristic appearance of night time VLF propagation after sunset (about 8:30 pm, CDT). Fig. 40b shows the one-way phase variation measured simultaneously at the Fairhope transponder station with that data of Fig. 40a. The calibration of the actual phase is only approximate, but the plot does indicate the relative change in diurnal phase as previously indicated. It is also interesting to note again that the closed-loop system has a response time of about 200 sec for a step change in phase (Gold Hill Transmitter) of 12 μ sec; this compares favorably with the 99 sec response time predicted.

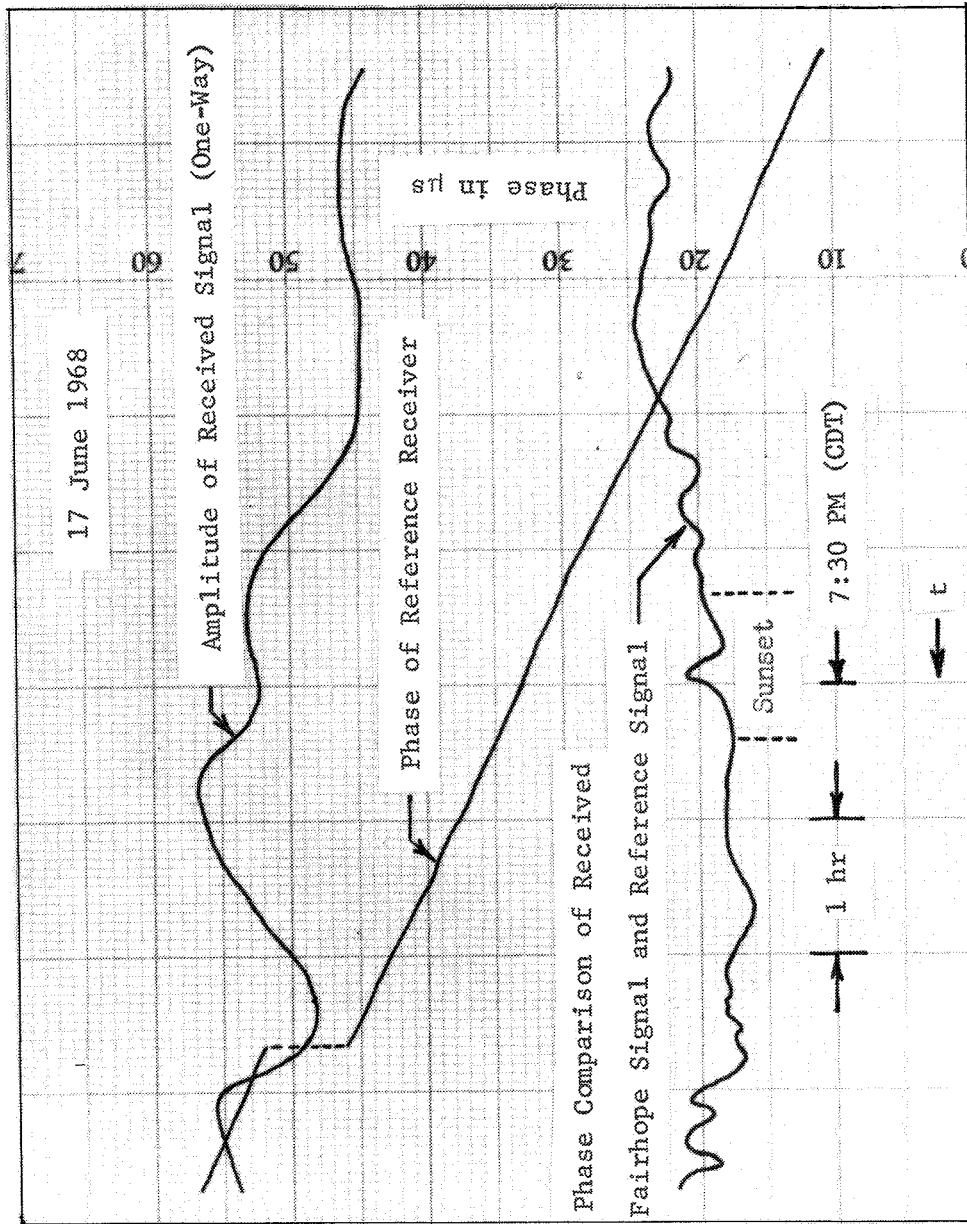


Fig. 40a--A Typical phase comparison recording for the closed-loop system (Control Station data.)

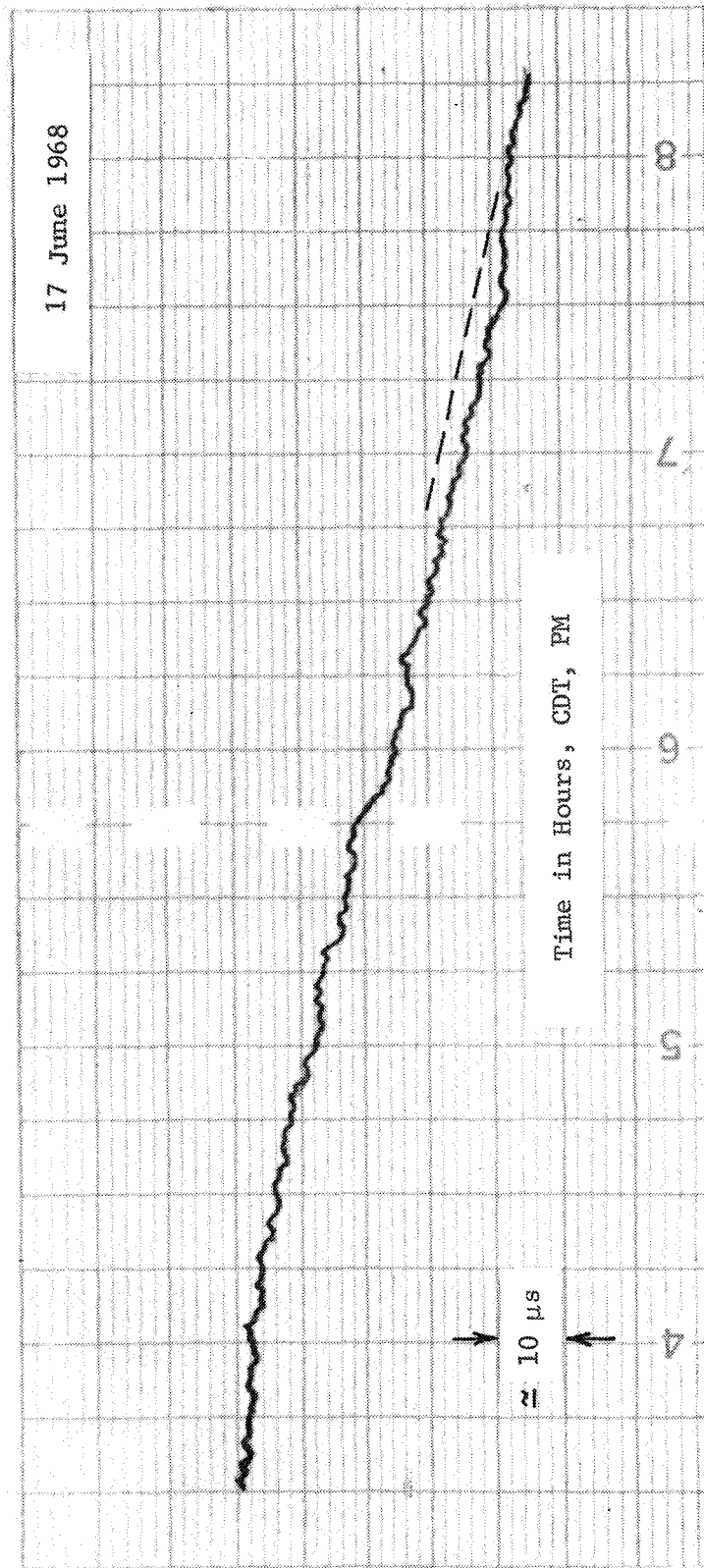


Fig. 40b -- A typical phase comparison recording for the closed-loop system:
One-way phase Variation, Fairhope receiver (Simultaneous with (a)).

The actual values of the design parameters obtained here are not exact, as is characteristic of any engineering design, particularly propagation studies. Even the system itself, of course, is to be employed to study statistically the phase stability of propagation over this path because the phase characteristics are variable and, hence, cannot be determined precisely. Even so, the over-all results compared quite satisfactorily, and this completed system represents a unique tool for the study of VLF propagation over short distances.

LIST OF REFERENCES

REFERENCES

1. Graf, E. R., Smith, C. E., McDevitt, F. R. and Sims, R. J., "A New Method for High Accuracy Prediction of Sunspot Activity as an Aid in Deep Space Communication," IEEE Region III Conv. Record, 21.5.1 (1968).
2. Davies, K., Ionospheric Radio Propagation, Washington, D. C.: U. S. Govt. Print. Office, (1965).
3. Pierce, J. A. Mitchell, H. T., and Essen L., "World-Wide Frequency and Time Comparison by Means of Radio Transmissions," Nature, 174, 922 (1954).
4. Morgan, A. H., "Distribution of Standard Frequency and Time Signals," Proc. IEEE, 55, 827(1967).
5. Casselman, C. J., Heritage, D. P. and Tibbals, M. L., "VLF Propagation Measurements for the Radux-Omega Navigation System," Proc. IEEE, 47, 829 (1959).
6. Reder, F. H., Winkler, G. M. R., and Bichart, C., "Results of a Long-Range Clock Synchronization Experiment," Proc. IEEE, 49, 1028 (1961).
7. Hopkins, H. G., and Reynolds, L. G., "An Experimental Investigation of Short-Distance Ionospheric Propagation at Low and Very Low Frequencies," Conv. IEE Record, Radio Section, 21 (1953).
8. Bain, W. C., et al., "The Ionospheric Propagation of Radio Waves of Frequency 16 Kc/s over Distances of About 540 KM," IEE, London, England, Monogram 37 (1952).
9. Bracewell, R. N., et al., "The Ionospheric Propagation of Low- and Very-Low Frequency Radio Waves over Distances less than 1000 KM," Proc. IEE, 98, 221 (1951).
10. Straker, T. W., "The Ionospheric Reflection of Radio Waves of Frequency 16 KC/s over Short Distances," Proc. IEE, 102C, 396 (1955).
11. Bracewell, R. N., "The Ionospheric Propagation of Radio Waves of Frequency 16 kc/s over Distances of about 200 KM," IEE, London, England, Monogram 34R (1952).

12. Jordan, E. C., Electromagnetic Waves and Radiating Systems. Englewood Cliffs, N. J.; Prentice-Hall, Inc. (1950).
13. T. M. Lowe, Jr. and Associates, Inc., Land Survey of Antennas Positions in Baldwin and Lee County, Alabama, (Atlanta, Ga., 1966).
14. Budden, K. G., The Wave-Guide Mode Theory of Wave Propagation. Logos Press (1961).
15. Wait, J. R., "The Mode Theory of VLF Ionospheric Propagation for Finite Ground Conductivity," Proc. IEEE, 45, 760 (1957).
16. Pierce, J. A., "Intercontinental Frequency Comparison by Very Low Frequency Radio Transmissions," Proc. IEEE, 45, 798 (1957).
17. Belrose, J. S., et al., "The Engineering of Communications Systems for Low Radio Frequencies," Proc. IEEE, 47, 661 (1959).
18. Watt, A. D. VLF Radio Engineering. New York, N.Y.; Permagon Press (1967).
19. Watt, A. D., and Plush, R. W. "Power Requirements and Choice of an Optimum Frequency for a World-wide Standard-Frequency Broadcasting Station," Journal Res. NBS, 63D, 35 (1959).
20. Graf, E. R. and Smith, C. E., "An Investigation of the Design Criterion for a Phase Stability Study System of VLF Propagation over Short Distances," Auburn University, Auburn, Ala., NAS8-5231 Rept. 9 (December 1965).
21. Norton, K. A. "The Calculation of Ground-Wave field Intensity over a Finetely Conducting Spherical Earth," Proc. IEEE, 26, 623 (1941).
22. Wait, J. R., "Diffractive Corrections to the Geometrical Optics of Low Frequency Propagation," NBS, Boulder, Colo., Rep.-5572 (1958).
23. Skolnik, M. I., Introduction to Radar Systems. New York, N. Y.; McGraw-Hill Book Co. (1963).
24. Brown, G. H., "Ground Systems as a Factor in Antenna Efficiency," Proc. IEEE, 25, 753 (1937).
25. Kraus, J. D. Antennas, New York, N. Y.; McGraw-Hill Book Co. (1950).
26. Wait, J. R., and Pope, W. A. "Input Resistance of L. F. Unipole Antennas," Wireless Engr., 32, 366 (1963).
27. Abbott, F. R., "Design of Optimum Buried-Conductor RF Ground Systems," Proc. IEEE 40, 846 (1952).

28. Smith, C. E. and Johnson, E. M., "Performance of Short Antennas," Proc. IEEE, 35, 1026 (1947).
29. Smeby, L. C., "Short Antenna Characteristics-Theoretical," Proc. IEEE, 37, 1185 (1949).
30. Walter, J. C., "Very-Low-Frequency Antennas are Going Back to Work," Electronics, 38, 80 (1965).
31. Gangi, A. F., et al., "The Characteristics of Electrically Short, Umbrella Top-Loaded Antennas," IEEE Trans. AP, 13, 864 (1965).
32. Jasik, H., Antenna Engineering Handbook. New York, N. Y.; McGraw-Hill Book Co. (1961).
33. Wait, J. R. and Conda, A. M., "Pattern of an Antenna on a Curved Lossy Surface," IEEE Trans. AP, 6, 348 (1958).
34. Norton, K. A. "Transmission Loss in Radio Propagation-II," NBS, Boulder, Colo., Tech. Note-12 (1959).
35. Wait, J. R., Electromagnetic Waves in a Stratified Media, New York, N. Y.; Permagon Press (1962).
36. Austin, L. W., "Some Quantative Experiments in Long-Distance Radio Telegraphy," J. Res. NBS, 7, 315(1911).
37. Terman, F. E. Radio Engineers Handbook. New York., N. Y.; McGraw Hill Book Co. (1943).
38. Butterworth, S. "Effective Resistance of Inductance Coils at Radio Frequencies," Exp. Wireless and Wireless Engineering, 3, 203 (1926).
39. Norton, K. A., Shultz, E. L., and Yarbrough, H., "The Probability Distribution of the Phase of the Resultant Vector Sum of a Constant Vector Plus a Rayleigh Distributed Vector", J. Appl. Phys., 23, 137 (1952).
40. Schwartz, M. Information Transmission, Modulation, and Noise. New York, N. Y.; McGraw-Hill Book Co. (1959).
41. Rice, S. O., "Statistical Properties of a Sine Wave Plus Random Noise," Bell Sys. T. J., 27, 138 (1948).
42. General Radio Company, "Input Noise, Its Influence on Counter and Pulse-Generator Performance and Its Measurement," The Experimenter 40, 3, (1966).

APPENDICES

PRECEDING PAGE BLANK NOT FILMED.

APPENDIX A

List of Symbols

<u>Symbol</u>	<u>Definition</u>	<u>Usual Units</u>
A	ground wave attenuation factor	-
A_p	peak amplitude of a sinusoidal voltage signal	v
A_{rms}	rms value of A_p	v
a	antenna physical height	ft
C_f	terrain cutback-factor	-
C_{Ae}	equivalent antenna capacitance	pf
D_m	ionospheric Convergence factor	-
D	distance to extremities of umbrella antenna support wires	ft
d	vertical distance from top of umbrella antenna to insulator	ft
d_i	diameter of coil	ft
\bar{E}_t	total electric field strength	v/m
$ \bar{E}_g $	magnitude of ground wave electric field	v/m
$ \bar{E}_{s,m} $	magnitude of the m^{th} sky wave electric	v/m
$\bar{E}(t)$	time dependent electric field	v/m
$ \bar{F}_s $	magnitude of unattenuated field strength from a vertical radiator @ 1 m	mv/m
f	frequency	Hz
f_o	frequency at which a monopole antenna is $\lambda/4$ in length	Hz

<u>Symbol</u>	<u>Definition</u>	<u>Usual units</u>
f_c	cut-off frequency (3 db)	Hz
F	magnitude factor in coil calculation	-
$G_t(i_g)$	normalized voltage gain of an antenna	-
G	radian height of an antenna	radians
h	angular height of an antenna	degrees
h_i	height of ionosphere	km
h_e	effective height of an antenna	km
i_g	angle of incidence at earth's surface	degrees
I_o	antenna current	amperes
L_g	propagation distance measured along the earth's surface	mi
$L_{s,m}$	propagation distance of the m^{th} sky wave	mi
L_t	launching loss	-
Log	log to base 10	-
\log	log to base e	-
L	inductance	henry
ℓ	length of coil	ft
ℓ_1	layer gradient scale factor (conductivity change of a 2.71 ratio)	km
M	changing vertical moment on an antenna	amp m
N	number of ribs	-
n	numerical constant	-
n_t	number of coil turns	-
P_r	radiated power	W

<u>Symbol</u>	<u>Definition</u>	<u>Usual units</u>
P_i	total input power to system	W
P_G	total power loss in ground	w
P_w	power loss in wires	w
P_e	power loss in ground adjacent to wires	w
P_x	power loss in ground beyond wires	w
Q	quality factor	-
R_L	loss resistance	Ω
R_r	radiation resistance	m Ω
R_I	inductor loss resistance	Ω
R_g	ground loss resistance	Ω
R_A	antenna structural loss resistance	Ω
R_{ac}	ac resistance	Ω
R_{dc}	dc resistance	Ω
R_{Ae}	effective shunt resistance	-
$R_{g }$	ground reflection coefficient	-
R_m	composite ionospheric reflection coefficient	-
$ R $	ionospheric reflection coefficient in the plane incident	-
r_1	antenna tower radius	ft
r_2	umbrella rib radius	in
S	turns spacing for coils	in
t_t	total system time response	s
T	fundamental period of a sinusoid of frequency f	s

<u>Symbol</u>	<u>Definition</u>	<u>Usual units</u>
v_o	velocity of light in free space	m/s
V_b	antenna base voltage	kV
V_t	voltage between coil turns	V
w	power input to antenna	W
X_A	capacitive reactance of antenna	Ω
X_L	inductive reactance	Ω
Z	antenna input impedance	Ω
β	free-space propagation constant	radians/m
ΔA_p	amplitude change in A_p	V
ΔT	differential period increment	s
Δt	differential time increment	s
$\delta \phi_p$	rms phase error	radians
$\delta \phi_m$	rms mechanical error	radians
δt	rms time error	s
ϵ_a	permittivity	farads/m
ϵ_r	relative permittivity	-
ϵ_o	permittivity of free space	farads/m
θ	$90 - i_g$	degrees
θ_1	angular distance	radians
λ	wavelength	m
λ_o	free space wavelength	m
η	efficiency	percent
σ	conductivity	mho/m

<u>Symbol</u>	<u>Description</u>	<u>Usual units</u>
τ	time constant	s
τ_t	composite time constant	s
τ_n	n^{th} time constant	s
ϕ_g	ground wave phase	degrees
ϕ_I	antenna current phase	degrees
ϕ_A	ground attenuation factor phase	degrees
ϕ_d	diurnal phase shift	degrees
$\phi_{s,m}$	sky wave phase	degrees
ϕ_R	phase of ionospheric reflection coefficient	degrees
ϕ_P	phase of a sinusoid	degrees
ϕ	angle of incidence at the ionosphere	degrees

APPENDIX B
A COMPUTER-AIDED MEASUREMENT OF SNR
EMPLOYING A TIME INTERVAL COUNTER

The accuracy of any phase measurement of a sinusoid, as well as the ultimate sensitivity of any communication system, is limited by the noise present within the bandwidth of the over-all system. This noise manifests itself by varying the parameters of the observed signals both in effective amplitude and phase. Consequently, the extraction of information from this combination of signal and noise is limited by the uncertainty of the signal parameters. The theoretical description of a sinusoid, plus random noise, for both phase measurements and communications applications can be obtained from various approximate and completely statistical techniques.³⁹⁻⁴¹ These descriptions of this problem relate the desired signal parameters in terms of the existing signal-to-noise ratios (SNR).

For a brief review of the signal-to-noise problem, consider the simple geometric relationships between the signal and the statistical parameters of the added noise as shown in Fig. 8. It can be shown that the root-mean-square (rms) errors of the signal parameters can be expressed by relationships between the known signal parameters and the existing SNR. A very simple technique to obtain these relationships is described by Skolink²³ as applied to radar applications for large

SNR. If a noise component is introduced in the transmission system with a monochromatic sinusoid, as shown in Fig. 8, then the apparent amplitude is increased above the actual value by an amount $\Delta A_p = n(t)$. If the error in the time at the zero-axis crossing as a result of the added noise is now considered, then, from Fig. 8,

$$\Delta t = \frac{n(t)}{\text{zero-crossing slope}} \quad (105)$$

Therefore, the rms time error can be expressed as

$$\delta t = (n(t)^2)^{\frac{1}{2}} / A_p \omega \quad (106)$$

where $(n(t)^2)^{\frac{1}{2}}$ is the rms value of the noise, the zero crossing slope is just the slope of the sinusoid for $t = 0$ or $A_p \omega \cos \omega t \big|_{t=0}$, A_p is the sinusoid amplitude, and ω is the radian frequency of the sinusoid. This effective time change is a result of the arithmetic summation of the signal and noise which changes the actual zero-crossing of the waveform. The rms error of the period T , which is the time between two successive zero crossings, can easily be obtained if the two zero-crossing measurements are independent. If this assumption is valid, then the rms period error δT is just $2^{\frac{1}{2}}$ multiplied by the square root of the sum of the squares of the rms time error, or $\delta T = (2)^{\frac{1}{2}} \delta t$ in this case. The rms period error is, from (106)

$$\delta T = (2)^{\frac{1}{2}} (n(t)^2)^{\frac{1}{2}} / A_p \omega \quad (107)$$

or

$$\delta T = T/2\pi(\text{SNR})^{\frac{1}{2}} \quad (108)$$

where $T = 1/f$ and SNR is power signal-to-noise ratio, $(A_p^2/\overline{n(t)^2})^{\frac{1}{2}} = (2\text{SNR})^{\frac{1}{2}}$. Thus, the SNR can be obtained from (108) in terms of the rms period error as

$$\text{SNR} = (T/2\pi\delta T)^2 \quad (109)$$

The validity of this expression holds only for the basic model where large SNR's and independent zero crossings are assumed.

The equations for both the rms time and phase errors have been widely used in the aerospace and radar fields to predict the accuracy of range measurements from known SNR's. However, as indicated in (109), it is evident that the SNR can be specified completely from the measurement of the period or frequency of the signal and the determination of the rms period error. In many cases, the absolute period of the signal is a priori information; and, thus, the determination of the rms error in the period is all that is required to specify the SNR for a given operating condition. This result is quite important since it means that the SNR can be determined from a single calculation of the rms period error for a statistical sample of period measurements. The rms period error can be calculated from the m^{th} period error

$$\Delta T_m = T_m - T \quad (110)$$

where T_m is the measured period and T is the actual period of the signal. For a large number of the measured time errors in the period of a monochromatic sinusoid plus noise, the rms period error can be calculated from

$$\delta T = (\overline{\Delta T^2})^{\frac{1}{2}} \approx \left(\sum_{n=1}^K (\Delta T_n)^2 / K \right)^{\frac{1}{2}} \quad (111)$$

where n is the n^{th} measured period error for $n = 1, 2, 3 \dots K$. The results of (111) will approach the theoretically derived statistical value for large values of K , and the existing SNR can be calculated from (109).

A time interval counter, which has a highly stable clock frequency, can be employed to measure the period or time lapsed between successive zero crossings of a monochromatic sinusoid plus random noise. From this measured period data, a simple digital computer program (or specialized computer) can be employed to calculate the existing SNR from (109), (110), and (111).

There are two basic errors that could occur in the measurement. These are (1) uncertainty of the trigger-level at the zero-crossing point,⁴² and (2) period variations introduced independently of the noise by the counter clock and the actual sinusoid. The error t_1 introduced by the inability of a counter to trigger the counting procedure at the zero crossing is, from Fig. 41,

$$t_1 = \frac{t_u}{\text{slope}} \approx \frac{T t_u}{A_p 2\pi \cos \theta_1} \quad (112)$$

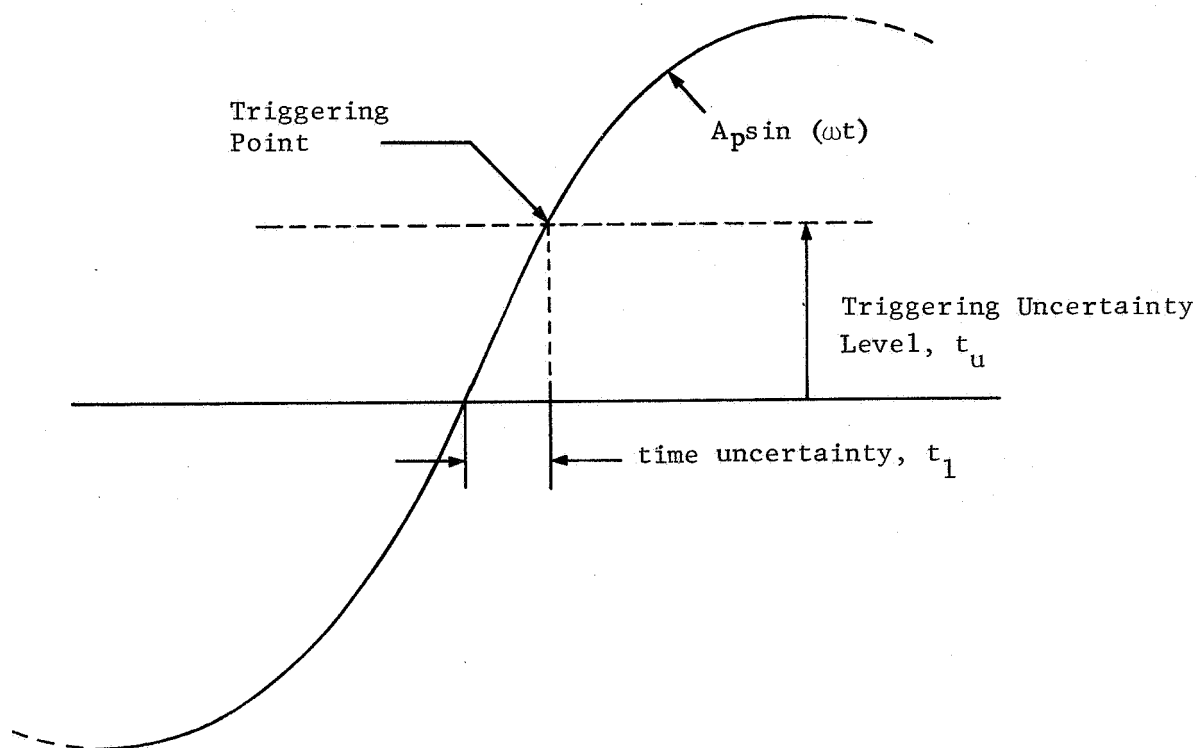


Fig. 41 -- The effects of uncertainty in trigger level on the SNR measurement.

where t_1 is time uncertainty of the period, t_u is trigger level uncertainty, and $\theta_1 = \omega t_1$, the angle between the input voltage zero crossing and the triggering point $A_p > t_u$. The normalized period error ϵ_m is from (112)

$$\epsilon_m = \frac{t_1}{T} \approx \frac{t_u}{2\pi A_p} \left(\frac{1}{\cos \theta_1} \right) \quad (113)$$

The error introduced by trigger uncertainty is a function of the ratio t_u/A_p and inversely related to the cosine of θ_1 . Hence, to minimize this error, not only must $A_p > t_u$, but the trigger sensitivity level must be maintained at a low level so the $\cos \theta_1 \approx 1$ for all measurements. Actually, the system is so sensitive to this type error that the condition $A_p \gg t_u$ must be established if error free measurements are to be obtained for these two factors. The triggering level uncertainty error may also be emphasized if the trigger-reset levels are not established around zero amplitude. This result is valid for narrow-band systems, where the time rate-of-change of the signal plus noise can be considered approximately equal to that of the signal. For wide bandwidths, the actual slope within the triggering level and zero-crossing region will determine the ultimate period error of (112).

If an error ϵ_n is introduced in the actual period measurement as a result of period instability of the clock or the input signal, then, the rms period error δT is

$$\delta T = \left(\sum_{n=1}^K (\Delta T_n + \epsilon_n)^2 / K \right)^{1/2} \quad (114)$$

or

$$\delta T = \left[\sum_{n=1}^K (\Delta T_n^2 / K) (1 + (2\epsilon_n / \Delta T_n)) \right]^{\frac{1}{2}} \quad (115)$$

for $\epsilon_n \ll \Delta T_n$ and $n = 1, 2, 3 \dots K$. Thus, the frequency or period errors of the clock and signal are actually masked somewhat for the case where $\epsilon_n \ll \Delta T_n$. However, if no added noise is present, (114) becomes

$$\delta T = \sum_{n=1}^K \frac{\epsilon_n^2}{K} \quad (116)$$

which determines the basic limiting value for measuring SNR with the system.

Measurements of the period of a 1 kHz signal on a one period basis have been made for known SNR's in a narrow-bandwidth system. Random noise obtained from a General Radio Type 1390-B generator was summed after amplification with a 1 kHz signal from a Rhode and Schwarz frequency standard. The arithmetic summation of signals was processed through a narrow-band filter, and the signal and noise were measured independently with a true rms voltmeter. The period counts, which were obtained with a Hewlett-Packard Model 2245 counter with time-interval plug-in, were recorded in digital form, and processed on a computer to calculate the signal-to-noise ratios. The ratio of peak signal to sensitivity or trigger level was approximately 25 to 1 for the measurements, which corresponds to an angle ϕ_p of 2.3° . It was found after some experimentation that a set of 100 data points ($K = 100$)

constituted a good statistical sample for the measurements described here. Computer calculations for the measured SNR are presented in Fig. 42. These results indicate that a very high degree of accuracy can be obtained in using a computer-aided technique employing a time interval counter. It is interesting to note that computed accuracy decreases above 60 db as the limiting system SNR, which is based on (116), is approached.

This technique is, in general, limited to the low frequency spectrum as a result of the counter limitations; however, frequency translation techniques may possibly be used to obtain measured values of SNR at higher frequencies.

This technique was developed to monitor the SNR for this type of long-term phase stability propagation study. The period measurements are to be recorded on magnetic tape along with the phase information for the propagation study. The relative accuracy of the phase measurement is then to be determined on an almost continuous basis as the phase data is analyzed on a digital computer.

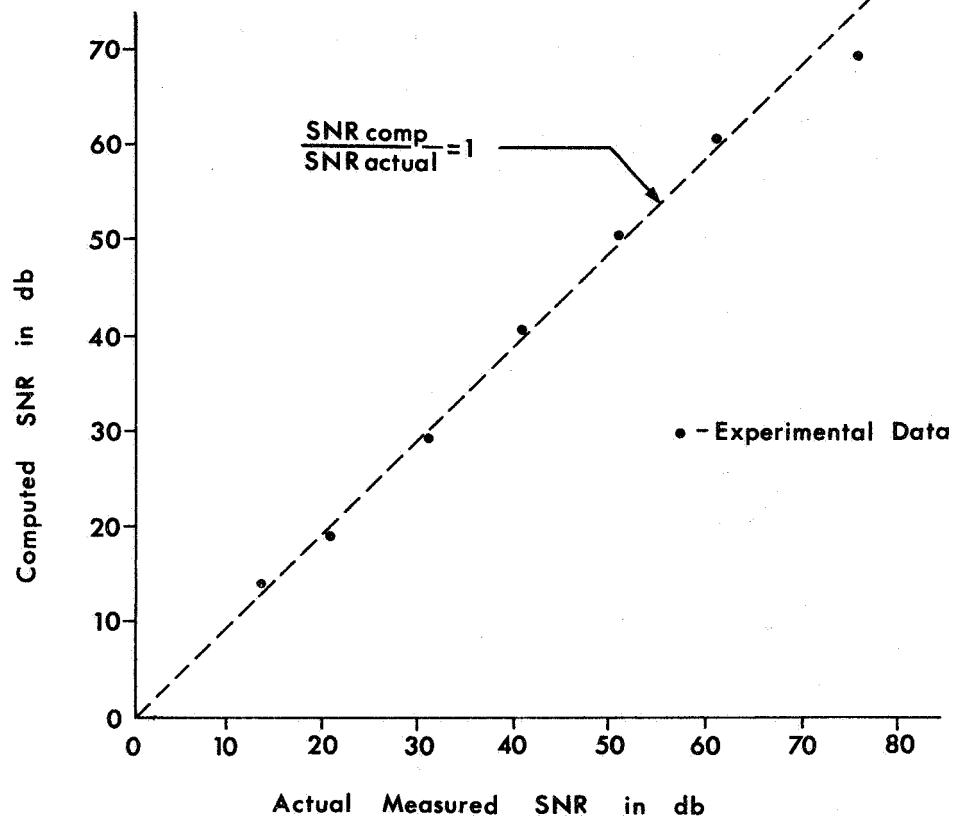


Fig. 42 -- Actual versus computed SNR